2014

Multifunctional, tunable catalysts from interfacially cross-linked reverse micelles

Li-Chen Lee
Iowa State University

Multifunctional, tunable catalysts from interfacially cross-linked reverse micelles

by

Li-Chen Lee

A dissertation submitted to the graduate faculty

in partial fulfillment of the requirements for the degree of

DOCTOR OF PHILOSOPHY

Major: Chemistry

Program of Study Committee:

Yan Zhao, Major Professor
Aaron Sadow
Javier Vela
Ning Fang
Wenyu Huang

Iowa State University

Ames, Iowa

2014

TABLE OF CONTENTS

ACKNOWLEDGEMENTS

First and foremost I would like to thank my adviser, Professor Yan Zhao, for his invaluable guidance, patience, and support. I also thank my committee members, Professors Aaron Sadow, Javier Vela, Ning Fang, and Wenyu Huang, for their suggestions and helpful advice throughout the course of this research. A special thank goes to late Professor Victor S-Y Lin. His memory will be with me always and I will be ever grateful to his assistance.

In addition, I would also like to thank my friends, colleagues, the department faculty and staff for making my time at Iowa State University a wonderful experience.

Last, but certainly not least, are my family members who have been very supportive throughout my Ph.D. I could not have finished this without all of you.

CHAPTER 1.

GENERAL INTRODUCTION

Dissertation Organization

This dissertation is composed of 6 chapters. The first chapter is a review of the application of core-shell organic nanoparticles in catalysis. The second chapter was published in *Organic Letters* in 2012. The interfacially cross-linked reverse micelle (ICRM) was synthesized and studied in selective azidation reaction. The ICRMs contained cross-linked quaternary ammonium groups in the hydrophilic core and thus can extract anions from an aqueous phase. They were shown to catalyze size-selective biphasic reaction between sodium azide and alkyl bromides. Good size selectivity was obtained for alkyl bromides with similar structures. The selectivity was influenced strongly by the size of the water pool and proposed to happen as a result of the "sieving" effect of the alkyl corona. The third chapter was published in *Helvetica Chimica Acta.* in 2012. Palladium salts were extracted into the hydrophilic core of ICRM and formed efficient nanocatalysts in the Heck coupling of a wide range of alkyl acrylates and iodobenzenes in good to excellent yields. The catalytic cores were readily accessible to most reagents. No palladium black was observed even after several reaction cycles. An important benefit of the ICRMs is their good miscibility with common organic molecules, allowing us to perform the Heck reactions without any solvents. The fourth chapter was published in *ACS Catalysis* in 2014. Gold clusters encapsulated within ICRMs were found to be efficient catalyst systems for intermolecular hydroamination of alkynes at room temperature instead of at 100 °C commonly required for gold nanoparticles. Different metal oxides introduced into the micelle core by sol-gel chemistry interacted with

the gold clusters and modulated their catalysis, with silicon oxide being the most effective cocatalyst. The fifth chapter was published in *Journal of the American Chemical Society* in 2014. Extraction of tetrachloroaurate into the hydrophilic core of ICRM produced an artificial "metalloenzyme" with highly unusual catalytic properties. The ICRM pulled the substrate toward the catalytic metal, which converted it efficiently to the product that was rapidly ejected. These features enabled greatly reduced catalyst loading, constant high reaction rate throughout the course of the reaction, lack of hydrolyzed side product, and substrate selectivity unobserved in conventional gold catalysts. The sixth chapter was submitted for publication in 2014. ICRMs readily accommodated anionic gold and palladium metal salts in their ammonium-lined hydrophilic cores and allowed facile control of the metallic composition, as well as the metal oxides in the vicinity of the metals. Deposition onto a solid support (P25 TiO_2) followed by thermal treatment of Pd-Au-containing ICRMs yielded bimetallic nanoclusters with tunable properties. The catalysts allowed efficient oxidation of benzyl alcohol under relatively mild conditions with minimal amounts of oxidant (hydrogen peroxide) in water without any organic solvent. Dr. C. Xiao of Prof. W. Huang research group performed the characterizations of solid support bimetallic nanoparticles.

Literature Reviews

Metal nanoparticles find many applications in both homogeneous and heterogeneous catalysis because their large surface area translates to a high percentage of surface atoms useful for catalysis.[1-5] However, it is challenging to control the active sites and selectivity in the reactions, as metal nanoparticles tend to vary greatly in size, shape and aggregational

state. Since organic structures may help control both the size and the reactivity of the supported metal particles, there have been intensive efforts to identify suitable organic supports to stabilize metal nanoparticles.[6, 7] Organic dendrimers have been shown to afford a range of useful features including tailored solubility, size selectivity, and improved surface deposition.[8, 9] Other reported templates include proteins,[10] polymer microgels,[11] and star polymers.[12]

Organic core-shell particles have a wide range of applications in different fields, such as drug delivery,[13-15] biosensing,[16] chemical separation,[17] biomaterials, [18] and catalysis.[19-24] Since both the core and the shell materials could be modified, core-shell particles can be highly functional and tunable. Current applications of different core/shell nanoparticles are summarized in a review article by Karele et al.[25]

Hybrid of organic and inorganic nanoscale phases can possess properties very different from the bulk phases. The inverted unimolecular micelles were prepared by Meckinh *et al*. Amphiphilic polymers with a polar dendritic core and an apolar shell can form reverse micelles in organic solution. They have also studied other systems based on hyperbranched polymers that are more synthetically accessible. [26] The reduction of a metal salt can indeed proceed in a unimolecular micelle as a 'nanoreactor' to afford a metal particle. The organic polymer shell provides solubility of the metal particle in apolar organic solvents. These metal colloids can be employed as catalysts for hydrogenation and hydroformylation reactions in hydrocarbons as reaction media. Taton *et al* have demonstrated surface-templated self-assembly of copolymers around nanoparticles as a route to well-defined core-shell nanostructures.[27] The characteristics of the component polymer blocks could determine the core-shell architectures in which the dimensions and properties of the nanostructures. In

the absence of ligand chemistry, micelle encapsulation will allow shell functionalization, biomolecular conjugation, and polymer processing to be performed on nano-materials.

Reverse micelles (RMs) are widely utilized as media for catalysis and templates to prepare core-shell inorganic nanomaterials; however, the size and content of inorganic materials were difficult to be controlled because of the fast collision of RMs and exchange of surfactants. We recently reported a simple method to capture RMs by covalent fixation. [28, 29] Unlike dynamic RMs that constantly exchange surfactants and internal contents with one another, the interfacially cross-linked RMs (ICRMs) are stable core-shell organic nanoparticles with tunable properties. The size of their hydrophilic core, the alkyl density on the surface, and internal contents can be changed systematically either during the synthesis or through postmodification. The interfacially cross-linked reverse micelles (ICRMs) turned out as highly unusual properties as templates for metal nanoparticle synthesis. Also, the templates synthesis was fast and straightforward to control.

In this dissertation, I present several applications of these core-shell materials in catalysis. I used ICRMs as size-selective phase transfer catalysts or as organic templates to prepare gold clusters several nanometers in size or clusters consisting of a few atoms. Nanoalloys were simply obtained by combining two metal precursors in the same reaction. Noble metal clusters have shown great promise in their applications in photonics and catalysis.

References

(1) Lee, H.; Habas, S. E.; Kweskin, S.; Butcher, D.; Somorjai, G. A.; Yang, P. *Angew. Chem., Int. Ed.* **2006**, *45*, 7824 − 7828.

(2) Narayanan, R.; El-Sayed, M. A. *J. Am. Chem. Soc.* **2003**, *125*, 8340 − 8347.

(3) Tian, N.; Zhou, Z. Y.; Sun, S. G.; Ding, Y.; Wang, Z. L. *Science* **2007**, **316**, 732 − 735.

(4) Wang, C.; Daimon, H.; Lee, Y.; Kim, J.; Sun, S. *J. Am. Chem. Soc.* **2007**, *129*, 6974 − 6975.

(5) Tsung, C. K.; Kuhn, J. N.; Huang, W.; Aliaga, C.; Hung, L. I.; Somorjai, G. A.; Yang, P. *J. Am. Chem. Soc.* **2009**, *131*, 5816 − 5822.

(6) Negishi, Y.; Takasugi, Y.; Sato, S.; Yao, H.; Kimura, K.; Tsukuda, T. *J. Am. Chem. Soc.* **2004**, *126*, 6518 − 6519.

(7) Schaaff, T. G.; Knight, G.; Shafigullin, M. N.; Borkman, R. F.; Whetten, R. L. *J. Phys. Chem. B* **1998**, *102*, 10643 − 10646.

(8) Zheng, J.; Petty, J. T.; Dickson, R. M. *J. Am. Chem. Soc.* **2003**, *125*, 7780 – 7781.

(9) Tran, M. L.; Zvyagin, A. V.; Plakhotnik, T. *Chem. Commun.* **2006**, 2400 – 2401.

(10) Xie, J.; Zheng, Y.; Ying, J. Y. *J. Am. Chem. Soc.* **2009**, *131*, 888 − 889.

(11) Zhang, J. G.; Xu, S. Q.; Kumacheva, E. *Adv. Mater.* **2005**, *17*, 2336 − 2340.

(12) Shen, Z.; Duan, H. W.; Frey, H. *Adv. Mater.* **2007**, *19*, 349 − 352.

(13) Das, M.; Mardyani, S.; Chan, W. C. E.; Kumacheva, E. *Adv. Mater.* **2006**, *18*, 80 − 83.

(14) Nayak, S.; Lee, H.; Chmielewski, J.; Lyon, L. A. *J. Am. Chem. Soc.* **2004**, *126*, 10258 − 10259.

(15) Soppimath, K. S.; Tan, D. C.-W.; Yang, Y.-Y. *Adv. Mater.* **2005**, *17*, 313 − 323.

(16) Hu, Z.; Chen, Y.; Wang, C.; Zheng, Y.; Li, Y. *Nature* **1998**, *393*, 149 − 152.

(17) Atansov, V. M. Ph.D. Thesis, Johannes Gutenberg-Universitat, Mainz, Germany, 2004.

(18) Bouillot, P.; Vincent, B. *Colloid Polym. Sci.* **2000**, *278*, 74 − 79.

(19) Sahiner, N.; Godbey, W. T.; McPherson, G. L.; John, V. T. *Colloid Polym. Sci*. **2006**, *284*, 1121 − 1129.

(20) Bergbreiter, D. E.; Liu, Y. S.; Osburn, P. L. *Polym. Prepr. (Am. Chem. Soc., Div. Polym. Chem.)* **1998**, *39*, 298.

(21) Biffis, A.; Minati, L. *J. Catal*. **2005**, *236*, 405 − 409.

(22) Biffis, A.; Orlandi, N.; Corain, B. *Adv. Mater.* **2003**, *15*, 1551 − 1555.

(23) Lu, Y.; Mei, Y.; Ballau ff , M.; Dreschler, M. *J. Phys. Chem. B* **2006**, *110*, 3930 − 3937.

(24) Lu, Y.; Mei, Y.; Drechsler, M.; Ballauff, M. *Angew. Chem., Int. Ed.* **2006**, *45*, 813 − 816.

(25) Karele, S.; Gosavi, S. W.; Urban, J.; Kularni, S. K. *Curr. Sci*. **2006**, *91*, 1038 − 1052.

(26) L. Antonietti, C. Aymonier, U. Schlotterbeck, V.M. Garamus, T. Maksimova, W. Richtering, S. Mecking. *Macromolecules* **2005**, *38*, 5914 − 5920.

(27) Kang, Y.; Taton, T. A. *Angew. Chem., Int. Ed*. **2005**, *44*, 409 − 412.

(28) Zhang, S.; Zhao, Y. *ACS Nano* **2011** , *5*, 2637 − 2646.

(29) Zhang, S.; Zhao, Y. *Langmuir* **2012** , *28*, 3606 − 3613.

CHAPTER 2.

SIZE-SELECTIVE PHASE-TRANSFER CATALYSIS WITH INTERFACIALLY CROSS-LINKED REVERSE MICELLES

A paper published in *Organic Letters*, **2012**, *14*, 784-787.

Li-Chen Lee, Yan Zhao

Abstract

Cross-linking of the reverse micelles (RMs) of a triallylammonium surfactant afforded organic nanoparticles with introverted cationic groups. The cross-linked reverse micelles catalyzed size-selective biphasic reaction between sodium azide and alkyl bromides. Size selectivity of up to 9:1 was obtained for alkyl bromides with similar structures. The selectivity was influenced strongly by the size of the water pool and proposed to happen as a result of the "sieving" effect of the alkyl corona.

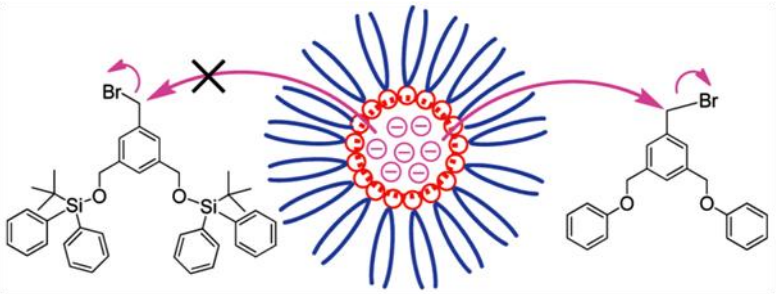

Introduction

Enzymes carry out highly efficient and selective catalysis in active sites tailored for their specific functions. The active site not only has different polarity from the bulk solvent but also size, shape, and functional groups essential to the molecular recognition and catalysis of the enzyme. Chemists have adopted a similar strategy and devoted much effort to

the development of nanoreactors for enzyme-like catalysis.[1] By encapsulating orthoester in an anionic water-soluble nanoreactor, Bergman and Raymond were able to achieve acid catalysis in basic solution.[2] Rebek and co-workers placed a carboxyl group inside a cavitand for the regioselective ring-opening of epoxides.[3] Ramamurthy and Gibb were able to control the photoreactions of ketones using water-soluble molecular capsules.[4] Fujita and colleagues demonstrated that, when packed in a metal organic nanocapsule, unreactive naphthalenes could undergo regio-and stereoselective Diels-Alder reactions.[5] Badjic and co-workers developed cavitand "baskets" with conformational gating to control reactivity.[6] Warmuth employed hemicarcerand to modulate the photochemical and thermal reactions of reactive intermediates such as nitrene and carbene.[7] We recently reported the synthesis of interfacially cross-linked reverse micelles (ICRMs) from cationic surfactants **1** and **2** (Scheme 1).[8] These surfactants form RMs in a chloroform/heptane mixture in the presence of a small amount of water. The nanosized water pool in the middle of the RM concentrates the water-soluble dithiothreitol (DTT) near the headgroups of the surfactants. The high local concentrations of alkene and thiol near the water surfactant interface facilitate the already efficient thiolene radical chain reaction,[9] enabling the dynamic self-assembled RMs to be captured in the original size by covalent bonds.[10]

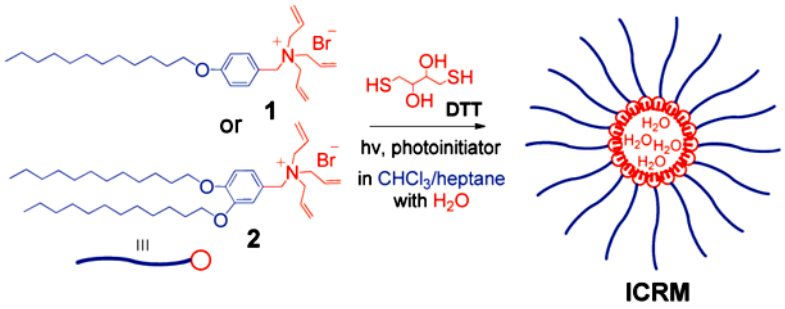

Scheme 1. Preparation of the interfacially cross-linked reverse micelle (ICRM) and the benzyl bromides used in the study

We reasoned that the introverted ammonium groups of the ICRMs should make them potential phase-transfer catalysts (PTCs). Unlike conventional PTCs, however, the ICRMs have the phase-transferred anions located in or near the nanosized internal cavity. Because both the surface alkyl density and the size of the water pool can be tuned easily in our synthesis, we hypothesized that only substrates small enough to access the nucleophilic anions would be able to react. The size selectivity is akin to the "reactive sieving" displayed by tRNA synthetase[11] and synthetic foldamers.[12]

Results and Discussion

To test the hypothesis, we examined the biphasic reaction between sodium azide and alkyl bromides (**3-8**) in a water/chloroform mixture. As shown in Table 1, in the absence of the ICRMs, most bromides were unreactive under our experimental conditions. The small bromides (**3** and **4**) had somewhat higher background reactivity, probably because their higher water-solubility allowed them to enter the azide-containing aqueous phase more easily. In the presence of both ICRMs, the small azides (**3** and **4**) reacted quantitatively. A bulky bromide (**5**), on the other hand, was only converted in 23 and 38% yield, respectively, by the two ICRMs. Because compound **6**, which is similar to **5** electronically but less sterically demanding, gave 80-90% yield under the same conditions, steric interactions were mainly responsible for the selectivity. The ICRMs overall were amazingly "permeable", as bromide **7** with two tert-butyl groups and a dodecyloxy chain gave over 70% yield. A single dodecyloxy chain was even less of a problem; bromide **8** reacted quantitatively in the biphasic reaction.

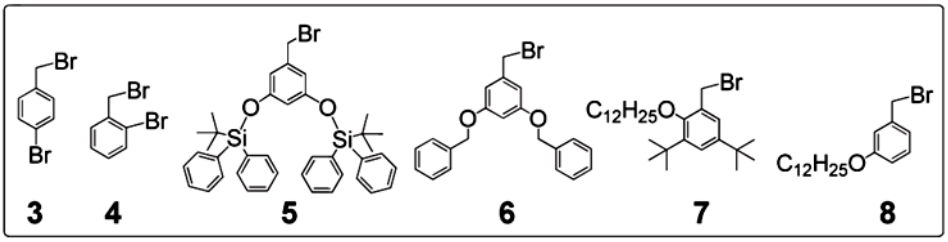

A surprising result in the phase-transfer catalysis is the similar activity of ICRM (**1**) and ICRM (**2**) for the majority of the substrates. Although an alkyl bromide may not have to get into the hydrophilic core of the ICRM to react with the azide, it has to penetrate the alkyl corona to a certain degree to access the nucleophiles in or near the ICRM core. For this reason, one would expect that the double-tailed surfactant should afford ICRMs with a stronger "sieving" effect. Nevertheless, the two ICRM(s) gave essentially indistinguishable results for the majority of the bromides. For the bulkiest bromide (**5**), the ICRM derived from the double-tailed surfactant actually was more active, giving 1.7 times as much product as that by the single-tailed one (Table 1, entry 3).

Table 1. Percent yield of benzyl azide obtained in the biphasic reaction between NaN_3 and various benzyl bromides (RBr)[a]

entry	RBr	yield with ICRM (**1**) (%)	yield with ICRM (**2**) (%)	yield with no ICRM (%)
1	**3**	>95	>95	8
2	**4**	>95	>95	9
3	**5**	23	38	0
4	**6**	82	89	0
5	**7**	74	74	3
6	**8**	>95	>95	2

a. The reactions were carried out with 0.1 mmol of RBr, 0.3 mmol of NaN_3, and 20 mol % of the cross-linkable surfactant in the ICRMs in a mixture of water (1 mL) and $CDCl_3$ (1 mL) under vigorous stirring for 24 h. W_0 = $[H_2O]/[surfactant]$ = 15. The ICRMs were prepared according to a previously published procedure.[8] The reaction yields were determined by ^1H NMR spectroscopy.

The above result may be explained by our previous study of the ICRMs.[8] Normally, one would anticipate an alkyl-covered organic nanoparticle to be fully soluble in non-polar solvents. The ICRMs prepared from the single-tailed surfactant, however, have gaps in between the alkyl chains due to the bulkiness of the headgroup and the geometry of a spherical particle, i.e., more space at the periphery than at the center. These features make ICRM(**1**) extremely prone to interparticle aggregation even in nonpolar solvents such as chloroform. As aggregation occurs, the alkyl chains on the ICRM surface interdigitate, not only promoting the van der Waals interactions among the alkyl chains but also expelling solvent molecules trapped in between the alkyl chains into the bulk ; an entropically favorable process. At the particles get closer, the (long-range) electrostatic interactions from the charged micellar cores also become significant. These interactions are sufficiently strong in ICRM (**1**) that it is completely insoluble in highly nonpolar solvents such as hexane. In our previous study, ICRM (**2**) was found to be free of aggregation because the higher density of the alkyl chains on the surface makes alkyl-interdigitation sterically impossible.

Quite likely, it was the aggregation of ICRM (**1**) that made it much less "permeable" to bromide **5**. Although this PTC has larger gaps in between the surface alkyl groups, the gaps are closed by the alkyl interdigitation.

Conceivably, the larger the gap, the higher is the driving force for the interparticle aggregation and the "tighter" the alkyl shell, making the ICRM of the single-tailed surfactant more discriminating.

The reactions in Table 1 were performed with an excess of azide. To better characterize the size selectivity, we carried out competitive azidation with two bromides

present in the same solution and only 1 equiv of azide. Figure 1 shows the ^{1}H NMR spectra of bromides **5**, **6**, and a 1:1:1 mixture of **5**/**6**/NaN_3 after 24 h at room temperature. According to the integration, while ca. 70% of **6** was converted to the azide, barely 10% of **5** reacted.

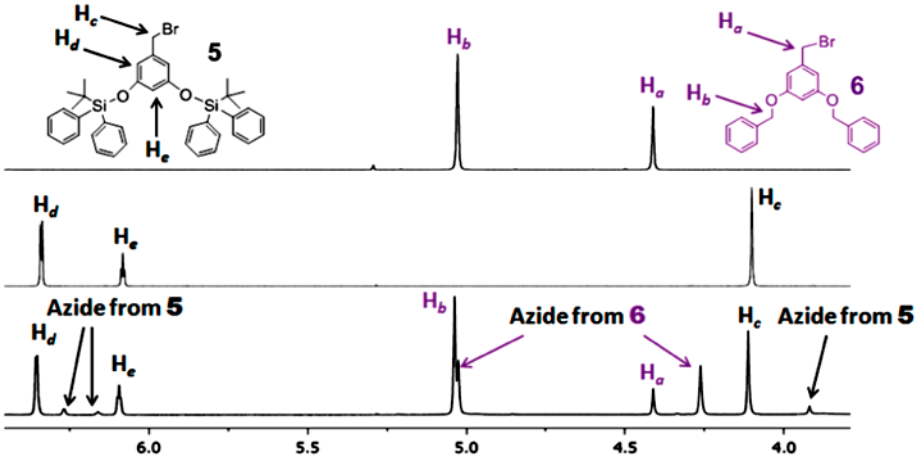

Figure 1. Competitive azidation of **5** and **6** at W_0 = 5. The ^{1}H NMR spectra from top to bottom are for **6**, **5**, and the 1:1:1 mixture of **5**/**6**/NaN_3 at room temperature after 24 h.

The size of the hydrophilic core can be tuned by the amount of water used in the RM formulation.[13] Figure 2a shows the yields in the competitive azidation of bromides **5** and **6**. The ICRMs prepared at W_0 = [H_2O]/[surfactant] = 15 was clearly less selective than those at lower W_0 . Note that it was the bulkier substrate (**5**) that was affected more by the size of the water pool, not the smaller one. As shown by Figure 2b, the highest selectivity for **6**/**5** was ~ 7:1, which was significantly higher than that displayed by conventional phase-transfer catalysts such as CTAB (cetyltrimethylammonium bromide) or TBAB (tetrabutylammonium bromide).

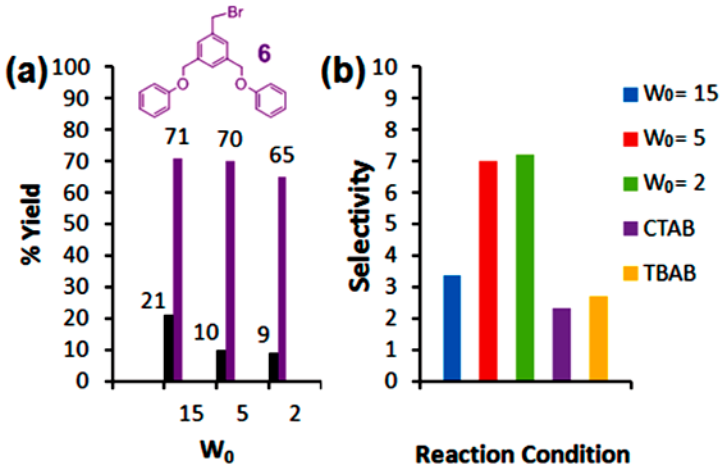

Figure 2. (a) Competitive azidation of **5** and **6** catalyzed by ICRM(**1**) with different W_0 = [H_2O]/[Surfactant]. The figure is color-coded according to the molecules, with the black bars showing the conversion of **5**. The numbers over the bars are the percent yields of the corresponding azides. (b) Comparison of the substrate-selectivity in the competitive azidation under different conditions. CTAB = cetyltrimethylammonium bromide. TBAB = tetrabutyl-ammonium bromide.

Similar competitive azidation was performed for **7**/**5** and **8**/**5** (Figure 3). When another bulky bromide (**7**) was present, **5** became more reactive, affording 14-23% azidation under the same reaction conditions. Meantime, the total yields decreased, ranging from 51-68% for **7**/**5** to 74-92% for **6**/**5** and 79-91% for **8**/**5**. Clearly, bulky substrates in general have difficulty approaching the entrapped azide ions.

For all three pairs, the selectivity was the lowest at the highest W_0. In general, the bromides were more reactive at higher W_0 but the effect was more pronounced for the bulkier bromide (**5**) than for the less bulky ones (**6** and **8**). An increase of W_0 from **5** to **15**, for example, doubled the product yield for **5** while **6** and **8** were hardly affected (Figures 2a and 3b).

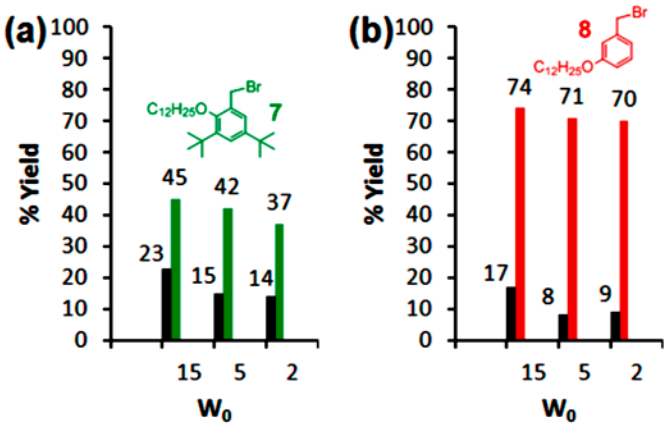

Figure 3. Competitive azidation of (a) **5** and **7** and (b) **5** and **8** catalyzed by ICRM (**1**) with different W_0. The figure is color-coded according to the molecules, with the black bars showing the conversion of **5**.

The ICRMs could be affected by the water/surfactant ratio in several ways. As W_0 decreases, the water pool inside the ICRM becomes smaller, the number of the (cross-linked) surfactants in the ICRM decreases, and the curvature of the nanoparticle becomes larger. The first two factors affect the number of azide ions per ICRM and the last the aggregation of the ICRMs. For an S_N2 reaction in a homogeneous solution, the reaction rate depends on the inherent reactivity of the reactants, their concentrations, and temperature. For a microphase-separated system such as what we have, many factors could affect the reaction rates including the local concentration of the azide ions and how the bromide approaches the azide.

Although the total concentration of azide ions was the same under in all the experiments, the local concentration of azide could be different at different W_0. Because all the bromides in our study became more reactive at higher W_0, it is possible that the local concentration of azide ions might have increased with the W_0. The higher local concentration

of azide, however, could not explain why the sterically most demanding bromide (**5**) always benefited most from the increase in the water-to-surfactant ratio. Since the smaller or slimmer bromides should be better able to react with the entrappedazide (as evident from their higher yields), they should benefit more from an increase in the effective concentration of azide ions if no other factors are involved.

Our current postulation is that the alkyl density outside the ICRM core is the main determining factor for the size selectivity. For the single-tailed ICRM, as discussed earlier, interparticle aggregation "tightens" the alkyl shell and increases the selectivity. A lower W_0 increases the curvature of the ICRM core, widens the gaps in between the alkyl chains, and leads to stronger interparticle aggregation. The alkyl density around micellar core would increase as a result, making it more difficult for the bulky substrate to react. The smaller bromides were not affected significantly by the W_0 possibly because they could penetrate the alkyl corona fairly easily at all W_0.

Conclusions

ICRMs are prepared in a one-step synthesis from the cross-linkable surfactant. Their facile synthesis represents a tremendous benefit when they are compared with other functionalized nanoreactors such as dendrimers. Selectivity up to 9:1 has been achieved for similar bromides such as **5** and **8**. Further derivatization of these organic core shell nanoparticles should provide additional functions and convert them into useful biomimetic nanoreactors.

Experimental section

General Method. All reagents and solvents were of A. C. S. certified grade or higher, and were used as received from commercial suppliers.

Synthesis

Compounds **3** and **4** are commercially available. The syntheses of compounds **5**, **6** and **8** have been reported on the literature.[14, 15] The preparation and characterization of the ICRM(**1**) and ICRM(**2**) were reported previously.[16]

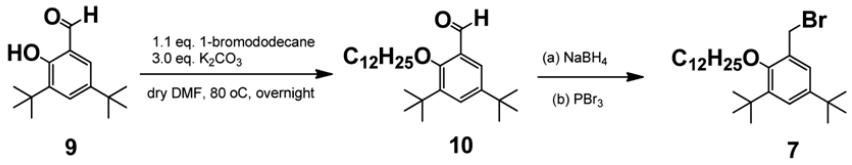

Scheme 2. Synthesis of compound **7**.

3,5-Di-tert-butyl-2-(dodecyloxy)benzaldehyde(10). Potassium carbonate (0.7 g, 2.5 mmol) was added to a solution of 3,5-di-tert-butyl-2-hydroxybenzaldehyde (**9**) (0.2 g, 0.85 mmol) in DMF (5 mL) at room temperature. After the mixture was stirred at 60 °C for 1 h, 1-bromooctane (0.25 mL, 0.94 mmol) was added slowly. The reaction mixture was stirred overnight at 80 °C under N_2, cooled to room temperature, and poured over 200 mL of icy water. The mixture was extracted with EtOAc (3 × 10 mL). The combined organic phase was washed with brine (10 mL), dried over $MgSO_4$, and concentrated in vacuo to give a yellow oil (0.40 g), which was used in the next step without further purification.

3,5-Di-tert-butyl-2-(dodecyloxy)benzyl bromide (7). The yellow oil obtained above was dissolved in anhydrous THF (5 mL) and added dropwise to a stirred suspension of $NaBH_4$ (64 mg, 1.7 mmol) in anhydrous THF (5 mL) at 0 °C. The reaction mixture

was stirred at room temperature overnight and was quenched with water (5 mL). The solid formed was removed by filtration and the filtrate was concentrated in *vacuo*. The residue was dissolved in $CHCl_3$ (10 mL). The resulting solution was washed with brine (3 × 10 mL), dried over anhydrous Mg_2SO_4 , and concentrated in vacuo to give a white solid (0.36 g). The solid was dissolved in $CHCl_3$ (5 mL), to which a solution of PBr_3 (0.16 mL, 1.7 mmol) in $CHCl_3$ (5 mL) was added at 0 °C. The reaction mixture was stirred for 3 h at room temperature and slowly poured into water (ca. 20 mL). The product was extracted with $CHCl_3$ (3 × 10 mL). The combined organic phase was washed with brine (3 × 10 mL), dried over anhydrous $MgSO_4$, concentrated in vacuo, and purified by column chromatography over silica gel with hexane as the eluent to afford a white solid (0.39 g, 90%). ^{1}H NMR (400 MHz, $CDCl_3$, δ): 7.29 (s, 2H), 4.57 (s, 2H), 3.98 (t, J = 6.8 Hz, 2H), 1.864 (m, 2H), 1.54–1.27 (m, 21H), 0.88 (t, J = 6.4 Hz, 3H); ^{13}C-NMR (100 MHz, $CDCl_3$, δ)154.74, 146.23, 142.51, 131.02, 127.28,125.50, 74.60, 35.71, 34.74, 32.18,31.67, 30.43, 29.87, 29.61, 26.24, 22.95, 14.43 ; HRMS(m/z): M^+ calcd for C_{27} H_{47}BrO, 466.2805; found 466.2787.

General procedure for Azidation. The alkyl bromide (0.1 mmol), the appropriate ICRM corresponding to 0.02 mmol of the cross-linked surfactant, and sodium azide (19.5 mg, 0.3 mmol) were dissolved in a mixture of water (1.0 mL) and $CDCl_3$ (1.0 mL). After the biphasic mixture was stirred vigorously at room temperature for 24 h, the organic phase was separated, dried over $MgSO_4$, and analyzed by the ^{1}H NMR spectroscopy to determine the percent yield.

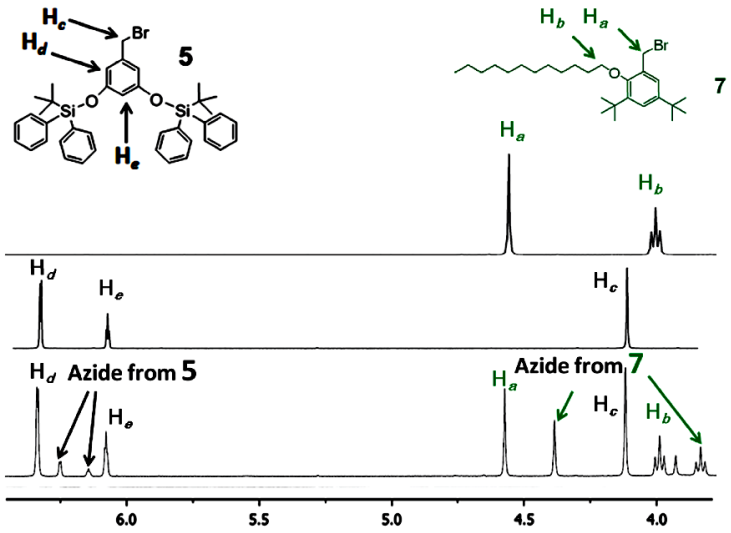

Figure 4. Competitive azidation of **5** and **7** at W_0=5. The ^{1}H NMR spectra from top to bottom are for **7**, **5**, and the 1:1:1 reaction mixture of **5**/**7**/NaN_3 at room temperature after 24 h.

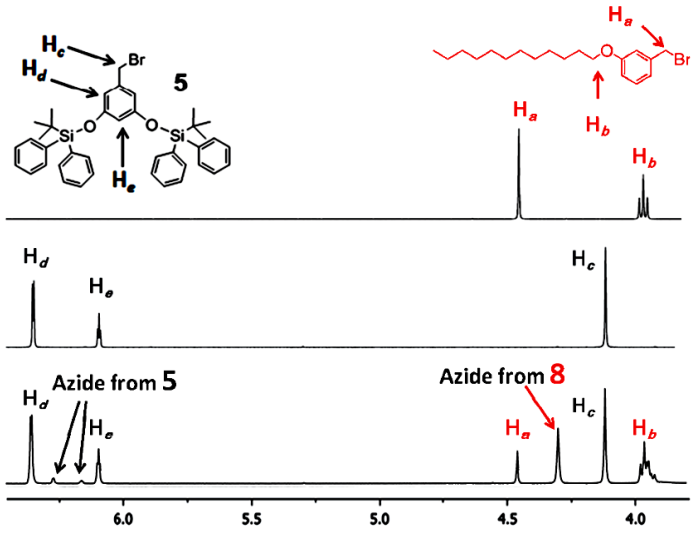

Figure 5. Competitive azidation of 5 and 8 at W_0 =5. The ^{1}H NMR spectra from top to bottom are for **8**, **5**, and the 1:1:1 reaction mixture of 5/8/NaN_3 at room temperature after 24 h.

^{1}H and ^{13}C NMR spectra of key compounds

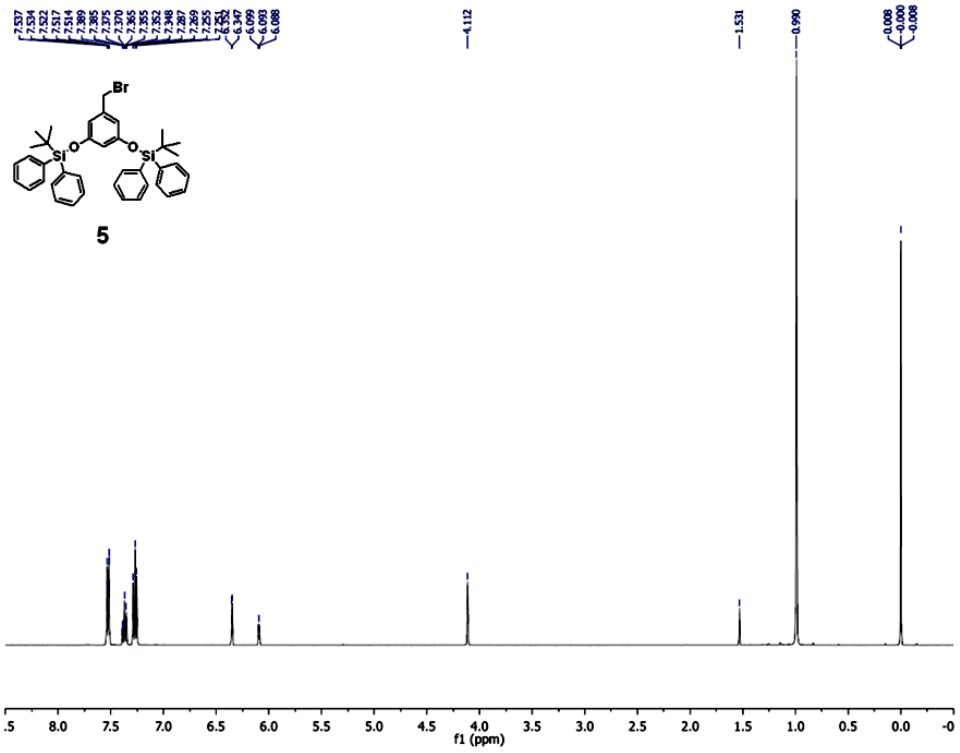

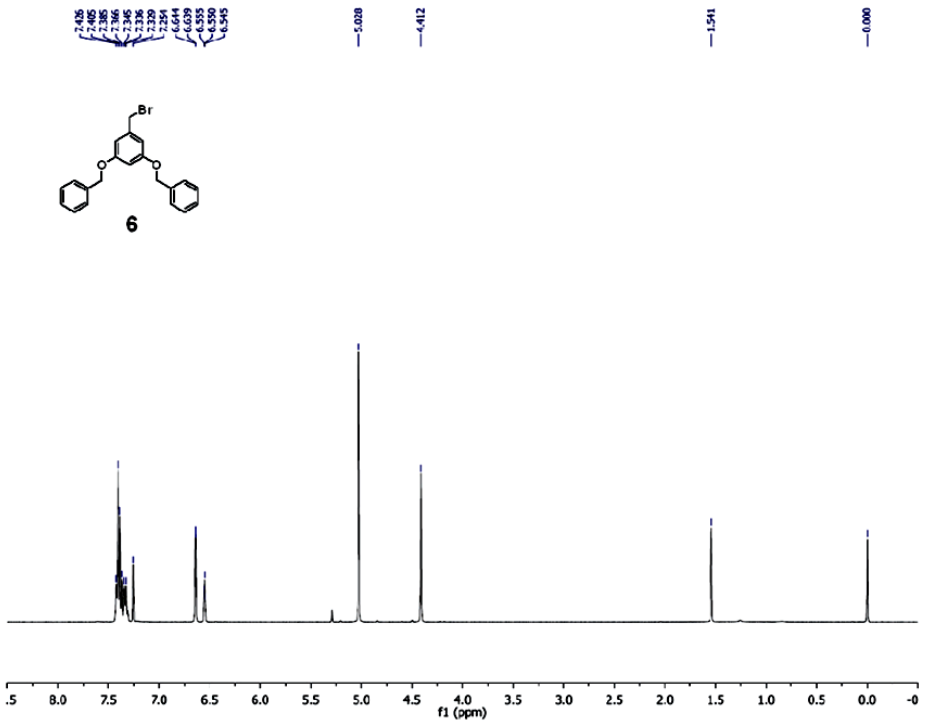

^{1}H and ^{13}C NMR spectra continued

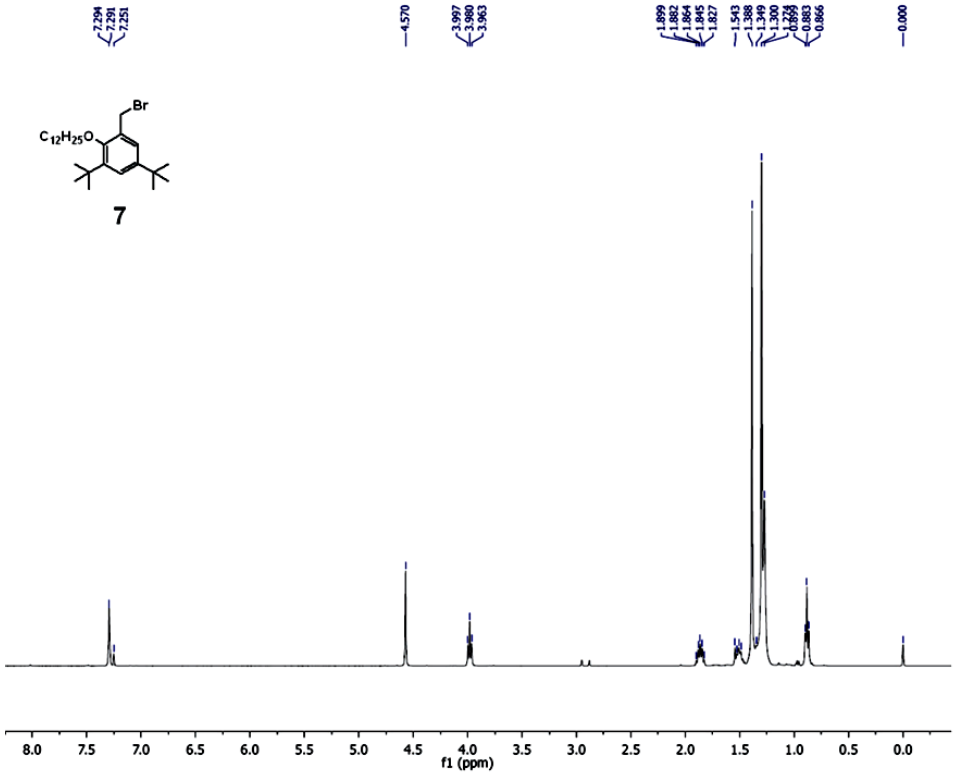

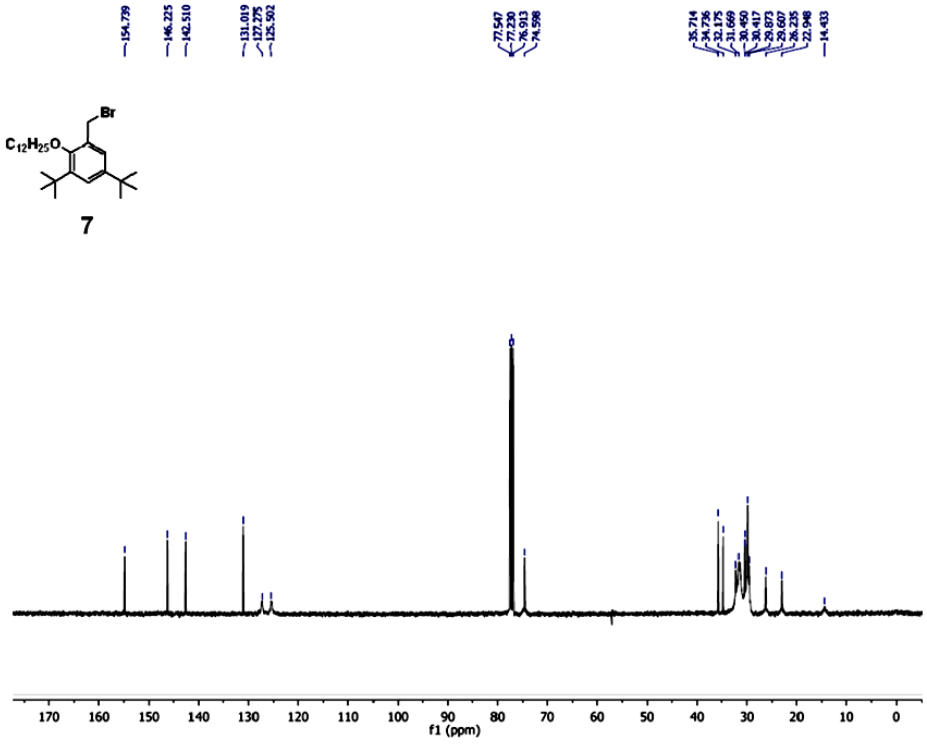

^{1}H and ^{13}C NMR spectra continued

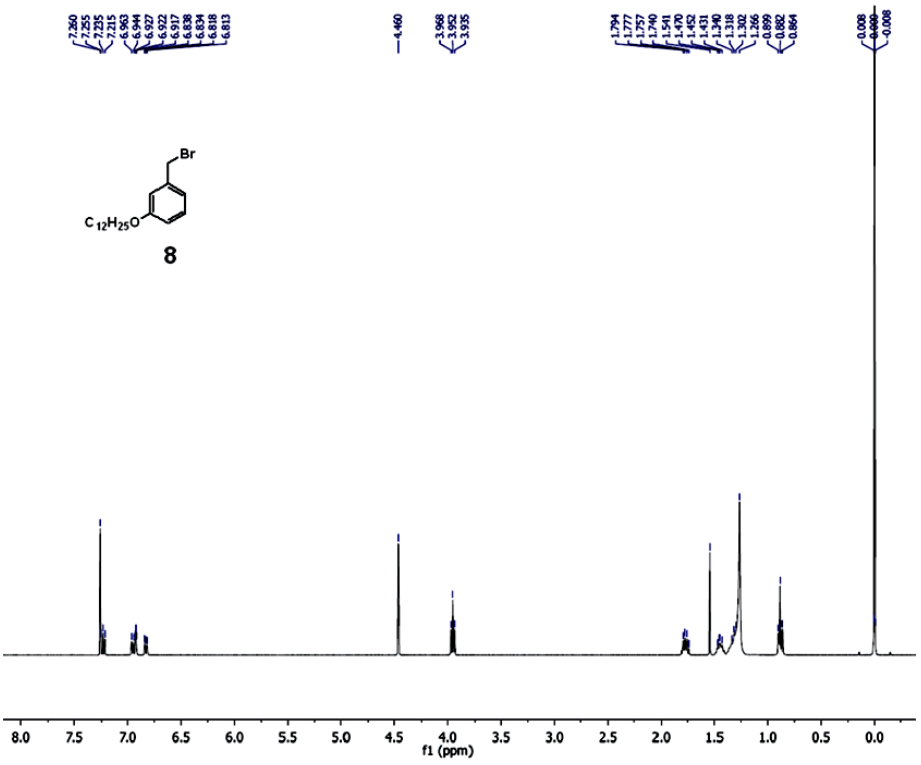

Acknowledgment. We thank the U.S. Department of Energy Office of Basic Energy Sciences (Grant No. DE-SC0002142) for supporting the research.

References

(1) Fiedler, D.; Leung, D. H.; Bergman, R. G.; Raymond, K. N. *Acc. Chem. Res*. **2004**, *38*, 349–358. (b) Vriezema, D. M.; Aragones, M. C.; Elemans, J.; Cornelissen, J.; Rowan, A. E.; Nolte, R. J. M. *Chem. Rev*. **2005**, *105*, 1445–1489. (c) Rebek, J. *Angew. Chem., Int. Ed*. **2005**, *44*, 2068–2078. (d) Yoshizawa, M.; Klosterman, J. K.; Fujita, M. *Angew. Chem., Int. Ed*. **2009**, *48*, 3418–3438.

(2) Pluth, M. D.; Bergman, R. G.; Raymond, K. N. *Science* **2007**, *316*, 85–88.

(3) Shenoy, S. R.; Pinacho Cris ostomo, F. R.; Iwasawa, T.; Rebek, J. *J. Am. Chem. Soc***. 2008**, *130*, 5658–5659.

(4) Gibb, C. L. D.; Sundaresan, A. K.; Ramamurthy, V.; Gibb, B. C. *J. Am. Chem. Soc*. **2008**, *130*, 4069–4080.

(5) Murase, T.; Horiuchi, S.; Fujita, M. *J. Am. Chem. Soc.* **2010**, *132*, 2866–2867.

(6) (a) Wang, B. Y.; Bao, X. G.; Yan, Z. Q.; Maslak, V.; Hadad, C. M.; Badjic, J. D. *J. Am. Chem. Soc.* **2008**, *130*, 15127–15133. (b) Bao, X. G.; Rieth, S.; Stojanovic, S.; Hadad, C. M.; Badjic, J. D. *Angew. Chem., Int. Ed.* **2010**, *49*, 4816–4819. (c) Rieth, S.; Hermann, K.; Wang, B. Y.; Badjic, J. D. *Chem. Soc. Rev.* **2011**, *40*, 1609–1622.

(7) (a) Warmuth, R.; Makowiec, S. J. Am. Chem. Soc. 2007, 129, 1233–1241. (b) Lu, Z.; Moss, R. A.; Sauers, R. R.; Warmuth, R. *Org. Lett.* **2009**, *11*, 3866–3869.

(8) Zhang, S.; Zhao, Y. *ACS Nano* **2011**, *5*, 2637–2646.

(9) (a) Hoyle, C. E.; Lee, T. Y.; Roper, T. *J. Polym. Sci., Part A: Polym. Chem.* **2004**, *42*, 5301–5338. (b) Dondoni, A. *Angew. Chem., Int. Ed.* **2008**, *47*, 8995–8997.

(10) Only one other example was reported to capture RMs in the original size. See: (a) Jung, H. M.; Price, K. E.; McQuade, D. T. *J. Am. Chem. Soc.* **2003**, *125*, 5351–5355. (b) Price, K. E.; McQuade, D. T. *Chem. Commun.* **2005**, 1714–1716.

(11) Fukunaga, R.; Fukai, S.; Ishitani, R.; Nureki, O.; Yokoyama, S. *J. Biol. Chem.* **2004**, *279*, 8396–8402.

(12) (a) Smaldone, R. A.; Moore, J. S. *J. Am. Chem. Soc.* **2007**, *129*, 5444–5450. (b) Smaldone, R. A.; Moore, J. S. *Chem.-Eur. J.* **2008**, *14*, 2650–2657.

(13) Pileni, M. P. *Structure and Reactivity in Reverse Micelles*; Elsevier: Amsterdam, 1989.

(14) Freeman, A.W.; Chrisstoffels, L. A. J.; Frechet, J. M. J. *J. Org. Chem.* **2000**, *65*, 7612.

(15) Lee, S. B.; Choo, H.; Hong, J.-I. *J. Chem. Res.* **1998**, 1290.

(16) Zhang, S.; Zhao, Y. *ACS Nano* **2011**, *5*, 2637-2646.

CHAPTER 3.

INTERFACIALLY CROSS-LINKED REVERSE MICELLES AS SOLUBLE SUPPORT FOR PALLADIUM NANOPARTICLE CATALYSTS

A paper published in *Helvetica Chimica Acta*, **2012**, *95*, 863-871.

Li-Chen Lee, Yan Zhao

Abstract

Reverse micelles (RM) were formed in heptane/$CHCl_3$ with a surfactant carrying the triallylammonium head group. Photo-cross-linking with dithiothreitol captured the RMs and afforded organic, soluble nanoparticles in a one-step reaction. Similar to dendrimers, the cross-linked reverse micelles could encapsulate palladium nanoparticles within their hydrophilic cores and protect them in catalytic reactions. Good to excellent yields were obtained in the Heck coupling of a range of alkyl acrylates and iodobenzenes. The catalytic activity of the palladium nanoparticles was maintained in several repeated runs.

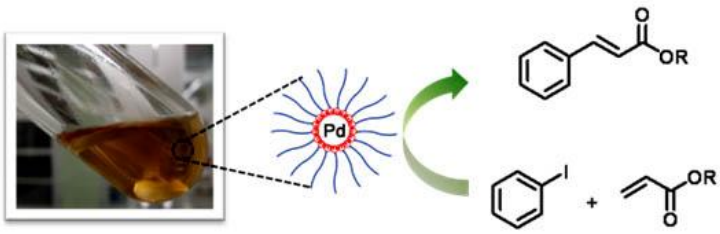

Introduction

By staying in the same phase and being readily accessible to reactants, homogeneous catalysts may achieve very high activity. Their mechanistic understanding and optimization in activity/selectivity are facilitated by the systematic tuning of the ligand environments and

active sites. Heterogeneous catalysts, on the other hand, often distinguish themselves by the ease of product separation, long-term stability, and recyclability. Chemists have long sought to bridge the gap between the two catalyst types and create either heterogenized homogeneous catalysts or soluble versions of heterogeneous catalysts.[1] Metal nanoparticles find many applications in both homogeneous and heterogeneous catalysis because their large surface area translates to a high percentage of surface atoms useful for catalysis.[1-4] When deposited on solid supports, however, metal nanoparticles tend to vary greatly in size, shape, and aggregational state, making it challenging to control the active sites and selectivity in the reactions.[5] For these and other reasons, there have been intensive efforts to identify suitable organic supports to stabilize metal nanoparticles, in the hope that the organic supports may not only create more uniform metal nanoparticles but also provide additional features not available to their inorganic counterparts.[1-4] Organic dendrimers,[6] for example, have been shown to offer a range of useful features including size selectivity[7], tailored solubility,[8, 9]and improved surface deposition.[5]

We recently reported a simple method to capture reverse micelles covalently.[10] Reverse micelles (RMs) are widely used as templates to create inorganic nanoparticles, but the dimension of the final materials templated by RMs rarely correlates directly with the size of the templates.[11, 12] The discrepancy derives from fast collision of RMs, accompanied by coalescence and rapid exchange of the internal contents.[13, 14] Although covalent fixation of RMs should in principle solve these problems, the same problems in the RM-templated synthesis (i.e., fast collision and coalescence) make it difficult to capture the dynamic noncovalent assemblies in the original states.[15, 16] Our covalent capture of RM relies on the three allyl groups in the headgroup of 4-(dodecyloxy)-*N*,*N*,*N*-triprop-2-en-1-ylbenzene

methan-aminium bromide (**1**), which create a high density of alkene functionality at the surfactant-H_2O interface (Scheme 1). When a H_2O -soluble cross-linker, dithiothreitol (*rel*-(2*R*,3*R*)-1,4-dimercaptobutane-2,3-diol; DTT), is used, the efficient thiol-ene radical addition[17-19] is facilitated by the proximity and high local concentration of the thiol and the alkene moieties. The high cross-linking density near the head group is also important to the successful capture of the RMs in the original size.[20, 21]

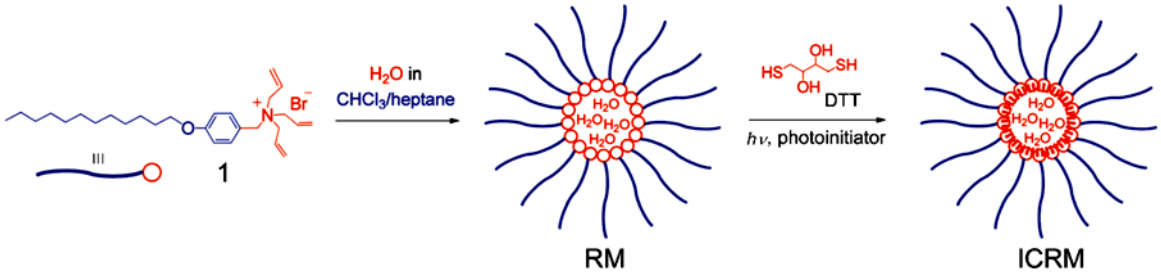

Scheme 1. Preparation of interfacially cross-linked reverse micelles (ICRMs) by the Thiol-Ene addition

In this work, we report our first step in using interfacially cross-linked RMs (ICRMs) as soluble support for Pd nanoparticles and demonstrate their applications in the *Heck* coupling. The *Heck* reaction belongs to an extremely important class of C,C bond-formation reactions.[22, 23] Although phosphine ligands are well-known to stabilize the catalytically active Pd^0 species for Heck reactions, they could be quite expensive. Similar to most homogeneous catalysts, recovery and reuse of catalysts are often impossible.[24] In addition to various inorganic supports,[24, 25] organic polymers,[26, 27] dendrimers,[28-31] lyotropic liquid crystal polymers,[32] block copolymer micelles,[33, 34] and polyhedral oligomeric silsesquioxane[35] have been reported to afford catalytically active Pd nanoparticles for the Heck coupling. With Pd-ICRM composites, we were able to perform efficient *Heck* reactions

between iodoarenes and various acrylates. No palladium black was observed even after several reaction cycles. An important benefit of the ICRMs is their good miscibility with common organic reactants, allowing us to perform the *Heck* reaction without any solvents.

Results and Discussion

ICRMs are unique templates for metal nanoparticles. Our previous work shows that single or bimetallic nanoparticles could be prepared simply by extraction of anionic metal salts such as $AuCl_4^-$ and $PtCl_6^{2-}$ followed by reduction.[10] Because the interior of the ICRMs mainly contains weak ligands such as bromide, thioether, and OH groups, we reasoned that they should serve as useful support for catalytic nanoparticles. Our hypothesis was that the metal particle inside an ICRM would be stabilized mainly by physical protection and thus remains catalytically active. The rationale for the work was that the ICRMs resemble dendrimers in the multivalent surface functionality and a well-defined core-shell structure but are prepared in a one-step synthesis. If they can duplicate the key benefits of dendrimer templates,[6] the ease of synthesis would make them attractive for large-scale applications.

The details of ICRM synthesis were reported previously.[10] Briefly, optically clear RM solutions were prepared in heptane/$CHCl_3$ 2 :1 with $[H_2O]/[1]=5$. $CHCl_3$ was included mainly to help dissolve DTT, the cross-linker, in the nonpolar mixture. Upon photolysis in the presence of 0.5 mol% of the photoinitiator 2,2'-dimethoxy-2-phenyl-acetophenone, an efficient thiol-ene radical reaction[17-19] took place. As reported previously, the ICRMs were characterized by a range of techniques including ^{1}H-NMR spectroscopy, dynamic light scattering (DLS), transmission electron microscopy (TEM), and IR spectroscopy.[10] The ICRMs can interact with one another through van der Waals interactions of the alkyl chains

on the surface. Their cores consist of charged ammonium head groups, and aggregation thus can benefit as well from electrostatic interactions, which could operate over a long distance. A double-tailed surfactant afforded ICRMs free of aggregation. We chose to use the single-tailed surfacant because the lower density of alkyl coronas was possibly beneficial to mass transfer. Although the ICRMs of the single-tailed surfactant **1** aggregated in a solvent-dependent fashion, the aggregates (13 nm in diameter in THF and ca. 200 nm in $CHCl_3$) were completely soluble in solvents with intermediate polarity but insoluble in highly polar (e.g., MeOH or H_2O) or highly nonpolar solvents such as hexane.

Because an ICRM contains numerous ammonium head groups in the interior, it is most suited to extract anionic metal precursors. When a solution of H_2PdCl_4 (10 mM) in H_2O (2 mL) was stirred with a solution of ICRM ([**1**]=10 mM) in $CHCl_3$ (2 mL), the orange phase turned colorless, and the organic layer became orange, indicating the successful extraction of the metal salts into the ICRMs.

Many reducing agents including sodium borohydride,[28, 31, 34] superhydride,[33] and EtOH[26] were reported to convert Pd^{II} to Pd^0. When the above described Pd-containing ICRM solution was heated to reflux in the presence of EtOH (2 mL) for 3 h, a brownish orange solution was obtained. No palladium black or precipitate was formed during the process, indicating that the reduced palladium was protected by the ICRMs. After evaporation of the solvents, the materials obtained could be redissolved in common organic solvents such as $CHCl_3$, CH_2Cl_2 , and THF. The solution was stable over at least a period of several months.

In our catalytic study (*vide infra*), we attempted *Heck* reactions with the Pd-ICRMs without EtOH treatment because Et_3N, the base used in our *Heck* coupling, is known to reduce Pd^{II} during the reaction.[24] Since the materials with and without EtOH reduction

essentially afforded the same yields (*vide infra*), we adopted the simpler preparative procedure without the reduction step.

The UV/VIS spectra of the ICRMs and the Pd-ICRMs with and without EtOH treatment are shown in Figure 1. The ICRMs had a major peak at 280 nm from the aromatic groups of the ICRMs (see structure of **1**). The major absorption of aqueous H_2PdCl_4 solution had a weak broad absorption at 420 nm. After loading with the palladium salt, the Pd-ICRMs had a very broad absorption band that started from 300 nm and tailed off into the VIS region. Overall, the materials obtained with and without EtOH reduction looked very similar. Possibly, some or all of the palladium salts were already reduced after extraction into the ICRMs. According to our previous study, $AuCl_4^-$ extracted into the cores of the ICRMs could reduce spontaneously.[10]

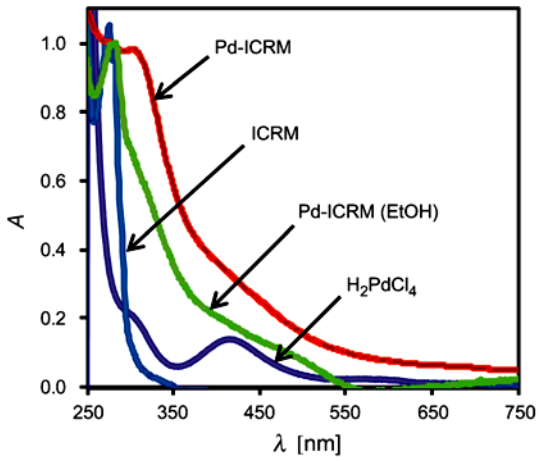

Figure 1. UV/VIS Spectra of $CHCl_3$ solutions of ICRM, Pd-ICRM, and Pd-ICRM after EtOH treatment. [**1**]=0.1 mM; [H_2PdCl_4]=0.1 mM. The spectra were adjusted in intensity for easier comparison.

We also characterized the Pd-ICRM without EtOH treatment by TEM. Figure 2 shows the representative micrograph of an unstained Pd-ICRM sample. The Pd nanoparticles

showed up as dark spots and averaged ca. 2 nm in diameter, in line with the core size of the ICRMs. The ICRMs also seemed to cluster together, possibly due to the aggregation of the alkyl shell.

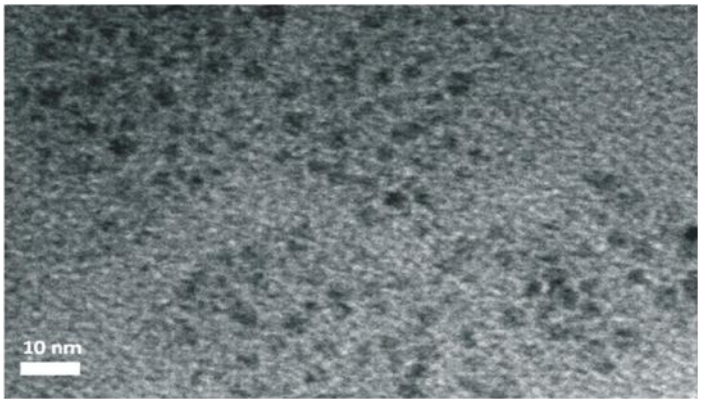

Figure 2. Micrograph of Pd-ICRM without EtOH treatment, obtained by TEM

Initially, we were not sure whether the Pd-ICRMs would be catalytically active and stable during reactions. Soluble palladium clusters are known to form from Pd-nanoparticles and are responsible for catalyzing cross-coupling reactions.[36, 37] Without ligands, Pd^0 is quite unstable and tends to quickly form palladium black and lose activity.[22-24] Therefore, after Pd-atoms depart from the ICRM cores and move into the solution, even if these atoms are initially active, they would aggregate easily and precipitate. To our delight, when a 1 :2 mixture of iodobenzene and butyl acrylate were heated with 1 mol% of Pd-ICRMs and 1.2 equiv. of Et_3N at 80 ^oC, reaction ran cleanly (Figure 3). After 18 h, the limiting reagent, iodobenzene, disappeared completely, and cinnamate was obtained as the only product. No solvent was needed in the reaction, suggesting that the Pd-ICRMs were completely miscible with the reactants, and the Pd metal inside the cores was readily accessible to the reactants. Importantly, the reaction mixture stayed completely clear at the end of the reaction, showing no formation of palladium black.

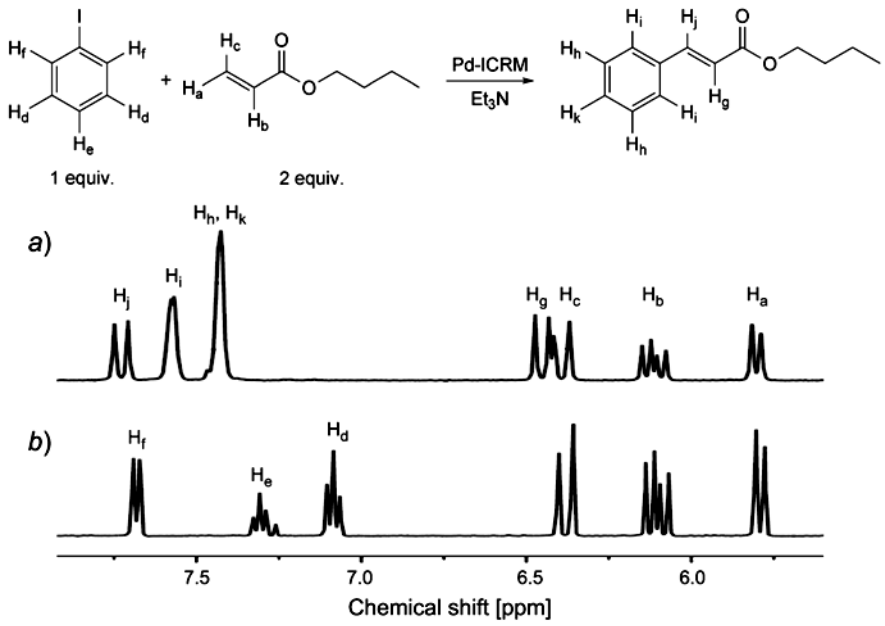

Figure 3. ^{1}H-NMR Spectra of a) the reaction mixture and b) a 1:2 mixture of iodobenzene and butyl acrylate

Table 1 shows the yields of the Heck reaction between various alkyl acrylates and iodobenzene catalyzed by the Pd-ICRMs. As mentioned earlier, EtOH reduction made no difference in the catalysis (Entries 1 and 2), possibly because either Pd^{II} was already reduced during the Pd-ICRM preparation or reduced by the Et_3N added.[24] *t*-Butyl acrylate and the hydrophilic 2-hydroxyethyl acrylate both gave good yields, suggesting that both hydrophobic and hydrophilic substrates are able to penetrate the core of the cross-linked reverse micelles. The 2-ethylhexyl acrylate was less reactive, giving a modest yield of 68% (Entry 5). Initially, we thought the lower yield was caused by the alkyl corona of the ICRM having ”filtering” effects, similar to those found in high-generation dendrimers.[7] To probe the reason for lower yield, we allowed a 1 :1 mixture of butyl acrylate and 2-ethylhexyl acrylate to react with 1

equivalent of iodobenzene and found that both acrylates were converted by similar rates. The lower conversion in 2-ethylhexyl acrylate, therefore, could not come from the filtering effect mentioned above. We also performed some control experiments. Without protection by the ICRMs, H_2PdCl_4 was insoluble in the reaction mixture and gave palladium black immediately. Although complete conversion of the butyl acrylate was also observed, the reaction, after 18 h, produced a large amount of black precipitate (Entry 6). In the absence of Pd, the ICRMs, as expected, were unable to promote the reaction (Entry 7).

Table 1. Pd-ICRM-catalyzed *Heck* reactions between alkyl acrylate and iodobenzene

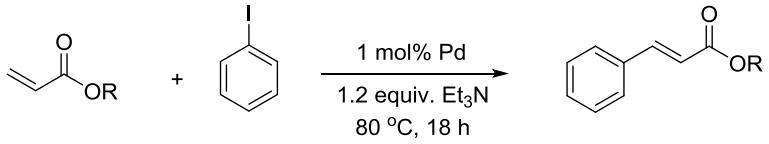

entry	reducing agent	yield (%)[a]
1	Bu	>95
2	Bu	>95[b]
3	*t*-Bu	94
4	2-hydroxyethyl	93
5	2-ethylhexyl	68
6	Bu	>95[c]
7	Bu	0[d]

[a] Yields of the products were determined by ^{1}H-NMR analysis. A yield of > 95% means that the reaction went to completion with no detectable amount of iodobenzene by ^{1}H-NMR spectroscopy. Typical reaction conditions: alkyl acrylate (1.0 mmol), iodobenzene (0.5 mmol), Et_3N (0.6 mmol), and Pd-ICRM (1 mol% of Pd with respect to iodobenzene); at 80 ^{o}C for 18 h. In Entry 4, 1 equiv. of acrylate was used. [b] Pd-ICRM with EtOH reduction was used. [c] H_2PdCl_4 was used. Although the reaction proceeded well, a large amount of palladium black formed during the coupling. [d] ICRMs in the absence of Pd were used.

The catalysis could happen in two possible ways. First, Pd^0 -atoms departed from the stock of palladium in the ICRM cores and moved into the solution to catalyze the reaction. Second, the reactions mostly took place on the surface of the Pd nano-particles, and catalytically active species never moved too far away from the ICRM cores. Our data could not rule out either mechanism. Because H_2PdCl_4 without the ICRMs also catalyzed the *Heck* coupling (Table 1, Entry 6), the ICRMs were not necessary for the reaction to occur. On the other hand, since H_2PdCl_4 without the ICRMs produced a large amount of palladium black, the ICRMs were clearly helpful by stabilizing Pd^0. Most likely, even if Pd^0 migrated from the ICRM cores and went into the solution to catalyze the reaction, the amount of Pd^0 departed must be so small that visible palladium, i.e., large aggregates of Pd^0 could not form. Alternatively, because the high tendency for Pd^0 to agglomerate, the Pd^0 atoms or small clusters that went into the solution may return and merge with the Pd nanoparticles within the ICRM cores. It should be noted that palladium black was never observed in Pd-ICRM-catalyzed reactions even in repeated runs (*vide infra*).

The results so far are quite promising. Despite the simpler synthesis and structure, the Pd-ICRMs gave comparable results as dendrimer-protected Pd nanoparticles in *Heck* coupling.[28-31] The good miscibility of the ICRMs with organic reactants is noteworthy, as solventless conditions are attractive for both economical and environmental points of view. To study the scope of the reaction, we examined the coupling between butyl acrylate and a range of substituted iodobenzenes, with electron-donating and -withdrawing groups at different positions. Most reactions proceeded well and gave good to excellent yields. On average, electron-deficient iodobenzenes gave somewhat higher yields than the electron-rich ones (Table 2).

Table 2. Pd-ICRM-catalyzed *Heck* reactions between butyl acrylate and substituted iodobenzenes

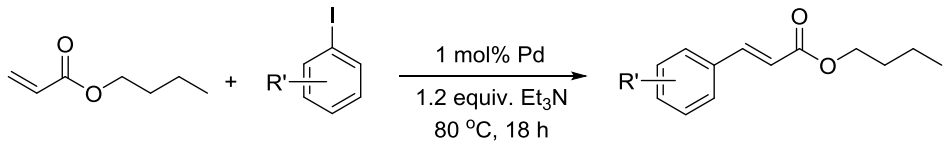

entry	R'	yield (%)[a]
1	H	>95
2	2-Me	82
3	2-MeO	78
4	2-Br	95
5	3-Br	>95
6	3-NO_2	>95
7	2-NO_2 and 5-MeO	88
8	4-Br	89
9	4-NO_2	78
10	4-CN	82
11	4-MeO	84

[a] Yields of the products were determined by 1 H-NMR analysis. A yield of > 95% means that the reaction went to completion with no detectable amount of iodobenzene by ^{1}H-NMR spectroscopy. Typical reaction conditions: alkyl acrylate (1.0 mmol), iodobenzene (0.5 mmol), Et_3N (0.6 mmol), and Pd-ICRM (1 mol-% of Pd with respect to iodobenzenes; at 80 ^{o}C for 18 h.

To test the reusability of the Pd-ICRMs, we took a mixture of butyl acrylate, iodobenzene, Et_3N, and 1 mol% Pd-ICRMs and heated it to 80 ^{o}C. After 18 h, another batch of reactants without the extra equivalent of butyl acrylate was added. ^{1}H-NMR spectroscopy indicated complete conversion of the iodobenzene. The procedure was repeated and, after the third cycle, the yield still remained quite good (85%). It is worth mentioning that the reaction mixture stayed clear throughout the three cycles and showed no formation of palladium black at the end of the third reaction cycle (Figure 4). The lower yield in the third cycle could result

from surface-poisoning of the nanoparticles. Similar results were reported in dendrimer-encapsulated Pd nanoparticles.[28] We also attempted to use the Pd-ICRMs for the *Heck* reactions of bromo- and chloroarenes but found them to be much less reactive. The results most likely derived from limitation of the Pd nanoparticles because similar observations were made in dendrimer-encapsulated Pd nanoparticles.[28-31]

Figure 4. Photograph of the reaction mixture of butyl acrylate and iodobenzene after the third catalytic cycle.

Conclusions

In summary, ICRMs are an excellent soluble support for catalytically active Pd nanoparticles. Good to excellent yields were obtained for the *Heck* coupling of a wide range of alkyl acrylates and iodobenzenes. The catalytic cores were readily accessible to most reagents. Compared to dendrimer templates, the ICRMs are much easier to prepare, via a one-step photo-cross-linking reaction. Extraction of metal salts is straightforward. Although the current systems only extract anionic salts, similar cross-linking concepts can be applied to

anionic and nonionic surfactants, as long as they carry multiple C=C bonds near the head group. The ICRMs are insoluble in polar organic solvents (MeOH or EtOH) and, if needed, can be easily recovered by precipitation. We demonstrated some success in reusing the catalysts for multiple runs. Given the simplicity of the synthesis and easy modification of the surfactants, ICRMs with a wide range of properties should be readily available, making these materials potentially useful in many catalytic applications.

Experimental Section

General. All reagents and solvents were of A.C.S. certified grade or higher, and were used as received from commercial suppliers. The synthesis and characterization of ICRMs were reported previously.[10] UV/VIS Spectra: Cary-50-Bio UV/VIS spectrophotometer; at r.t.. TEM: Philips-CM-30 instrument, operating at 200 kV. ^{1}H-NMR Spectra: Varian-VXR-400 and Bruker DRX-400 spectrometer; δ in ppm rel. to Me_4Si as internal standard, *J* in Hz.

Typical Preparation of Pd-ICRMs. An aq. soln. of H_2PdCl_4 (10 mM) was prepared by adding 0.4 M HCl (6 mL) to $PdCl_2$ (1.2 mmol) in H_2O (114 mL). A portion (2 mL) of H_2PdCl_4 soln. was added to an ICRM soln. in $CHCl_3$ (2 mL, [**1**]=10 mM). After stirring overnight, the mixture was allowed to sit at r.t. The orange org. phase was separated, washed with H_2O (3×), and concentrated to give an orange powder. For the UV/VIS measurement, 0.1 mL of the $CHCl_3$ soln. was diluted by 9.9 mL of $CHCl_3$ so that the concentration of the cross-linked [**1**] was 0.1 mM in the final sample.

Typical Preparation of Pd-ICRMs with EtOH as the Reducing Agents. The Pd-ICRMs were prepared as above. The $CHCl_3$ layer was separated and combined with 2 mL of EtOH. The resulting mixture was heated to reflux under N_2 for 3 h. After the soln. was cooled to r.t., the org. layer was washed with H_2O and concentrated to give a brownish orange powder. For the UV/VIS measurement, 2 mL of $CHCl_3$ was added back to the above-described brownish orange powder. A portion (0.1 mL) of the $CHCl_3$ soln. was diluted by 9.9 mL of $CHCl_3$ so that the concentration of cross-linked **1** was 0.1 mM in the final sample.

TEM Imaging. A soln. of Pd-ICRM in THF ([**1**]=1.0×10^{-4} M) was gently placed on a C-atom-coated copper grid (C-atom type A, 300 mesh). The TEM grid was dried overnight at r.t., and subjected to TEM observation.

Typical Procedure for the Heck Reaction. A small J. Young tube was charged with butyl acrylate (143.4 μL, 1 mmol), iodobenzene (56 μL, 0.5 mmol), Et_3N (83.6 μL, 0.6 mmol), and the Pd-ICRM catalyst ([Pd]/[**1**]=0.005 mmol). The mixture was stirred at 80 ^oC for 18 h with the tube closed. After the mixture was cooled to r.t., $CDCl_3$ was added, and yield of the reaction was determined by ^1H-NMR spectroscopy.

Acknowledgment. We thank the U.S. Department of Energy, Office of Basic Energy Sciences (grant DE-SC0002142), for supporting the research.

References

(1) G. A. Somorjai, A. M. Contreras, M. Montano, R. M. Rioux, *Proc. Natl. Acad. Sci.U.S.A.* **2006**, *103*, 10577.

(2) D. Astruc, in "Nanoparticles and Catalysis", Ed. D. Astruc, Wiley-VCH, Weinheim, Germany, 2008.

(3) A. T. Bell, *Science (Washingtopn, DC, U.S.)* **2003**, *299*, 1688.

(4) C. Burda, X. Chen, R. Narayanan, M. A. El-Sayed, *Chem. Rev.* **2005**, *105*, 1025.

(5) G. A. Somorjai, Y. M. Li, *Top. Catal*. **2010**, *53*, 832.

(6) R. M. Crooks, M. Zhao, L. Sun, V. Chechik, L. K. Yeung, *Acc. Chem. Res*. **2001**, *34*, 181.

(7) M. Zhao, R. M. Crooks, *Angew. Chem., Int. Ed*. **1999**, *38*, 364.

(8) V. Chechik, M. Zhao, R. M. Crooks, *J. Am. Chem. Soc*. **1999**, *121*, 4910.

(9) V. Chechik, R. M. Crooks, *J. Am. Chem. Soc*. **2000**, *122*, 1243.

(10) S. Zhang, Y. Zhao, *ACS Nano* **2011**, *5*, 2637.

(11) J. H. Fendler, "Membrane Mimetic Chemistry", Wiley, New York, 1982.

(12) M. P. Pileni, "Structure and Reactivity in Reverse Micelles", Elsevier, Amsterdam, 1989.

(13) M. P. Pileni, *Langmuir* **1997**, *13*, 3266.

(14) M.-P. Pileni, *Nat. Mater*. **2003**, *2*, 145.

(15) G. Voortmans, A. Verbeeck, C. Jackers, F. C. De Schryver, *Macromolecules* **1988**, *21*, 1977.

(16) G. Voortmans, F. C. De Schryver, in "Polymerization in and of Inverse Micelles", Ed. M. P. Pileni, Elsevier, Amsterdam, 1989.

(17) A. Dondoni, *Angew. Chem., Int. Ed*. **2008**, *47*, 8995.

(18) C. E. Hoyle, T. Y. Lee, T. Roper, *J. Polym. Sci. Pol. Chem*. **2004**, *42*, 5301.

(19) R. K. Iha, K. L. Wooley, A. M. Nystrçm, D. J. Burke, M. J. Kade, C. J. Hawker, *Chem. Rev*. **2009**, *109*, 5620.

(20) H. M. Jung, K. E. Price, D. T. McQuade, *J. Am. Chem. Soc.* **2003**, *125*, 5351.

(21) K. E. Price, D. T. McQuade, *Chem. Commun*. **2005**, 1714.

(22) R. F. Heck, *Acc. Chem. Res*. **1979**, *12*, 146.

(23) R. F. Heck, "Palladium Reagents in Organic Synthesis", Academic Press, London, 1985.

(24) I. P. Beletskaya, A. V. Cheprakov, *Chem. Rev*. **2000**, *100*, 3009.

(25) A. Biffis, M. Zecca, M. Basato, *J. Mol. Catal. A: Chem*. **2001**, *173*, 249.

(26) S. Pathak, M. T. Greci, R. C. Kwong, K. Mercado, G. K. S. Prakash, G. A. Olah, M. E. Thompson, *Chem. Mater*. **2000**, *12*, 1985.

(27) K. Okamoto, R. Akiyama, H. Yoshida, T. Yoshida, S. Kobayashi, *J. Am. Chem. Soc*. **2005**, *127*, 2125.

(28) L. K. Yeung, R. M. Crooks, *Nano Lett*. **2000**, *1*, 14.

(29) E. H. Rahim, F. S. Kamounah, J. Frederiksen, J. B. Christensen, *Nano Lett*. **2001**, *1*, 499.

(30) L. K. Yeung, C. T. Lee Jr., K. P. Johnston, R. M. Crooks, *Chem. Commun*. **2001**, 2290.

(31) K. R. Gopidas, J. K. Whitesell, M. A. Fox, Nano Lett. **2003**, *3*, 1757.

(32) J. H. Ding, D. L. Gin, *Chem. Mater*. **2000**, *12*, 22.

(33) S. Klingelhçfer, W. Heitz, A. Greiner, S. Oestreich, S. Fçrster, M. Antonietti, *J. Am. Chem. Soc*. **1997**, *119*, 10116.

(34) I. P. Beletskaya, A. N. Kashin, A. E. Litvinov, V. S. Tyurin, P. M. Valetsky, G. van Koten, *Organometallics* **2005**, *25*, 154.

(35) C.-H. Lu, F.-C. Chang, *ACS Catal*. **2011**, *1*, 481.

(36) M. T. Reetz, J. G. de Vries, *Chem. Commun*. **2004**, 1559.

(37) D. Astruc, *Inorg. Chem*. **2007**, *46*, 1884.

CHAPTER 4.

ROOM TEMPERATURE HYDROAMINATION OF ALKYNES CATALYZED BY GOLD CLUSTERS IN INTERFACIALLY CROSS-LINKED REVERSE MICELLES

A paper published in *ACS Catalysis*, **2014**, *4*, 688-691.

Li-Chen Lee, Yan Zhao

Abstract

The microenvironment around a catalyst could have profound influence on catalysis. Gold clusters encapsulated within interfacially cross-linked reverse micelles catalyzed hydroamination of alkynes at room temperature instead of at 100 °C commonly required for gold nanoparticles. Different metal oxides introduced into the micelle core by sol-gel chemistry interacted with the gold clusters and modulated their catalysis, with silicon oxide being the most effective cocatalyst.

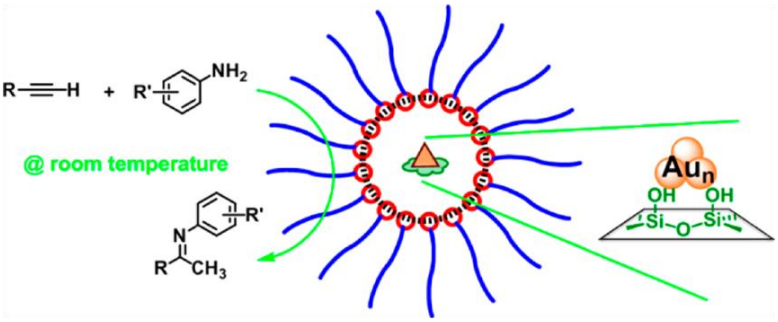

Introduction

Gold nanoparticles (AuNPs) can catalyze a wide range of reactions, including hydrogenation, oxidation, carbon-carbon bond formation, and C-N bond formation.[1] In recent years, gold clusters, consisting of a few to tens of metal atoms, have attracted much research interest.[1, 2] In comparison with their larger AuNP counterparts, metal clusters are

characterized by an even higher surface-to-volume ratio. The abundance of low-coordinated gold atoms on the surface potentially could afford exceptional catalytic activity.[3]

An important reaction catalyzed by gold catalysts is hydroamination of alkyne, an atom-economical reaction to a wide range of fi ne chemicals.[4] Although the intramolecular reaction occurs rather readily, intermolecular hydroamination is quite challenging. The latter could be catalyzed by homogeneous Au(I) or Au(III) complexes in the presence of acid promoters and special ligands.[5] The acid promoters were reported to be replaced by acidic sites when Au(III) complexes were supported on Sn-containing MCM-41; the same report indicated that colloidal gold displayed no catalytic activity under similar conditions.[5e] When deposited on a chitosan-silica support, AuNPs could catalyze intermolecular hydroamination of alkynes, although rather harsh conditions (100 °C for 22 h) were required.[6] Very recently, AuNPs supported on TiO_2 were found to catalyze similar hydroamination at mild temperatures (40 °C) under visible light irradiation.[7]

We recently reported a simple method to capture reverse micelles (RMs) by covalent fixation.[8] Unlike dynamic RMs that constantly exchange surfactants and internal contents with one another, the interfacially cross-linked RMs (ICRMs) are stable core-shell organic nanoparticles with tunable properties. The size of their hydrophilic core,[8] the alkyl density on the surface,[8,9] and internal contents[8,10] can be changed systematically either during the synthesis or through postmodification.

Herein, we report that gold clusters encapsulated within ICRMs are efficient catalysts for hydroamination of alkynes at room temperature. The benefit of Au_n@ICRMs (i.e., gold clusters encapsulated within ICRMs) is that the ICRM serves as both the template

and the support for the catalysts, and the microenvironment around the catalyst could be tuned through introducing metal oxide into the ICRM core.

The synthesis and characterization of ICRMs from cross-linkable surfactants **1** and **2**, as well as the template synthesis of Au_n@ICRMs, have been documented in detail previously.[8,10a] Briefly, the cross-linkable surfactant was dissolved in a heptane/chloroform mixture in the presence of a small amount of water (Scheme 1). The size of the water pool in the middle of the RM was determined by the water/surfactant ratio (i.e., W_0).

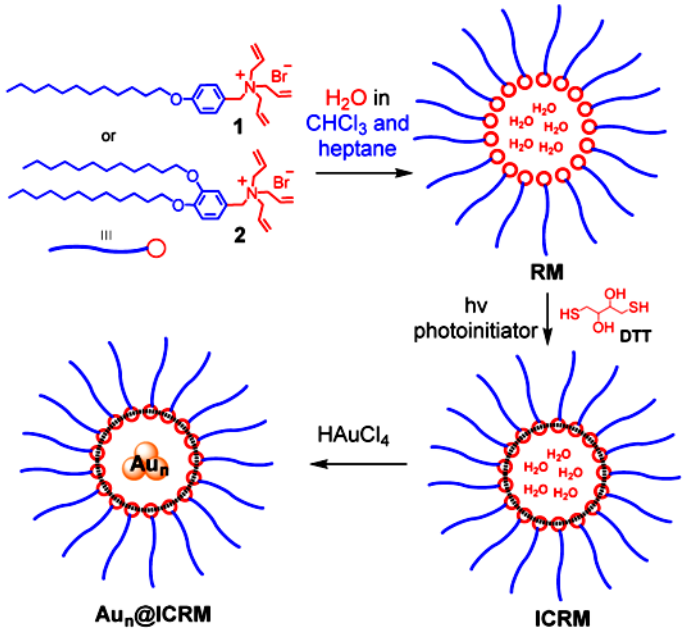

Scheme 1. Preparation of Au_n@ICRM

UV irradiation in the presence of dithiothreitol (DTT, a hydrophilic cross-linker) and 2,2 ′-dimethoxy-2-phenylaceto-phenone (a photoinitiator) for 10-15 min was generally sufficient to cross-link the core of the RM to afford the ICRM. When a solution of the ICRM in chloroform was stirred with an aqueous solution of $HAuCl_4$, the aurate ions exchanged with the bromide in the ICRM core and underwent a two-step elimination-disproportionation

reaction (eqs 1 and 2) to afford gold clusters, with the overall reaction shown in eq 3.[10a] The size of the gold clusters (Au_4 to Au_{23}) was mainly controlled by W_0 and the aurate loading (aurate/surfactant ratio) in the template synthesis. The gold clusters stayed inside the ICRM core probably because the overall Au_n-bromide complex was anionic and needed to stay inside the ICRM to help the ammonium-lined ICRM core to maintain charge neutrality. At high aurate loading (>50%), not all aurate was reduced to Au(0), according to our previous study.[10a]

$$AuX_4^- \leftrightarrows AuX_2^- + X_2 \qquad (1)$$

$$3AuX_2^- \leftrightarrows AuX_4^- + 2Au(0) + 2X^- \qquad (2)$$

$$2AuX_4^- \leftrightarrows 2Au(0) + 3X_2 + 2X^- \qquad (3)$$

Our model hydroamination was between 1-octyne and aniline. To our delight, the alkyl corona of the ICRMs made Au_n@ICRMs freely soluble in the reactants and allowed us to carry out the reaction under solvent-free conditions. The reaction was performed at room temperature for 18 h with 1 mol % Au as the catalyst. Similar to what was reported in the literature,[6] because some of the imine product hydrolyzed under typical reaction conditions, we added water at the end of the reaction to hydrolyze the product into ketone to facilitate determination of the yield by ^{1}H NMR spectroscopy (Figure 1). In the absence of aniline, 1-octyne was recovered under the same reaction conditions; thus, the 2-octanone obtained at the end of the reaction was NOT a result of simple hydration of alkyne catalyzed by gold.

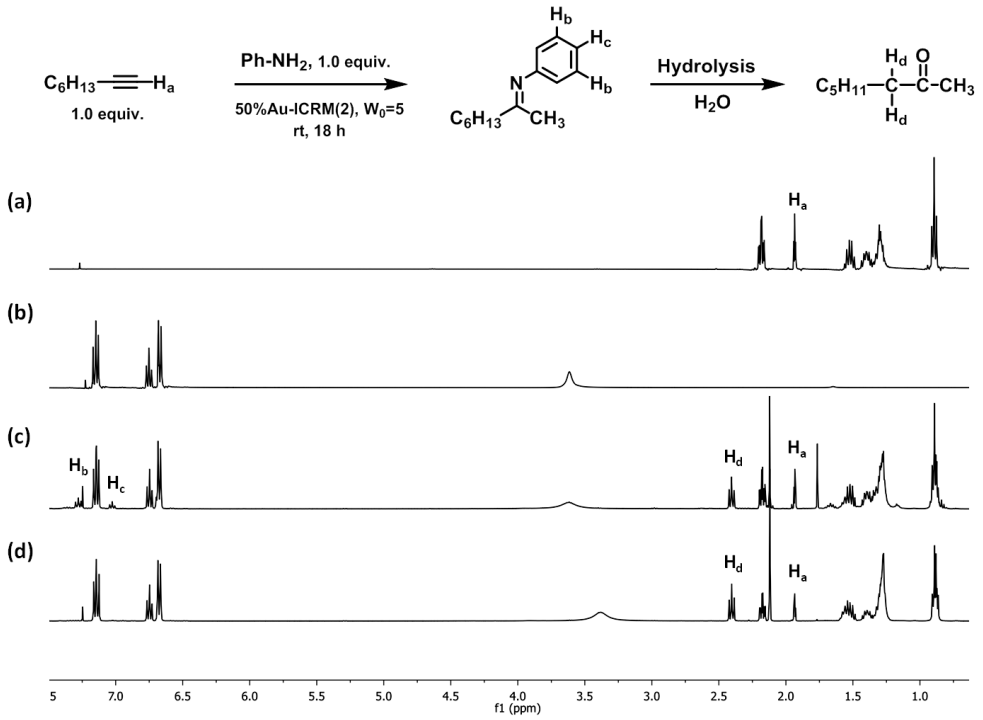

Figure 1. ^{1}H-NMR Spectra of (a) 1-octyne, (b) aniline, (c) the reaction mixture after hydroamination catalyzed by Catalyst was 1 mol % of Au_n@ICRM(2) with W_0 = [H_2O]/[surfactant] = 5, aurate loading = [$HAuCl_4$]/[surfactant] = 50%, and (d) after addition of water to hydrolyze the imine.

Results and Discussion

Table 1 summarizes the reaction yields under different reaction conditions. We compared Au_n@ICRMs prepared with the single-tailed surfactant **1** and the double-tailed **2**. We also varied the amount of aurate loading in the template synthesis and W_0 for the ICRMs.

The most surprising result was the drastically different performance of Au_n@ICRM(**1**) and Au_n@ICRM(**2**). Regardless of the gold loading in template synthesis, Au_n@ICRM(**1**) was completely inactive (Table 1, entries 1-2). In contrast, Au_n@ICRM(**2**) displayed progressively higher activity with increasing gold loading in the core (entries 3-5). In addition to the alkyl density of the ICRM, the water/surfactant ratio was also critical to the

catalysis. The reaction yield decreased at either W_0 = 2 or 20 for Au_n@ICRM(**2**) while the gold loading in the ICRM core and the overall amount of gold were kept the same (entries 6-7). Without gold in the core, the ICRM was completely inactive, as expected (entry 8). Au(III) in the form of $AuCl_4^-$ was not a good catalyst itself, affording only 20% yield under the same reaction conditions, and formed gold black during the reaction (entry 9).

The main difference between ICRM(**1**) and ICRM(**2**) was the alkyl density on the shell. According to our previous study,[8] ICRM(**1**), having a low density of alkyl groups, aggregates easily in many solvents (chloroform, THF, acetone) through alkyl interdigitation. ICRM(**2**), on the other hand, tends to exist as single nanoparticles. The same study also demonstrated that the template synthesis of gold clusters afforded similar results for the two ICRMs.

The enormously different reaction yields in Table 1 indicate that the catalytic hydroamination was sensitive to ICRM aggregation or some other differences between the two Au_n@ICRMs. We noticed that gold black was formed in the case of Au_n@ICRM(**1)** at the end of the reaction. Thus, the gold clusters encapsulated in the single-tailed ICRMs were not only inactive but also unstable under the reaction conditions. The formation of bulk gold suggests that the gold in ICRM(**1**) migrated out of the hydrophilic core in the presence of the reactants. Since both Au_n@ICRMs are stable indefinitely in the absence of the reactants,[8,10a] the gold migration/agglomeration might have been facilitated by the reactants (alkyne and amine) that could complex with gold and was understandably easier when the ICRMs aggregate.

Table 1. Hydroamination of 1-octyne with aniline catalyzed by Au_n@ICRMs[a]

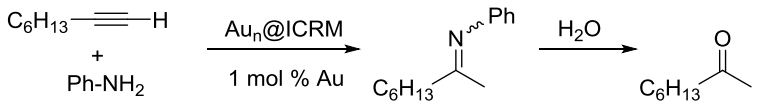

entry	ICRM	Au loading	W_0	yield (%)[b]
1	ICRM(**1**)	30%	5	0[c]
2	ICRM(**1**)	50%	5	0[c]
3	ICRM(**2**)	10%	5	0
4	ICRM(**2**)	30%	5	49
5	ICRM(**2**)	50%	5	69
6	ICRM(**2**)	50%	2	60
7	ICRM(**2**)	50%	20	42
8	ICRM(**2**)	0%	5	0[d]
9	$HAuCl_4$	--	--	20[c]

[a] Reaction conditions: 0.25 mmol of 1-octyne, 0.25 mmol of aniline, and 1 mol% of catalyst at room temperature for 18 h. [b] The reaction yield was determined by ^{1}H NMR spectroscopy. [c] Metal black precipitates formed during the reaction. [d] The reaction was carried out with the ICRMs only without gold in the core.

The size of the gold clusters formed in the template synthesis with ICRMs depends on both the amount of aurate loading and W_0.[8,10a,11] Generally, the size of the gold clusters formed could be determined by the emission wavelengths of the particles. [8,12] Our previous work indicates that, for ICRM(**1**) at W_0 = 5, 10% aurate loading in the template synthesis yielded mostly $Au_{9\text{-}10}$ clusters in the ICRM core, with an emission wavelength of 487 nm.[10a] For Au_n @ICRM(**2**) with W_0 = 5, the aurate/surfactant ratios (10, 30, and 50%) all afforded a main emission peak at 481 nm, indicative of similar gold clusters (Figures 2). (As a reference, Au_8 clusters emit at ~ 450 nm.)[13] Meanwhile, a minor emission peak at 640 nm gradually increased with the increase in the gold loading, corresponding to the formation of Au_{18} clusters.[13] However, because the increase of W_0 from 2 to 5 to 20 progressively enhanced the 640 nm peak (Figure 3) but Au_n@ICRM(**2**) with W_0 = 5 afforded the highest

yield among the three, the catalytic activity of the gold clusters in the ICRMs was not simply a function of the cluster size. Other important parameters must also exist in the system.

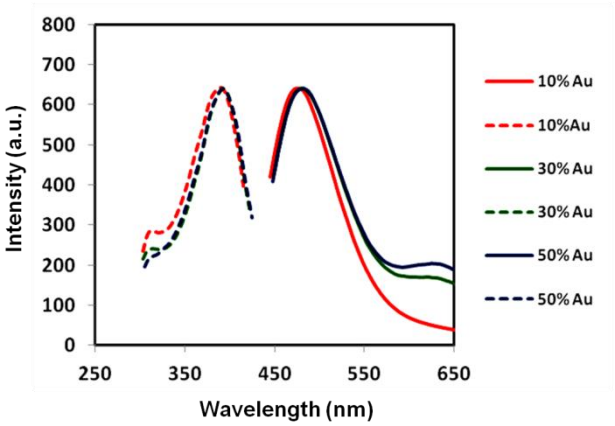

Figure 2. Normalized emission (solid lines) and excitation (dashed lines) spectra of Au_n@ICRM(**2**) with different aurate loading. W_0 = [H_2O]/[surfactant] = 5. [Cross-linked **2** in the ICRM] = 3.0 mM.

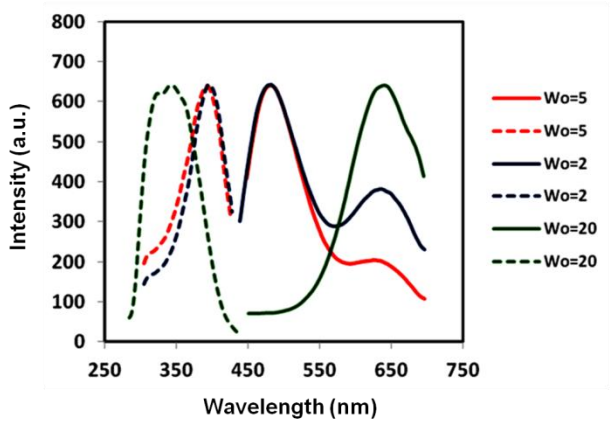

Figure 3. Normalized emission (solid lines) and excitation (dashed lines) spectra of Au_n@ICRM(**2**) with different W_0. [Cross-linked **2** in the ICRM] = 3.0 mM. Aurate loading = [$HAuCl_4$]/[surfactant] = 50%.

In addition to cluster size, we examined the effects of different reduction methods in the template synthesis on the gold-catalyzed hydroamination. Our previous work already

established that Au(III) could undergo the reaction shown in eq 3 when bromide was the counteranion in the ICRM core.[10a] It is known that Au(III) undergoes reduction readily under UV irradiation.[14] In our hands, because Au n @ICRM(**2**) with and without UV treatment gave identical yields in the hydroamination (Table 2, entries 1-2), the gold catalysts should be in the reduced form, Au(0). We were not surprised by the result because aniline could reduce both Au(I) and Au(III).[15]Thus, even if a small amount of oxidized gold was present before the catalysis, it should be reduced by a large excess of aniline during the hydroamination.[16]

Table 2. Hydroamination of 1-octyne with aniline catalyzed by Au_n@ICRM(2)[a]

entry	counteranion	reducing agent	yield (%)
1	Br	none	69
2	Br	UV	69
3	Br	$NaBH_4$	6
4	Cl	none	9
5	Cl	UV	12
6	Cl	$NaBH_4$	<5

[a] Reaction conditions: 0.25 mmol of 1-octyne, 0.25 mmol of aniline, and 1 mol% of catalyst at room temperature for 18 h.

Reduction of the ICRM-encapsulated aurate by sodium borohydride has been shown to produce AuNPs instead of clusters.[8] The AuNPs, with a characteristic brown color from the surface plasmon absorption,[17] gave only 6% yield in the hydroamination, confirming the higher activity of the cluster-based catalysts.

In the literature, bromide has been shown to poison the catalytic properties of, at least, larger AuNPs.[18] Much to our surprise, bromide in the ICRM core turned out critical to the catalysis. As seen from Table 2 (entries 4-6), with chloride as the counteranion, Au_n

@ICRM(**2**) showed poor activity, regardless of the reducing conditions. The stability of gold clusters is affected by both the intrinsic stability of the gold core and the surface ligands.[19] For halides, the binding affinity follows the order of $F^- < Cl^- < Br^- < I^-$.[20] Bromide adsorption on the gold surface is quite strong and has been used to control the growth of gold nanomaterials.[21] Our results suggest that bromide adsorption played important roles in the stability/activity of the gold clusters within ICRM(**2**).

It is well-known that catalytic properties of metal particles on metal oxide support are strongly affected by the support.[22] A unique feature of Au_n@ICRMs is the location of the gold clusters in the hydrophilic core of the cross-linked reverse micelles. Because reverse micelles are frequently used as templates to prepare inorganic nanoparticles,[23] we could easily incorporate metal oxides in the ICRM core to fine-tune the catalysis.

To introduce metal oxide into the ICRM core, we first added 5 equiv of water[24] relative to the surfactant to a chloroform solution of Au_n@ICRM(**2**). A chloroform-soluble, hydrolyzable metal oxide precursor-e.g., $Si(OMe)_4$ for SiO_2, $SnCl_4$ for SnO_2, (*s*-$BuO)_3Al$ for Al_2O_3, and $Ti(OiPr)_4$ for TiO_2-was then added. Since the sol-gel reaction required water that was located in the ICRM core, hydrolysis was expected to occur near/inside the hydrophilic core. In general, hydrolysis was allowed to proceed for 24 h (48 h for SiO_2) at room temperature and shown to be complete by the released alcohol side product monitored by ^{1}H NMR spectroscopy. The metal oxide-modified Au_n@ICRM(**2**) in all cases were completely soluble in chloroform. In contrast, the same sol-gel synthesis in the absence of Au_n@ICRM(**2**) yielded precipitate in the chloroform solution.

Table 3 shows that hydroamination was strongly influenced by the metal oxide around Au_n@ICRM(**2**). In the absence of metal oxide, the hydroamination catalyzed by

Au_n@ICRM(**2**) gave 83% yield (with 2 mol % gold to substrate). SiO_2 was clearly the best cocatalyst, affording quantitative yield under the same conditions, possibly as a result of the acidity of the silica surface. A control experiment, with a physical mixture of Au_n@ICRM(**2**) and SiO_2@ICRM(**2**), showed no improvement in the reaction yield (data not shown). SiO_2 @ICRM(**2**) itself showed no activity (entry 6). Our study also showed that SnO_2 had little impact, and Al_2O_3 lowered the yield slightly. The most unusual result was TiO_2. In heterogeneous catalysis, TiO_2 is known to interact with AuNPs strongly to help the latter ' s deposition and stability.[25] In our hands, the small amount of TiO_2 completely shut down the catalysis. In addition, gold black was observed to form under the reaction conditions, indicating the instability of the gold clusters in the presence of TiO_2.[26] Our Au_n-SiO_2 @ICRM(**2**) generally worked well for terminal alkynes and diferent substituted anilines (Table 4), all at room temperature and without any special ligands. Aliphatic amines did not show any reactivity (data not shown), possibly because of their stronger basicity and complexation with gold.[5]

Table 3. Hydroamination of 1-octyne with aniline catalyzed by Au_n–M_xO_y@ICRM(2)[a]

entry	M_xO_y	yield (%)
1	None	83
2	SiO_2	>95
3	SnO_2	81
4	Al_2O_3	75
5	TiO_2	0[b]
6	SiO_2	0[c]

[a] Reaction conditions: 0.25 mmol of 1-octyne, 0.50 mmol of aniline, and 2 mol % of catalyst at room temperature for 18 h. [b] Metal black precipitates formed during the reaction. [c] The reaction was carried out with SiO_2–ICRM(**2**) without gold in the core

Table 4. Hydroamination of alkynes catalyzed by Au_n–SiO_2@ICRM(2)[a]

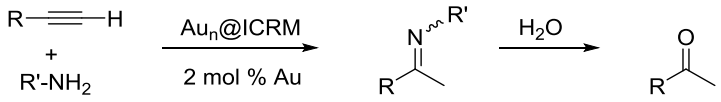

entry	R	R'	yield (%)
1	*n*-C_6H_{13}	Ph	>95
2	*n*-$C_{10}H_{21}$	Ph	94
3	Ph	Ph	86
4	*n*-C_6H_{13}	4-Br-Ph	>95[b]
5	*n*-C_6H_{13}	2-Br, 4-CH_3-Ph	>95
6	*n*-C_6H_{13}	3-Cl-Ph	>95

[a] Reaction conditions: 0.25 mmol of 1-octyne, 0.50 mmol of aniline, and 2 mol% of catalyst at room temperature for 24 h. [b] Chloroform (0.1 mL) was added to the reaction mixture to dissolve 4-bromophenylaniline, which was a solid as room temperature.

Conclusions

In summary, gold clusters encapsulated within ICRMs were found to be efficient catalyst systems for intermolecular hydroamination of alkynes at room temperature. The catalysts displayed a number of unusual features/trends from conventional AuNP catalysts, such as high activity, strong reliance on the bromide surface ligands, and unconventional interactions with locally introduced metal oxides (or their hydrates).[26] Given the large tunability of metal-encapsulated ICRMs,[8-10] these metal cluster - ICRM composites may open new possibilities in catalyst design and applications.

Experimental section

General. All reagents and solvents were of ACS certified grade or higher and were used as received from commercial suppliers. Routine ^{1}H and ^{13}C NMR spectra were recorded on a Varian VXR-400 and Bruker DRX-400 spectrometer. ESI-MS was performed on a

FINNIGAN TSQ700 mass spectrometer. Dynamic light scattering (DLS) was performed on a PD2000DLS^{PLUS} dynamic light scattering detector. Fluorescence spectra were recorded at ambient temperature on a Varian Cary Eclipse fluorescence spectrophotometer. UV-vis spectra were recorded at ambient temperature on a Cary 50 Bio UV-visible spectrophotometer.

Synthesis.

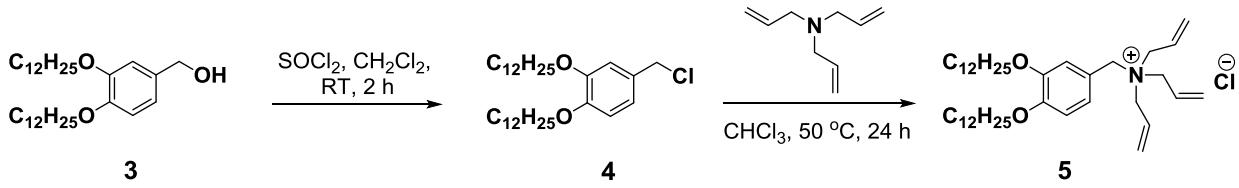

Scheme 2. Synthesis of compound **5**

3,4-Didodecyloxybenzyl chloride (4). A solution of excess $SOCl_2$ in CH_2Cl_2 (1 mL) was added slowly to a stirred solution of 3,4-didodecyloxybenzyl alcohol (**3**)[1] (0.20 g, 0.42 mmol) in CH_2Cl_2 (0.5 mL) at 0 °C. The reaction mixture was stirred for 2 h at room temperature and was concentrated by rotary evaporation to afford a brownish solid. The residue was dissolved in CH_2Cl_2 (5 mL). The organic solution was washed with aqueous $NaHCO_3$ solution until pH ~ 7, dried over anhydrous $MgSO_4$, and concentrated in vacuo to give a brownish wax (0.20 g, 96%). This compound was used directly in the following step without further purification. ^{1}H NMR (400 MHz, $CDCl_3$, δ): 6.91-6.87 (m, 2H), 6.81 (d, *J* = 8.0 Hz ,1H), 4.54 (s, 2H), 4.01-3.97 (dd, *J* = 12.2 Hz and 6.6 Hz, 4H), 1.83-1.78 (m, 4H), 1.45-1.26 (m, 38H), 0.88 (t, *J* = 7.2 Hz, 6H).

3,4-Didodecyloxybenzyltriallylammonium chloride (5). To a solution of 3,4-didodecyloxybenzyl chloride (**4**) (0.20 g, 0.4 mmol) in chloroform (2 mL) was added a solution of triallyammine (0.35 mL, 2.0 mmol) in chloroform (1 mL) at room temperature. The solution was then heated with stirring at 50 °C for 24 h. Water (2 mL) was added, followed by chloroform (5 mL). The organic layer was washed with 1M HCl aqueous solution (2 × 1 mL), brine (2 × 5 mL), dried over anhydrous $MgSO_4$, and concentrated *in vacuo*. The residue was purified by column chromatography over silica gel with CH_2Cl_2/MeOH = 20/1 to 10/1 as the eluents to give a white powder (0.21 g, 82%). ^{1}H NMR (400 MHz, CDCl 3 , δ): 7.31 (s, 1H), 7.15 (d, *J* = 8.4 Hz, 1H), 6.88 (d, *J* = 8.4 Hz, 1H), 6.07–5.96 (m, 3H), 5.76–5.66 (m, 6H), 4.91 (s, 2H), 4.19 (d, *J* = 7.2 Hz, 6H), 4.06-3.99 (m, 4H), 1.85–1.79 (m, 4H), 1.49–1.26 (m, 36H), 0.90 (t, *J* = 6.8 Hz, 6H). ^{13}C NMR (100 MHz, $CDCl_3$, δ); 150.99, 149.14, 128.33, 126.16, 125.22, 119.14, 118.03, 113.02,69.67, 68.97, 64.06, 61.65, 31.88, 29.68, 29.66, 29.61, 29.60, 29.48, 29.41, 29.32, 29.25, 29.12, 26.07, 26.00, 22.64, 14.09; ESI-MS (m/z): $[M - Cl]^+$ calcd for $C_{40}H_{70}NO_2^+$ 596.5401, found 596.5384.

General Preparation of Au_n-M_xO_y@ICRM(2). The preparation and characterization of Au_n@ICRMs were reported in detail previously.[1-2] To introduce metal oxide into the ICRM core, 20 mg of Au_n@ICRM(2) with [aurate]/[surfactant] = 50% and W_0 = 5 was first dissolved in 2 mL of $CHCl_3$. For easily hydrolyzed metal oxide precursors such as $SnCl_4$, (*s*-$BuO)_3Al$, and $Ti(OiPr)_4$, 2.7 μL of water was added. For $Si(OMe)_4$, 2.7 μL of 6M HCl aqueous solution was added to facilitate the hydrolysis of the metal oxide precursor. The mixture was stirred vigorously until the water droplets disappeared into the chloroform

solution. The appropriate metal oxide precursor ([metal oxide precursor]/[**2**] = 2.0) was then added to the solution with a Hamilton microsyringe. The mixture was stirred at room temperature for 24 h (48 h for $Si(OMe)_4$) to allow the hydrolysis to complete. The organic solvent was removed by rotary evaporation and the residue was washed with acetone to afford a yellowish power (ca. 20 mg) after drying under vacuum. Hydrolysis of the metal oxide precursors was monitored by ^{1}H NMR spectroscopy. The size of ICRMs was determined by dynamic light scattering.[1] The size of the gold clusters formed was generally characterized by UV-vis and fluorescence spectroscopy.[27, 28] For the optimized catalyst, i.e., Au_n–SiO_2@ICRM(2), the silica in the core of the ICRM was additionally characterized by solid-state ^{29}Si NMR spectroscopy.

General Procedure for Hydroamination. 1-Octyne (37 µL, 0.25 mmol), aniline (45 µL, 0.50 mmol), and the appropriate amount of the Au_n@ICRMs were stirred at room temperature for 18 h. Water (1 mL) was added to the stirred solution to hydrolyze the imine intermediate into the ketone. $CDCl_3$ (1 mL) was added to the mixture to extract the product (2-octanone) and the yield of the product was determined by ^{1}H NMR spectroscopy.

Characterization

Emission and Excitation Spectra

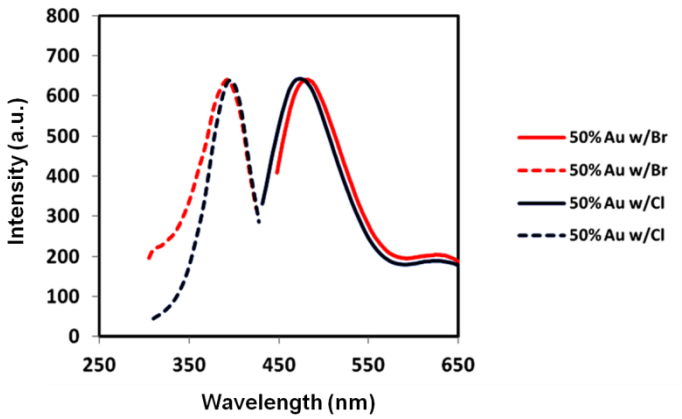

Figure 4. Normalized emission (solid lines) and excitation (dashed lines) spectra of Au_n@ICRM(2) with different counteranion in the core. W_0 = [H_2O]/[surfactant] = 5. [Cross-linked **2** in the ICRM] = 3.0 mM. Aurate loading = [$HAuCl_4$]/[surfactant] = 50%.

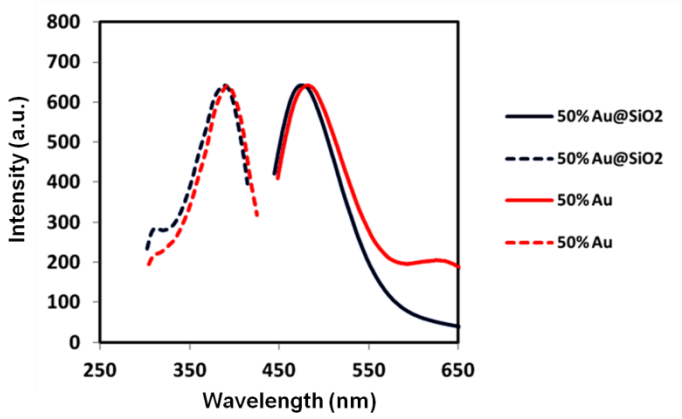

Figure 5. Normalized emission (solid lines) and excitation (dashed lines) spectra of Au_n@ICRM(2) with and without SiO_2 in the core. W_0 = [H_2O]/[surfactant] = 5. [Cross-linked **2** in the ICRM] = 3.0 mM. Aurate loading = [$HAuCl_4$]/[surfactant] = 50%.

UV-vis Absorption spectra

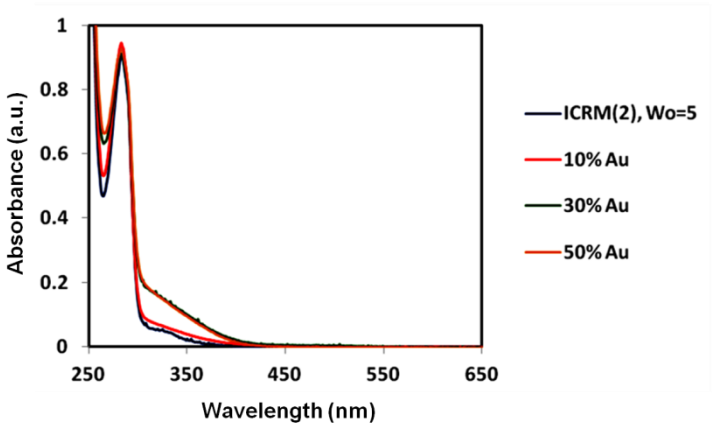

Figure 6. Absorption spectra of Au_n@ICRM(2) with different aurate loading. W_0 = [H_2O]/[surfactant] = 5. [Cross-linked **2** in the ICRM] = 0.2 mM. The absence of surface plasmon band indicates no formation of gold nanoparticles.

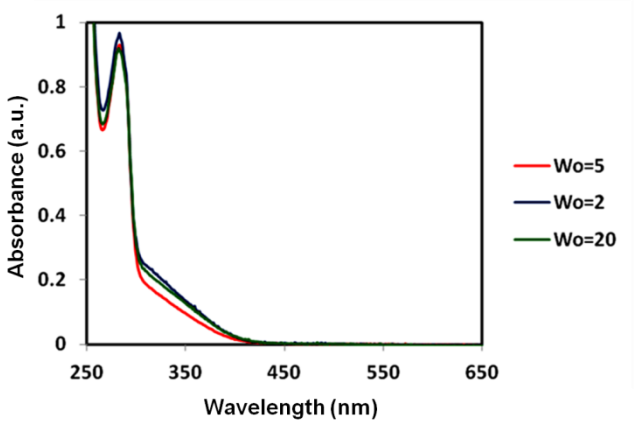

Figure 7. Absorption spectra of Au_n@ICRM(2) with different W_0. [Cross-linked **2** in the ICRM] = 0.2 mM. Aurate loading = [$HAuCl_4$]/[surfactant] = 50%. The absence of surface plasmon band indicates no formation of gold nanoparticles.

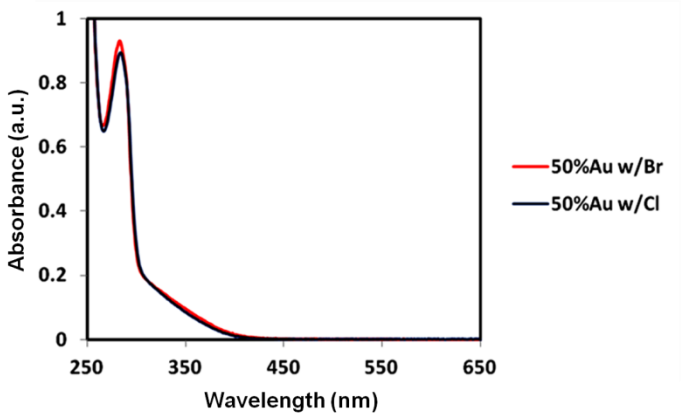

Figure 8. Absorption spectra of Au_n@ICRM(2) with different counteranion in the core. [Cross-linked **2** in the ICRM] = 0.2 mM. Aurate loading = [$HAuCl_4$]/[surfactant] = 50%. The absence of surface plasmon band indicates no formation of gold nanoparticles.

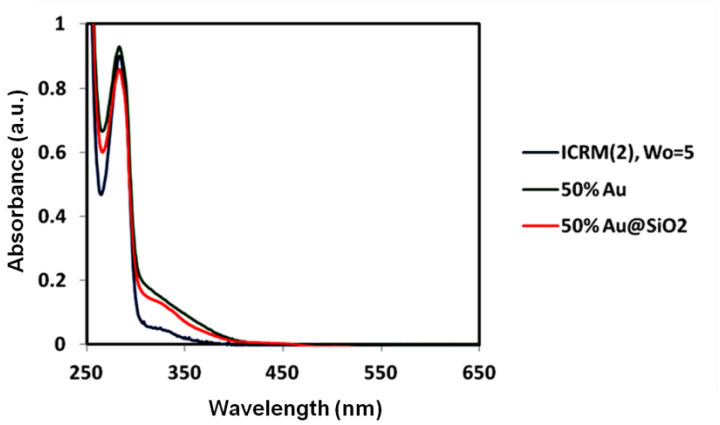

Figure 9. Absorption spectra of Au_n@ICRM(2) with and without SiO_2 in the core. [Cross-linked **2** in the ICRM] = 0.2 mM. Aurate loading = [$HAuCl_4$]/[surfactant] = 50%. The absence of surface plasmon band indicates no formation of gold nanoparticles.

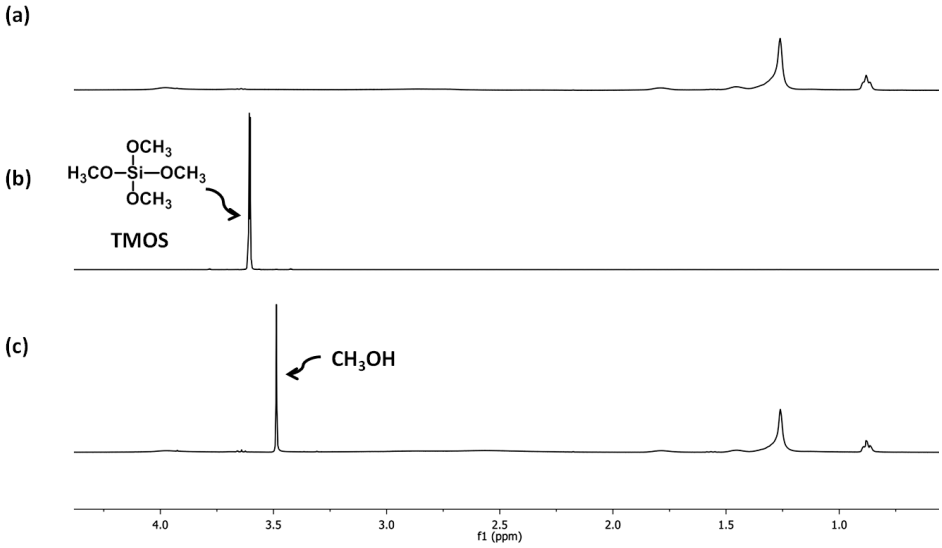

Figure 10. ^{1}H-NMR Spectra of (a) ICRM(2) with W_0=5, (b) tetramethoxysilane (TMOS), and (c) Au-SiO_2@ICRM(2) at the end of hydrolysis showing methanol as the by-product of the sol–gel chemistry.

^{29}Si-MAS NMR Spectra

T^2 and T^3: -50~-70 ppm $(\equiv SiO)_2Si(OH)R$, $(\equiv SiO)_3SiR$

Q^2, $Q^3$and Q^4 :-100 ppm, $(\equiv SiO)_2Si(OH)_2$ $(\equiv SiO)_3Si(OH)$ 、$(\equiv SiO)_4Si$

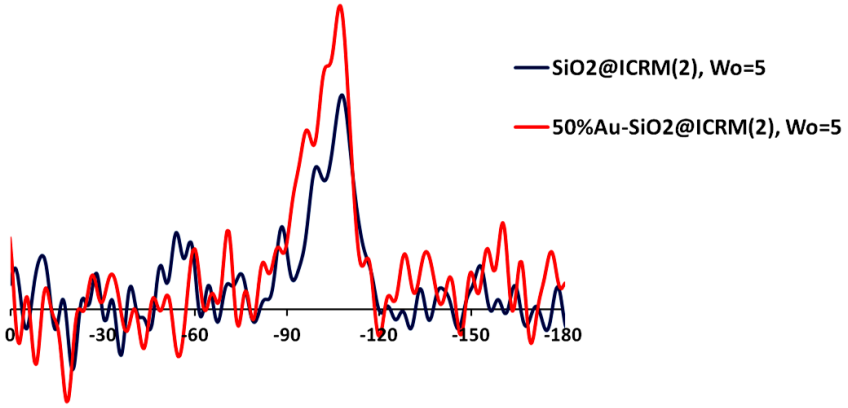

Figure 11. ^{29}Si-MAS NMR Spectra of SiO_2@ICRM(2) and Au_n–SiO_2@ICRM(2). W_0 = $[H_2O]$/[surfactant] = 5. Aurate loading in Au_n–SiO_2@ICRM(2) = $[HAuCl_4]$/[surfactant] = 50%.

(a)

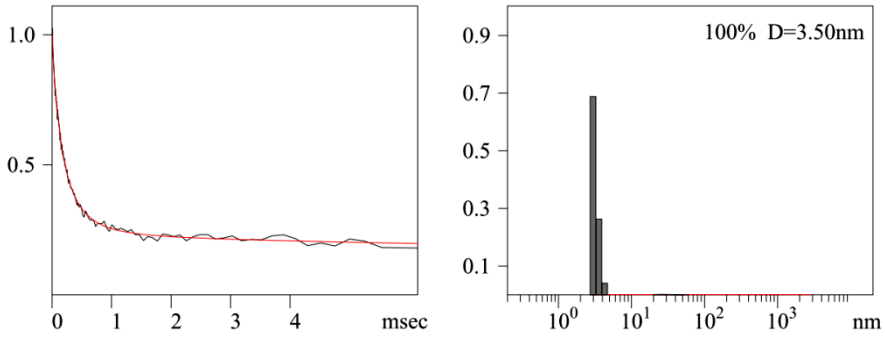

(b)

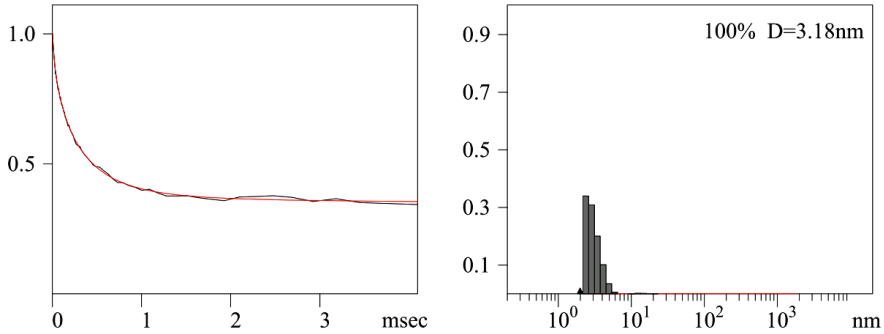

Figure 12. Correlation curves and distribution of hydrodynamic diameters of (a) Au_n@ICRM(2) and (b) Au_n–SiO_2@ICRM(2) in chloroform. W_0 = [H_2O]/[surfactant] = 5. Aurate loading = [$HAuCl_4$]/[surfactant] = 50%.

^{1}H and ^{13}C NMR spectra of key compounds

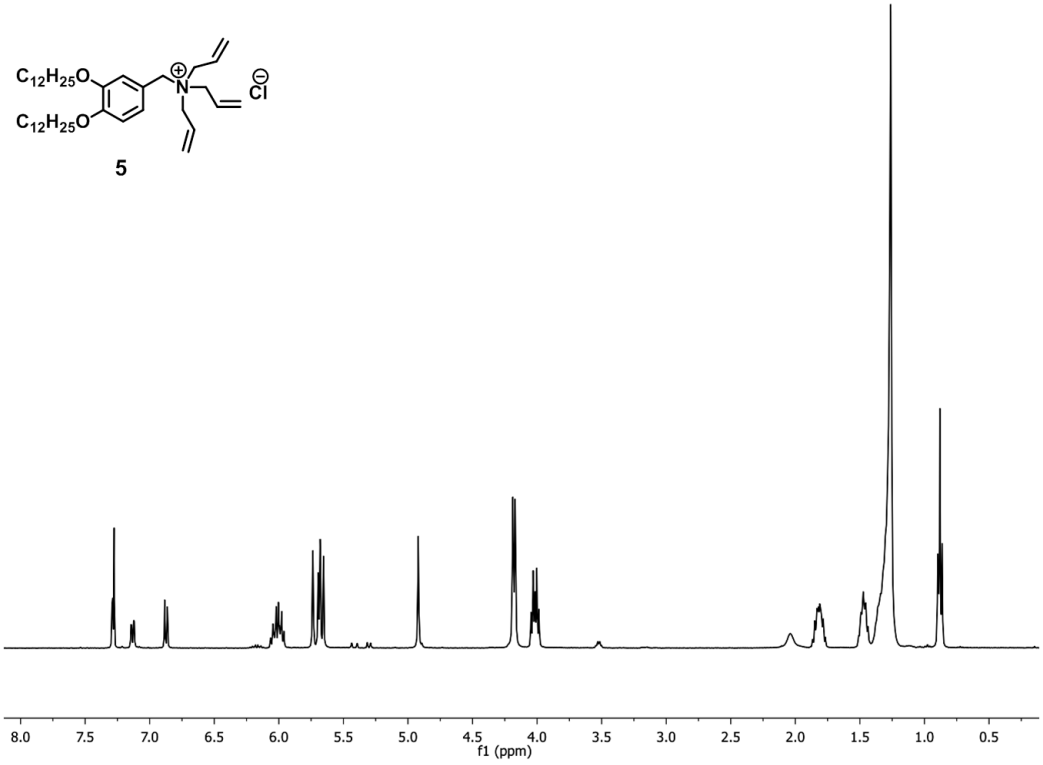

5

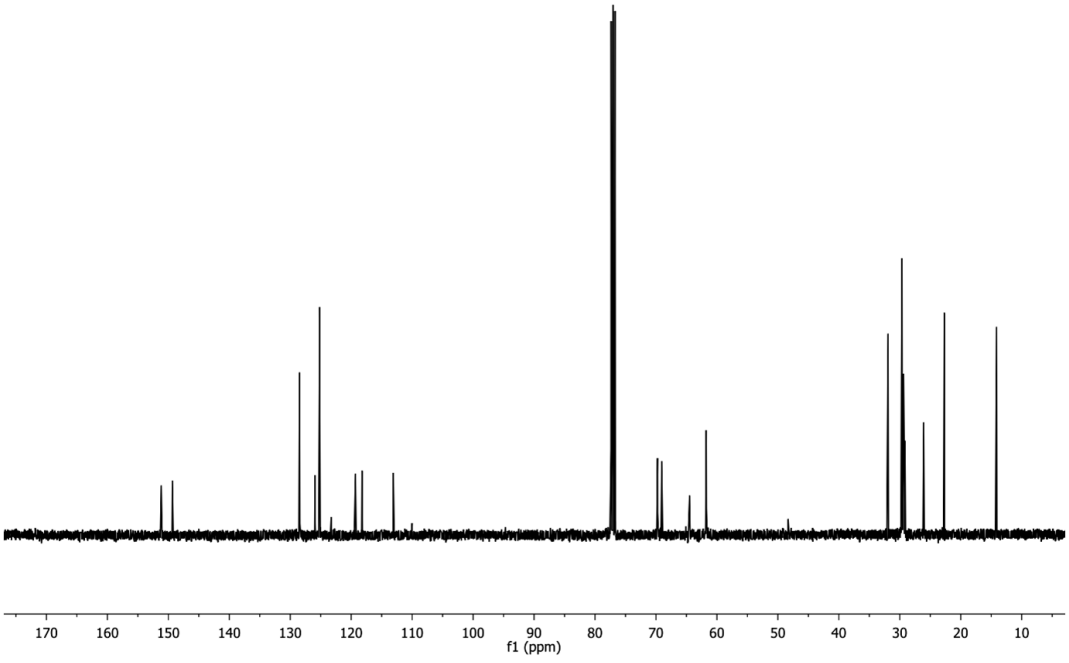

Acknowledgment. We thank the U.S. Department of Energy, Office of Basic Energy Sciences (Grant DE-SC0002142) for supporting the research. We thank Dr. Takeshi Kobayashi and Dr. Marek Pruski at the Ames Laboratory for acquiring the solid-state ^{29}Si NMR spectra of Au_n-SiO_2@ICRM(**2**).

References

(1) (a) Haruta, M. *Chem. Rec.* **2003**, *3*, 75. (b) Hashmi, A. S. K.; Hutchings, G. J. *Angew. Chem. Int. Ed.* **2006**, *45*, 7896. (c) Corma, A.; Garcia, H. *Chem. Soc. Rev.* **2008**, *37*, 2096. (d) Della Pina, C.; Falletta, E.; Prati, L.; Rossi, M. *Chem. Soc. Rev.* **2008**, *37*, 2077. (e) Della Pina, C.; Falletta, E.; Rossi, M. *Chem. Soc. Rev.* **2012**, *41*, 350. (f) Zhang, Y.; Cui, X. J.; Shi, F.; Deng, Y. Q. *Chem. Rev.* **2012**, *112*, 2467.

(2) (a) Sanchez, A.; Abbet, S.; Heiz, U.; Schneider, W. D.; Häkkinen, H.; Barnett, R. N.; Landman, U. *J. Phys. Chem. A* **1999**, *103*, 9573. (b) Lopez, N.; Janssens, T. V. W.; Clausen, B. S.; Xu, Y.; Mavrikakis, M.; Bligaard, T.; Nørskov, J. K. *J. Catal.* **2004**, *223*, 232. (c) Tsunoyama, H.; Sakurai, H.; Negishi, Y.; Tsukuda, T. *J. Am. Chem. Soc.* **2005**, *127*, 9374. (d) Herzing, A. A.; Kiely, C. J.; Carley, A. F.; Landon, P.; Hutchings, G. J. *Science* **2008**, *321*, 1331. (e) Liu, Y. M.; Tsunoyama, H.; Akita, T.; Xie, S. H.; Tsukuda, T. *ACS Catalysis* **2011**, *1*, 2.

(3) (a) Oliver-Meseguer, J.; Cabrero-Antonino, J. R.; Domínguez, I.; Leyva-Pérez, A.; Corma, A. *Science* **2012**, *338*, 1452. (b) Lee, S.; Molina, L. M.; López, M. J.; Alonso, J. A.; Hammer, B.; Lee, B.; Seifert, S.; Winans, R. E.; Elam, J. W.; Pellin, M. J.; Vajda, S. *Angew. Chem. Int. Ed.* **2009**, *48*, 1467.

(4) (a) Widenhoefer, R. A.; Han, X. Q. *Eur J Org Chem* **2006**, 4555. (b) Müller, T. E.; Hultzsch, K. C.; Yus, M.; Foubelo, F.; Tada, M. *Chem. Rev.* **2008**, *108*, 3795. (c) Beller, M.; Seayad, J.; Tillack, A.; Jiao, H. *Angew. Chem. Int. Ed.* **2004**, *43*, 3368. (d) Severin, R.; Doye, S. *Chem. Soc. Rev.* **2007**, *36*, 1407. (e) Mielby, J.; Kegnæs, S.; Fristrup, P. *ChemCatChem* **2012**, *4*, 1037.

(5) (a) Mizushima, E.; Hayashi, T.; Tanaka, M. *Org. Lett.* **2003**, *5*, 3349. (b) Zhang, Y.; Donahue, J. P.; Li, C.-J. *Org. Lett.* **2007**, *9*, 627. (c) Duan, H.; Sengupta, S.; Petersen, J. L.; Akhmedov, N. G.; Shi, X. *J. Am. Chem. Soc.* **2009**, *131*, 12100. (d) Han, Z.-Y.; Xiao, H.; Chen, X.-H.; Gong, L.-Z. *J. Am. Chem. Soc.* **2009**, *131*, 9182. (e) Corma, A.; Gonzalez-Arellano, C.; Iglesias, M.; Navarro, M. T.; Sanchez, F. *Chem. Commun.* **2008**, 6218.

(6) Corma, A.; Concepción, P.; Domínguez, I.; Forné, V.; Sabater, M. J. *J. Catal.* **2007**, *251*, 39.

(7) Zhao, J.; Zheng, Z.; Bottle, S.; Chou, A.; Sarina, S.; Zhu, H. *Chem. Commun.* **2013**, *49*, 2676.

(8) Zhang, S.; Zhao, Y. *ACS Nano* **2011**, *5*, 2637.

(9) Lee, L.-C.; Zhao, Y. *Org. Lett.* **2012**, *14*, 784.

(10) (a) Zhang, S.; Zhao, Y. *Langmuir* **2012**, *28*, 3606. (b) Lee, L.-C.; Zhao, Y. *Helv. Chim. Acta* **2012**, *95*, 863.

(11) Because the reduction of the aurate was induced by the bromide counteranion in the ICRM core, an increase of W_0 increased the number of the surfactant and thus the bromide counterion available for the reduction.

(12) Zheng, J.; Nicovich, P. R.; Dickson, R. M. *Annu. Rev. Phys. Chem.* **2007**, *58*, 409.

(13) Zheng, J.; Zhang, C.; Dickson, R. M. *Phys. Rev. Lett.* **2004**, *93*, 077402.

(14) Eustis, S.; Hsu, H.-Y.; El-Sayed, M. A. *J. Phys. Chem. B* **2005**, *109*, 4811.

(15) Newman, J. D. S.; Blanchard, G. J. *Langmuir* **2006**, *22*, 5882.

(16) The reduction was also evident by the formation of gold black in the reaction catalyzed by $HAuCl_4$ alone (Table 1, entry 9).

(17) (a) Hostetler, M. J.; Wingate, J. E.; Zhong, C. J.; Harris, J. E.; Vachet, R. W.; Clark, M. R.; Londono, J. D.; Green, S. J.; Stokes, J. J.; Wignall, G. D.; Glish, G. L.; Porter, M. D.; Evans, N. D.; Murray, R. W. *Langmuir* **1998**, *14*, 17. (b) Alvarez, M. M.; Khoury, J. T.; Schaaff, T. G.; Shafigullin, M. N.; Vezmar, I.; Whetten, R. L. *J. Phys. Chem. B* **1997**, *101*, 3706. (c) Schaaff, T. G.; Shafigullin, M. N.; Khoury, J. T.; Vezmar, I.; Whetten, R. L.; Cullen, W. G.; First, P. N.; GutierrezWing, C.; Ascensio, J.; JoseYacaman, M. J. *J. Phys. Chem. B* **1997**, *101*, 7885.

(18) (a) Oxford, S. M.; Henao, J. D.; Yang, J. H.; Kung, M. C.; Kung, H. H. *Appl. Catal., A* **2008**, *339*, 180. (b) Chandler, B. D.; Kendell, S.; Doan, H.; Korkosz, R.; Grabow, L. C.; Pursell, C. J. *Acs Catalysis* **2012**, *2*, 684.

(19) Negishi, Y.; Takasugi, Y.; Sato, S.; Yao, H.; Kimura, K.; Tsukuda, T. *J. Am. Chem. Soc.* **2004**, *126*, 6518.

(20) Habib, M. A. In *Comprehensive Treatise of Electrochemistry*; Bockris, J. O. M., Conway, B. E., Yeager, E., Eds.; Plenum Press: New York, 1980; Vol. 1, p 135.

(21) (a) Nikoobakht, B.; El-Sayed, M. A. *Langmuir* **2001**, *17*, 6368. (b) Gao, J.; Bender, C. M.; Murphy, C. J. *Langmuir* **2003**, *19*, 9065. (c) Sau, T. K.; Murphy, C. J. *Langmuir* **2005**, *21*, 2923. (d) Murphy, C. J.; Sau, T. K.; Gole, A. M.; Orendorff, C. J.; Gao, J.; Gou, L.; Hunyadi, S. E.; Li, T. *J. Phys. Chem. B* **2005**, *109*, 13857. (e) Pérez-Juste, J.; Pastoriza-Santos, I.; Liz-Marzán, L. M.; Mulvaney, P. *Coord. Chem. Rev.* **2005**, *249*, 1870. (f) Kawasaki, H.; Nishimura, K.; Arakawa, R. *J. Phys. Chem. C* **2007**, *111*, 2683. (g) Garg, N.; Scholl, C.; Mohanty, A.; Jin, R. C. *Langmuir* **2010**, *26*, 10271.

(22) (a) *Nanoparticles and Catalysis*; Astruc, D., Ed.; Wiley-VCH: Weinheim, Germany, 2008. (b) Bell, A. T. *Science* **2003**, *299*, 1688. (c) Somorjai, G. A.; Contreras, A. M.; Montano, M.; Rioux, R. M. *Proc. Natl. Acad. Sci. U. S. A.* **2006**, *103*, 10577. (d) Burda, C.; Chen, X.; Narayanan, R.; El-Sayed, M. A. *Chem. Rev.* **2005**, *105*, 1025. (e) Somorjai, G. A.; Li, Y. M. *Top. Catal.* **2010**, *53*, 832.

(23) Pileni, M. P. *Structure and Reactivity in Reverse Micelles*; Elsevier: Amsterdam, 1989.

(24) The reaction for the $Si(OMe)_4$ was facilitated by using 6 M HCl aqueous solution instead of water in the ICRM core.

(25) (a) Haruta, M. *Catal. Today* **1997**, *36*, 153. (b) Chen, M. S.; Goodman, D. W. *Chem. Soc. Rev.* **2008**, *37*, 1860.

(26) The sol-gel synthesis probably introduced metal oxide hydrates instead of metal oxides, as the synthesis was performed at room temperature. Nonetheless, the highly tunable activity by the locally introduced metal oxide (hydrates) was noteworthy.

(27) Zhang, S.; Zhao, Y. *ACS Nano* **2011**, *5*, 2637-2646.

(28) Zhang, S.; Zhao, Y. *Langmuir* **2012**, *28*, 3606-3613.

CHAPTER 5.

METALLOEZYME –MIMICKING SUPRAMOLECULAR CATALYSTS FOR HIGH ACTIVE AND SELECTIVE INTRAMOLECULAR ALKYNE CARBOXYLATION

A paper published in *JACS*, **2014**, *136*, 5579-5582

Li-Chen Lee, Yan Zhao

Abstract

Creation of synthetic catalysts with enzyme-like behavior is challenging despite strong interest in such systems. Extraction of tetrachloroaurate into the hydrophilic core of an interfacially cross-linked reverse micelle (ICRM) produced an artificial "metalloenzyme" with highly unusual catalytic properties. The ICRM pulled the substrate toward the catalytic metal, which converted it efficiently to the product that was rapidly ejected. These features enabled greatly reduced catalyst loading (30–100-times lower than typical levels used in literature examples), constant high reaction rate throughout the course of the reaction, lack of the hydrolyzed side product, and substrate selectivity unobserved in conventional gold catalysts.

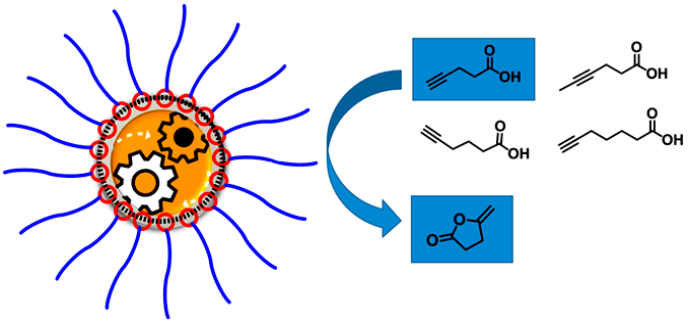

Introduction

Enzymes frequently perform chemical reactions with efficiency and selectivity difficult from a pure synthetic perspective. Different from most synthetic catalysts that

primarily accomplish their catalytic tasks by lowering the activation energy of a reaction, enzymes often are characterized by additional features including selective binding of the substrate via noncovalent forces, correct positioning of appropriate functional groups on the substrate and within the enzyme active site for optimal reactivity, and preferential binding of the substrate over the product.[1] Moreover, selectivity in enzymatic reactions is often accomplished through second-sphere or even more distal control instead of first-sphere interactions as in typical organic, metallic, and organometallic catalysts.[2]

In the last decades, supramolecular chemists have made tremendous progress in making receptors for small molecules.[3] Binding affinities approaching those in biological complexation (e.g., biotin–streptavidin) have been obtained in some cases.[4] Nonetheless, bottom-up construction of enzyme-like supramolecular catalysts remains challenging, especially those with the above mentioned biocatalytic features.[5] The challenge is understandable. If preparation of a catalytic center (organic, metallic, or organometallic) itself can require significant synthetic effort, building additional binding and regulating features around the catalytic center would certainly demand more sophisticated design and synthesis.[2, 5]

Herein, we report a facile bottom-up assembly of an artificial "metalloenzyme" for efficient intramolecular alkyne carboxylation. The supramolecular organization turns a mundane aurate salt into a highly active and selective catalyst with unusual features such as zero-order dependence of the reaction rate on the substrate and selectivity unobserved in conventional gold catalysts.

The design of the artificial "metalloenzyme" is based on our recently synthesized interfacially cross-linked reverse micelles (ICRMs).[6] As shown in Scheme 1, ICRM is

prepared by polymerization of cross-linkable surfactants such as **1** or **2** in the reverse micelle (RM) configuration. Our previous work utilized the thiol–ene addition reaction between **1** and dithiothreitol (DTT) to cross-link the RM. Surfactant **2** was cross-linked directly by free radical polymerization of the acrylamide. Because the ICRM core is lined with a layer of quaternary ammonium groups, the cross-linked micelle could easily extract tetrachloroaurate from aqueous solution into its hydrophilic core. The bromide counteranions within the ICRM(**1**) (i.e., ICRM prepared from **1**) in a prior work were shown to reduce aurate spontaneously to form luminescent gold nanoclusters (Au_4 to Au_{23}).[6-7] Complexed with the bromide ions, the overall negatively charged cluster prefers to stay within the positively charged ICRM core. Since gold nanoparticles can catalyze a variety of reactions[8] and gold clusters often have even higher activity due to their higher surface-to-volume ratio,[8-9] we reasoned that the gold clusters within ICRMs might be particularly active catalysts and ICRM could be used to facilitate the substrate binding. Essentially, in this artificial "metalloenzyme" (Au@ICRM), the metal cluster serves as the catalytic center[10] and the ICRM as a biomimetic scaffold to modulate the catalysis.[11]

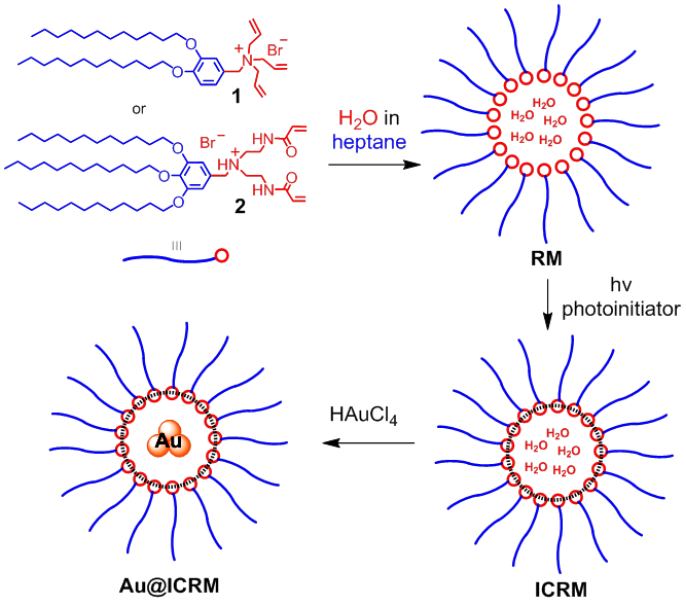

Scheme 1. Synthesis of ICRM from cross-linkable surfactant and incorporation of aurate.

Results and Discussion

One reaction catalyzed by gold is the cyclization of ω-alkynoic acid (Scheme 2). AuCl, $AuCl_3$, Au_2O_3, and other gold compounds have been reported to catalyze the reaction, typically at 3-10 mol % level.[12] We envisioned that Au@ICRM was ideally suited for this reaction for two primary reasons. First, the carboxylic acid group should be attracted to the ICRM core by the ammonium headgroups of the cross-linked surfactant in a nonpolar solvent. Even if a complete ion exchange (to form R'_4N^+ ^-OOCR and HBr) might not be favorable, to the extent this exchange could occur during the reaction, the substrate would be concentrated around the ICRM core. Not only would the effective concentration of the substrate near the catalytic center be enhanced, the nanometer-sized ICRM core suggests that the substrate and the catalyst would be in close proximity. Second, once cyclized, the substrate (**3**) loses the binding functionality (COOH) and the relative nonpolar product (**4**)

should prefer the nonpolar solvent instead of the hydrophilic ICRM core, vacating the binding site(s) for new substrates to come in. Thus, even with a simple structure, Au@ICRM should mimic key catalytic features of enzymes in substrate binding and product turn-over.

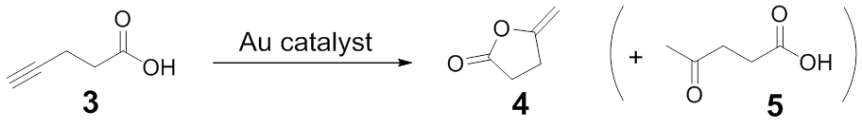

3 **4** **5**

Scheme 2. Gold-catalyzed cyclization of 4-pentynoic acid.

The initial experiments showed some promise. As shown in Table 1 (entries 1-2), 1 mol % Au@ICRM(**1**) was indeed able to catalyze the cyclization, albeit in fairly low yields (17-23%). An encouraging observation was the lack of hydrolysis of **4**, as the hydrolyzed product (**5**) was not observed at all. Apparently, even though the ICRM had a hydrophilic core and mostly likely some water in the core,[13] **4** must have been released sufficiently fast to avoid hydrolysis.

Table 1. Intramolecular cyclization of 4-pentynoic acid cata-lyzed by 1 mol % Au@ICRMs[a]

Entry	ICRM[b]	Au Loading[c]	Time (h)	Yield ([**4**]+[**5**])	Selectivity ([**4**]:[**5**])
1	ICRM(**1**), W_0 = 5	10%	3	17	--[d]
2	ICRM(**1**), W_0 = 5	20%	3	23	--[d]
3	ICRM(**2**), W_0 = 5	10%	3	>95	--[d]
4	ICRM(**2**), W_0 = 5	20%	3	>95	--[d]
5	ICRM(**2**), W_0 = 5	10%	1	>95	--[d]
6	ICRM(**2**), W_0 = 5	10%	1	75[e]	--[d]
7	ICRM(**2**), W_0 = 5	10%	1	22[f]	--[d]
8	ICRM(**2**), W_0 = 5	10%	1	6[g]	--[d]
9	ICRM(**2**), W_0 = 2	10%	1	>95	--[d]
10	ICRM(**2**), W_0 = 10	10%	1	>95	--[d]
11	--[h]	$HAuCl_4$	3	24	53:47
12	--[i]	$HAuCl_4$	3	0	--

[a] All reactions were performed with 0.25 mmol of 4-pentynoic acid with 1 mol % gold catalysts in 0.2 mL of benzene-d_6 at room temperature. The yield was determined by ^{1}H NMR spectroscopy. [b] ICRM(**1**) and ICRM(**2**) were prepared by polymerization of cross-linkable surfactant **1** and **2**, respectively. [c] Aurate loading was the aurate/surfactant ratio in the template synthesis of the gold clusters. [d] Hydrolyzed product **5** was not observed. [e] Solvent for reaction = 0.1 mL benzene-d_6 + 0.1 mL $CDCl_3$. [f] Solvent for reaction = 0.1 mL benzene-d_6 + 0.1 mL MeOH-d_4. [g] Solvent for reaction = 0.1 mL benzene-d_6 + 0.1 mL DMSO-d_6. [h] No ICRM was used and $HAuCl_4$ was used directly as the catalyst. [i] Uncross-linked surfactant **2** was used instead of the ICRM, with the ratio of [$HAuCl_4$]/[**2**] = 1:10.

To our delight, Au@ICRM(**2**) under the same conditions gave dramatically better results: even at 1 mol % catalyst loading (vs. 3-10 mol % used in the literature[12]), the reaction went to completion within 3 h at room temperature, also without any hydrolytic side reaction (Table 1, entries 3 & 4). Three hours of reaction time turned out unnecessary, as the reaction was complete in 1 h as well (entry 5). Notably, although Au@ICRM(**2**) was formed from $HAuCl_4$ under spontaneous reduction, $HAuCl_4$ itself was not a good catalyst and only afforded 24% yield with nearly half of the enol lactone hydrolyzed (entry 11). When uncross-linked **2** was used instead of the ICRM, no product was observed at all under identical conditions, confirming the importance of the cross-linking (entry 12). Our previous work

indicated that, without cross-linking, $HAuCl_4$ simply was extracted into the organic phase by these surfactants and turned into $AuBr_4^-$ via ligand exchange with the bromide counterions.[7]

To understand the oxidation state of the active Au catalyst involved, we performed the cyclization under different atmosphere, with reduced amount of catalyst (0.1-0.2 mol %) and shorter reaction time (1 h). As shown by Figure 1, oxidative conditions (under air or O_2) were clearly better than inert or reducing conditions (under N_2 or H_2). Thus, the most likely catalytic species was oxidized gold (I or III) on the gold cluster, consistent with other literature reports.[12]

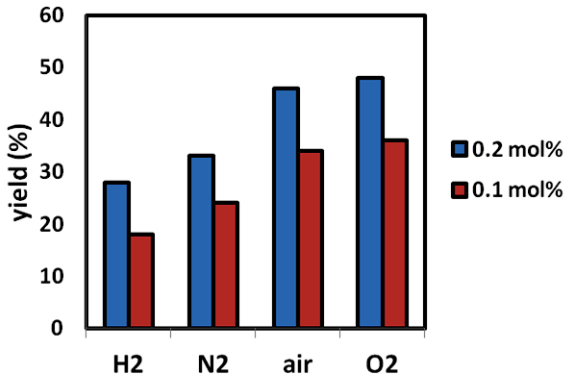

Figure 1. Yields of intramolecular cyclization of 4-pentynoic acid catalyzed by Au@ICRM(**2**) with 10% aurate loading and W_0 = 5 under different atmosphere at room temperature for 1 h.

Our hypothesized attraction of the substrate by the ICRM core was supported by solvent effects. Although the reaction proceeded smoothly in benzene (a nonpolar solvent), adding an equal volume of $CHCl_3$, MeOH, or DMSO to benzene lowered the reaction yield progressively, from quantitative all the way to 6% (Table 1, entries 5–8).

The importance of substrate binding to the catalysis was verified additionally by a competitive study. As shown by Figure 2, small-molecule carboxylic acids exhibited powerful inhibition of the cyclization, with even 1 mol % of the acid lowering the yield from quantitative to 40-80%. The inhibition followed a clear trend of acid size-acetic acid > dodecanoic acid > 1-adamantanecarboxylic acid. The strong inhibition suggests that a small number of highly active catalytic sites were responsible for the activity (considering that carboxylic acid was abundant in the reaction mixture from the starting material itself). It also appears that metal–ligand complexation between gold and alkyne was NOT the main driving force for the substrate binding. Otherwise, the carboxylic acid inhibitors, lacking the alkyne group, would not have been so effective at such low levels (1 mol %).

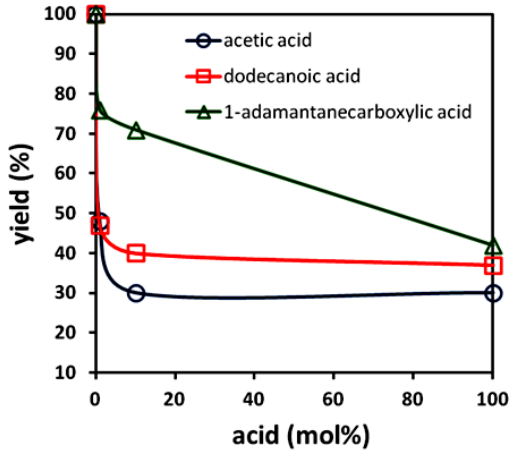

Figure 2. Reaction yield of cyclization of 4-pentynoic acid catalyzed by 1 mol % Au@ICRM(**2**) in the presence of carboxylic acid competitors.

We initially suspected the much higher activity of Au@ICRM(**2**) over Au@ICRM(**1**) was caused by different-sized gold clusters formed in the ICRM core. The size of the gold clusters formed in the ICRM-templated synthesis depends on the amount of aurate loading

(the aurate/surfactant ratio) and W_0 (water/surfactant ratio),[6-7,14] and typically could be determined by the emission wavelength of the gold clusters.[6, 15] Au@ICRM(**1**) at W_0 = 5 and 10-20% aurate loading emitted at 476 nm, corresponding to $Au_{9–10}$ clusters[6] (Figures 3). (As a reference, Au_8 clusters emit at ~450 nm.)[16] Au@ICRM(**2**), on the other hand, emitted at 440 nm (Figures 4) or blue-shifted by 36 nm from the emission of Au@ICRM(**1**). However, when we examined the effect of W_0 on the catalysis of Au@ICRM(**2**), the different particle size did not seem to be important. For example, Au@ICRM(**2**) at W_0 = 2 and 10 both gave quantitative yield in the intramolecular alkyne carboxylation (Table 1, entries 9-10) even though Au@ICRM(**2**) with W_0 = 10 clearly contained larger clusters than Au@ICRM(**1**).[17] Hence, the ICRM framework instead of the gold clusters most likely was controlling the catalytic activity.[18] In the literature, gold nanoparticles supported on various metal oxides were either completely inactive or gave very low yields at much higher catalyst loading.[12d]

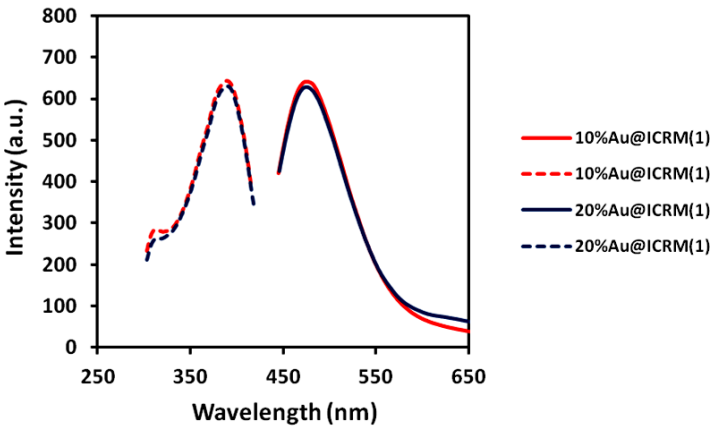

Figure 3. Emission (solid lines) and excitation (dashed lines) spectra of Au@ICRM(**1**) in chloroform with different aurate loading. W_0 = [H_2O]/[surfactant] = 5. [Cross-linked **1** in the ICRM] = 3.0 mM.

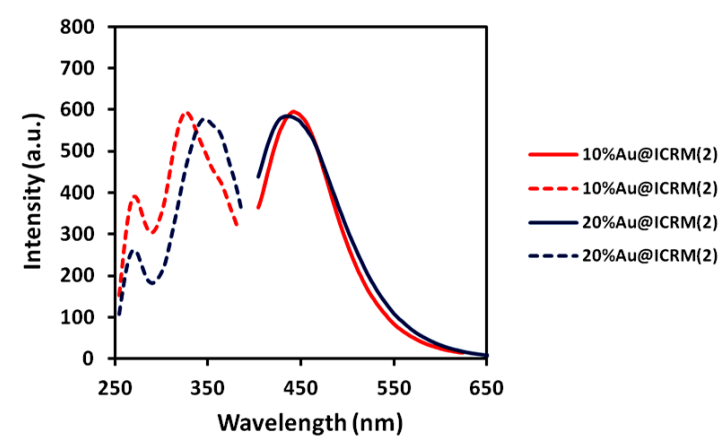

Figure 4. Emission (solid lines) and excitation (dashed lines) spectra of Au@ICRM(**2**) in chloroform with different aurate loading. W_0 = [H_2O]/[surfactant] = 5. [Cross-linked **2** in the ICRM] = 3.0 mM.

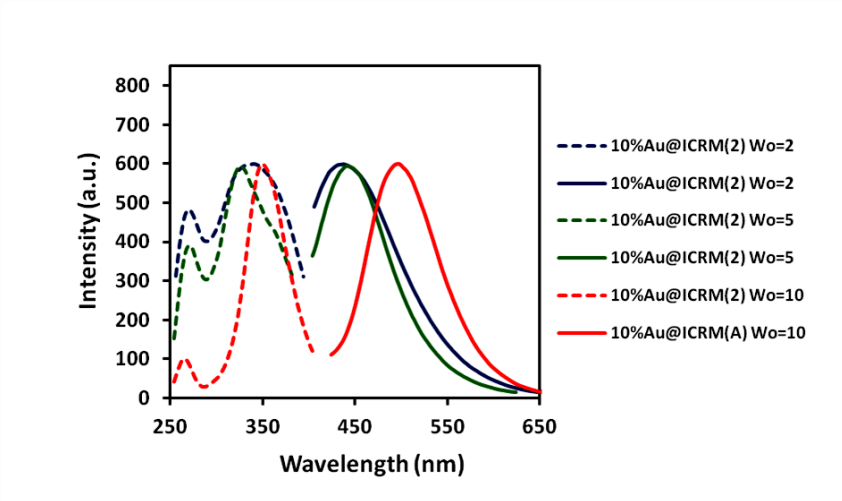

Figure 5. Emission (solid lines) and excitation (dashed lines) spectra of Au@ICRM(**2**) in chloroform with different W_0. [Cross-linked **2** in the ICRM] = 3.0 mM. Aurate loading = [$HAuCl_4$]/[surfactant] = 10%.

The results so far suggest that Au@ICRM(**2**) indeed appeared to function as an artificial "metalloenzyme" in cyclizing **3**. Noncovalent binding between the substrate and the ICRM was critical to the catalysis, as any disruption of this binding (by solvents or competitive carboxylic acids) dramatically hindered the conversion. The supramolecular

organization of the catalyst already made it far more active than conventional gold salts with or without special ligands.[12] Since the reaction went to completion in 1 h with 1 mol % catalyst, we decided to reduce the level of catalyst further.

The results were illuminating. At 0.1 mol % catalyst loading (30-100 times lower than what was used in the literature), the reaction still proceeded to completion within 4 h at room temperature. Most amazingly, unlike typical reactions that slow down as the starting material is consumed, cyclization of **3** catalyzed by Au@ICRM(**2**) showed practically no sign of slowing down all the way to the completion of the reaction (Figure 6).

The above results together point to a mechanism in which the carboxylic acid of **3** enabled its binding to Au@ICRM(**2**). The binding and product release must have been faster than the cyclization. In this way, the local concentration of the substrate near the catalyst was essentially constant throughout the reaction, as supported by the zero-order dependence of reaction rate on the substrate (Figure 6).

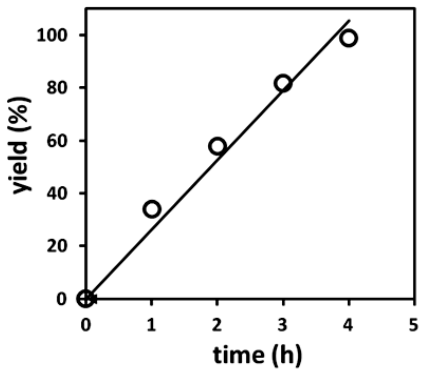

Figure 6. Reaction yield of cyclization of 4-pentynoic acid catalyzed by 0.1 mol % Au@ICRM(**2**) over time.

The importance of ICRM to the catalysis was already shown by the enormously different activity of Au@ICRM(**1**) and Au@ICRM(**2**). We then studied cyclization of

different substrates (**6**-**8**), curious whether the ICRM would impart any special substrate selectivity to the catalysis. Typical gold catalysts such as AuCl showed no distinction in cyclizing 4-pentynoic acid (**3**) or 5-hexynoic acid (**6**), although 6-heptynoic acid (**7**) showed lower reactivity.[12b, 12e] In our hands, only 7-18% cyclization occurred with **6** (Table 2, entries 1-3) in contrast to the quantitative conversion of 4- pentynoic acid **3** (Table 1, entries 5 and 9-10). Even when the reaction time was prolonged to 8 h, the reaction did not go to completion, giving 40-60% yield depending on the W_0 of the ICRM (Table 2, entries 4-6). Not only so, hydrolysis (10-15%) of the lactone product was observed for this compound. Not surprisingly, 6-heptynoic acid (**7**) was completely inactive even after 24 h (entry 7).

To understand the reason for the substrate selectivity, we studied another substrate, 4-hexynoic acid (**8**). Its contains the same number of carbon as the much less reactive **6** but forms the same five-membered ring enol lactone as the most reactive **3**. The reaction was clearly slower than that of **3** but faster than that of **6**: 19% at 1 h, 90% at 8 h, and quantitative at 24 h (Table 2, entries 8-10). Importantly, although both *Z* and *E* isomers formed for this product (as expected), no hydrolysis of the lactone occurred under the same reaction conditions.

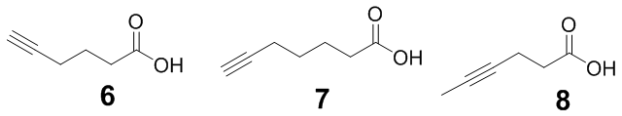

Table 2. Intramolecular cyclization of alkynoic acids catalyzed by 1 mol % Au@ICRM(**2**)

Entry	W_0	Substrate	Time (h)	% Yield
1	2	**6**	1	14
2	5	**6**	1	18
3	10	**6**	1	7
4	2	**6**	8	60[a]
5	5	**6**	8	54[a]
6	10	**6**	8	40[a]
7	2, 5, 10	**7**	8–24	0
8	5	**8**	1	19
9	5	**8**	8	90[b]
10	5	**8**	24	>95[b]

a Hydrolysis (10-15%) of the enol lactone was observed. b *Z*:*E* = 78/22.

Conclusion

Supramolecular engineering can be a powerful tool to modulate catalysis.[19] As demonstrated by this work, the high activity and selectivity for 4-pentynoic acid by Au@ICRM(**2**) did not originate from the catalytically active gold center but the organic ICRM framework that pulled the substrate from the environment to the catalyst. It is not entirely clear why Au@ICRM(**2**) had substrate reactivity unobserved in conventional gold catalysts. The catalyst, nonetheless, did appear to be "optimized" for the 5-membered-ring enol lactone: not only was **3** (and **8**) much more reactive than **6** and **7**, but also the five-membered-ring lactone was the only one showing no hydrolysis under identical reaction conditions. The most interesting finding was the role of carboxylic acid of **3** in the catalytic reaction. When it was

responsible for the (fast) binding of the substrate and meantime was the exact group to be converted in the catalysis, the entire system behaved like a catalytic nanomachine: the ICRM pulled the substrate to the catalytic center and the appropriately positioned gold cluster turned it into the product, which preferred the nonpolar environment instead of the ICRM core and was thus rapidly released. The result was extremely high activity compared to conventional gold catalysts (for similar reactions) and highly unusual zero-order kinetics. We believe these features are not unique with the Au@ICRMs. Similar designs potentially can turn other conventional catalysts into artificial "enzymes" having novel, useful, biomimetic functions.

Experimental Section

General. All reagents and solvents were of ACS certified grade or higher and were used as received from commercial suppliers. Routine ^{1}H and ^{13}C NMR spectra were recorded on a Varian VXR-400 and Bruker DRX-400 spectrometer. ESI-MS was performed on a FINNIGAN TSQ700 mass spectrometer. Dynamic light scattering (DLS) was performed on a PD2000DLS^{PLUS} dynamic light scattering detector. Fluorescence spectra were recorded at ambient temperature on a Varian Cary Eclipse fluorescence spectrophotometer. UV-vis spectra were recorded at ambient temperature on a Cary 50 Bio UV-visible spectrophotometer.

Synthesis

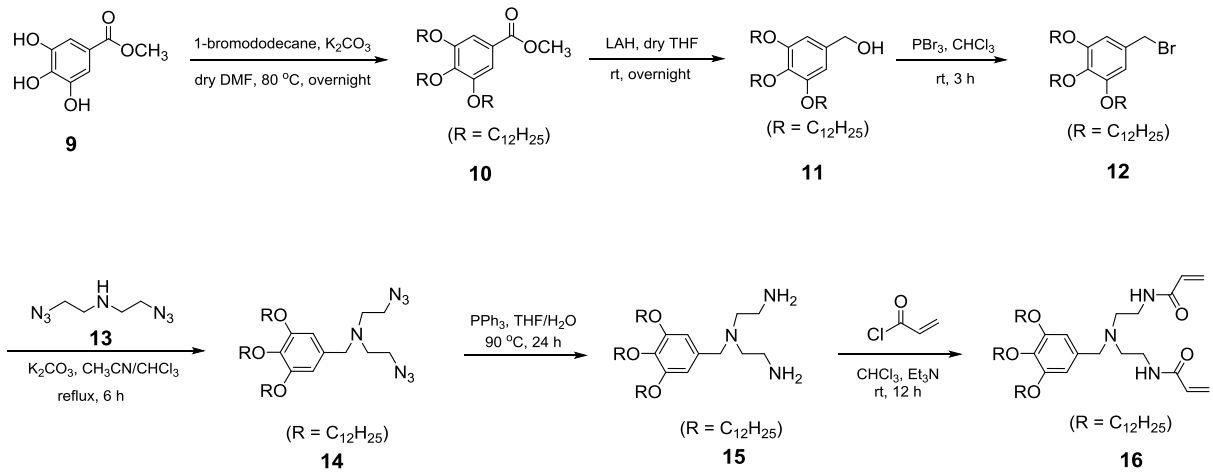

Scheme 2. Synthesis of compound **16**

Methyl 3,4,5-tris(dodecyloxy)benzoate (10).[20] Potassium carbonate (23.8 g, 172.20 mmol) was added to a solution of methyl 3,4,5-trihydroxybenzoate (**9)** (5.10 g, 27.54 mmol) in DMF (150 mL) at room temperature. After the mixture was stirred at 60 °C for 2 h, 1-bromododecane (21.3 mL, 88.0 mmol) was added slowly. The reaction mixture was stirred overnight at 80 °C, cooled to room temperature, and poured over 750 mL of icy water. The crude product was collected by suction filtration and purified by crystallization from acetone to give a yellow solid (20.0 g, quantitative). ^{1}H NMR (400 MHz, $CDCl_3$, δ): 7.24 (s, 2 H), 3.99 (t, 6 H), 3.88 (s, 3 H), 1.82-1.25 (m, 60 H), 0.86 (t, 9 H).

3,4,5-Tris(dodecyloxy)benzyl alcohol (11).[20] A solution of methyl 3,4,5-tris(dodecyloxy)-benzoate (**10)** (16.3 g, 23.6 mmol) in dry THF (125 mL) was added dropwise to a stirred suspension of $LiAlH_4$ (1.50 g, 38.7 mmol) in dry THF (40 mL) at 0 °C. The reaction mixture was stirred overnight at room temperature and was quenched carefully by methanol (10 mL) and water (10 mL). The solid formed was removed by filtration and the filtrate was concentrated *in vacuo*. The residue was dissolved in $CHCl_3$ (250 mL). The resulting solution was washed with water (2 × 100 mL), brine (2 × 100 mL), dried over anhydrous $MgSO_4$, and

concentrated *in vacuo* to give a white powder (11.0 g, 71%). ^{1}H NMR (400 MHz, $CDCl_3$, δ): 6.56 (s, 2H), 4.59 (s, 2H),4.02-3.88 (m, 6H), 1.86-1.26 (m, 60H), 0.88 (t, 9H).

3,4,5-Tris(dodecyloxy)benzyl bromide (12).[20] A solution of PBr_3 (0.50 mL, 5.3 mmol) in $CHCl_3$ (5 mL) was slowly added to a stirred solution of 3,4,5-tris(dodecyloxy)benzyl alcohol (1.80 g, 2.67 mmol) in $CHCl_3$ (30 mL) at 0 °C. The reaction mixture was stirred at room temperature for 3 h and slowly poured into water (20 mL). The product was extracted with $CHCl_3$ (2 × 30 mL). The combined organic phase was washed with brine (2 × 20 mL), dried over anhydrous $MgSO_4$, and concentrated *in vacuo* to give a white solid (1.70 g, 89%). ^{1}H NMR (400 MHz, $CDCl_3$, δ): 6.57 (s, 2H), 4.43 (s, 2H), 3.98-3.94 (m, 6H), 1.8-1.26 (m, 60H), 0.88 (t, 9H).

Compound (14). Bis-(2-azidoethyl)amine[21] (34 mg, 0.22 mmol) was dissolved in solution of compound **12** (80.0 mg, 0.11 mmol) and K_2CO_3 (46.0 mg, 0.33 mmol) in $CHCl_3$ (2 mL) and CH_3CN (3 mL). The reaction mixture was stirred at 80 °C for 6 h. The solid was removed by filtration and the filtrate was concentrated *in vacuo.* The residue was purified by column chromatography over silica gel using CH_2Cl_2 as the eluent to give a yellow oil (81.0 mg, 92%). ^{1}H NMR (400 MHz, $CDCl_3$, δ): 6.56 (s, 2H), 3.97-3.92 (dd, *J* = 13.6 Hz and 6.4 Hz, 6H), 3.59 (s, 2H), 3.28 (t, *J* = 6.0 Hz, 4H), 2.75 (t, *J* = 6.4 Hz, 4H), 1.82-1.72 (m, 6H), 1.46-1.26 (m, 54H), 0.88 (t, *J* = 6.8 Hz, 9H). ^{13}C NMR (100 MHz, $CDCl_3$, δ): 153.17, 137.28, 133.64, 106.71, 73.38, 69.07, 59.76, 49.44, 31.98, 31.96, 30.38, 29.80, 29.77, 29.74, 29.73, 29.70, 29.68, 29.66, 29.48, 29.47, 29.43, 29.41, 26.18, 26.14, 22.73, 14.14.; ESI-MS (*m*/*z*): $[M+H]^+$ calcd for $C_{47}H_{88}N_7O_3$, 798.6949; found 798.6944.

Compound (15). Ph_3P (197.0 mg, 0.75 mmol) was dissolved in solution of compound **14** (100.0 mg, 0.125 mmol) in THF (10 mL) and H_2O (1 mL). The reaction mixture was stirred at 80 ^{o}C for 24 h. After THF was removed by rotary evaporation, the mixture was extracted with $CHCl_3$ (3 × 10 mL). The combined organic phase was washed with 0.1 M NaOH (3 × 5 mL), dried over anhydrous $MgSO_4$, and concentrated by rotary evaporation. The residue was purified by column chromatography over silica gel using CH_2Cl_2/MeOH/Et_3N = 6:1:0.1 (v/v/v) as the eluent to give a yellow oil (58 mg, 62%). ^{1}H NMR (400 MHz, $CDCl_3$): 6.50 (s,

2H), 3.96-3.91 (dd, J = 12.8 Hz and 6.4 Hz, 6H), 3.50 (s, 2H), 2.76 (t, *J*= 6.0 Hz, 4H), 2.52 (t, *J* = 6.0 Hz, 4H), 1.82-1.72 (m, 6H), 1.46-1.26 (m, 54H), 0.88 (t, *J* = 6.8 Hz, 9H). ^{13}C NMR (100 MHz, $CDCl_3$, δ): 152.94, 137.12, 134.74, 107.03, 73.35, 69.10, 59.52, 57.48, 39.85, 31.90, 31.89, 30.32, 29.72, 29.70, 29.67, 29.66, 29.62, 29.60, 29.44, 29.42, 29.35, 29.33, 26.11, 26.11, 22.65, 14.07. ESI-MS (*m*/*z*): $[M+H]^+$ calcd for $C_{47}H_{92}N_3O_3$, 746.7139; found 746.7144.

Compound (16). Acryloyl chloride (41.2 µL, 0.52 mmol) was added dropwise to in solution of compound **15** (180 mg, 0.24 mmol) and triethylamine (0.2 mL, 1.44 mmol) in $CHCl_3$ (10 mL). The reaction mixture was stirred at room temperature for 12 h and slowly poured into water (5 mL). The product was extracted with $CHCl_3$ (3 × 5 mL). The combined organic phase was washed with brine (3 × 5 mL), dried over anhydrous $MgSO_4$. After $CHCl_3$ was removed by rotary evaporation, the residue was purified by column chromatography over silica gel using CH_2Cl_2/MeOH = 10:1 (v/v) as the eluent to give a white powder (168 mg, 82%). The compound was acidified with HBr in $CHCl_3$/CH_3OH to give compound **2**, which was used without further purification. ^{1}H NMR (400 MHz, $CDCl_3$, δ): 6.39 (s, 2H), 6.29-6.15(m, 4H), 5.59-5.57(dd, *J* = 7.6 Hz and 1.2 Hz, 2H), 3.92-3.85(m, 6H), 3.42-3.38(m, 6H), 2.6 (t, *J* = 5.4 Hz, 4H), 1.78-1.71 (m, 6H), 1.48-1.26 (m, 54H), 0.88 (t, *J* = 6.8 Hz, 9H). ^{13}C NMR (100 MHz, $CDCl_3$, δ): 166.07, 152.94, 137.04, 134.36, 130.99, 126.04, 107.38, 73.40, 69.05, 58.74, 53.42, 37.33, 31.93, 31.91, 30.34, 29.76, 29.74, 29.71, 29.69, 29.66, 29.64, 29.48, 29.45, 29.38, 29.36, 26.14, 22.68, 14.11. ESI-MS (*m*/*z*): $[M+H]^+$ calcd for $C_{53}H_{95}N_3O_5$, 854.7350; found 854.7343.

Preparation of ICRM(2). Preparation of ICRMs, detailed characterization of the materials, and the template synthesis of Au@ICRM have been reported previously.[22] Compound **2** (18.7 mg, 0.02 mmol) was dissolved in 0.5 ml of heptane, to which water (1.8 µL, 0.1 mmol) was added. The mixture was ultrasonicated at room temperature until the water droplet dissolved in the mixture and the solution became completely clear. After addition of 2-hydroxy-1-(4-(2-hydroxyethoxy)phenyl)-2-methylpropan-1-one (0.224 mg, 1 × 1 µmol), the mixture was irradiated in a Rayonet photoreactor for 2 h until alkenic protons in **2** were consumed. The

organic solvents were removed by rotary evaporation and the residue was washed by cold methanol and dried under vacuum to give a yellowish power (13.2 mg).

UV-vis Absorption spectra of Au@ICRMs

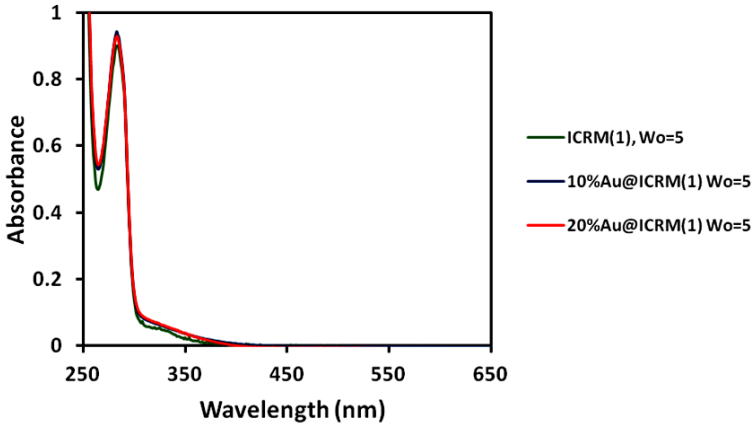

Figure 7. Absorption spectra of Au@ICRM(**1**) in chloroform with 10 and 20% aurate loading. [Cross-linked **1**] = 0.2 mM. W_0 = [H_2O]/[surfactant] = 5.

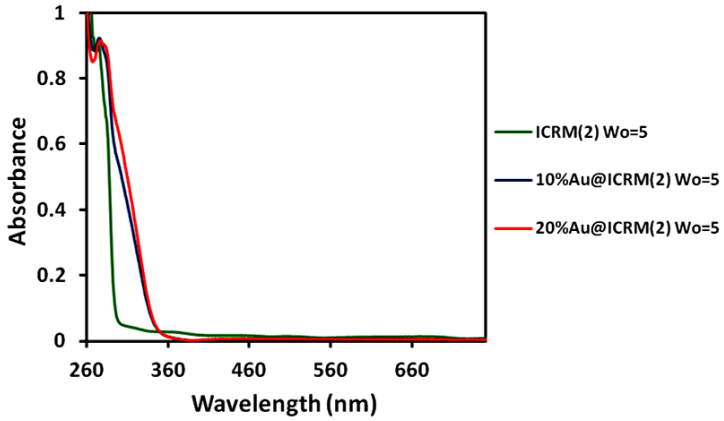

Figure 8. Absorption spectra of Au@ICRM(**2**) in chloroform with 10 and 20% aurate loading. [Cross-linked **2**] = 0.2 mM. W_0 = [H_2O]/[surfactant] = 5.

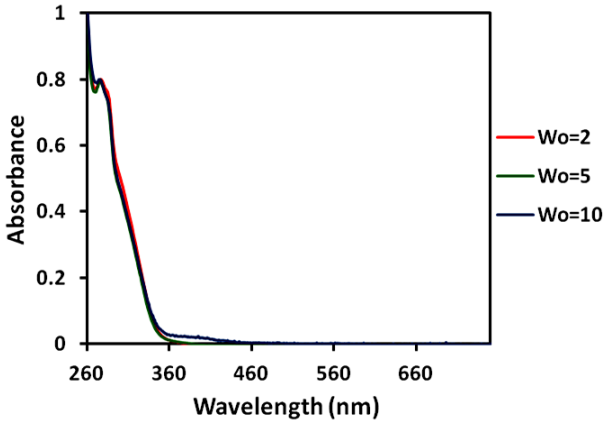

Figure 9. Absorption spectra of Au@ICRM(**2**) in chloroform with 10 % aurate loading. W_0 = [H_2O]/[surfactant] = 5.. [Cross-linked **2**] = 0.2 mM. W_0 = [H_2O]/[surfactant] = 2, 5, and 10.

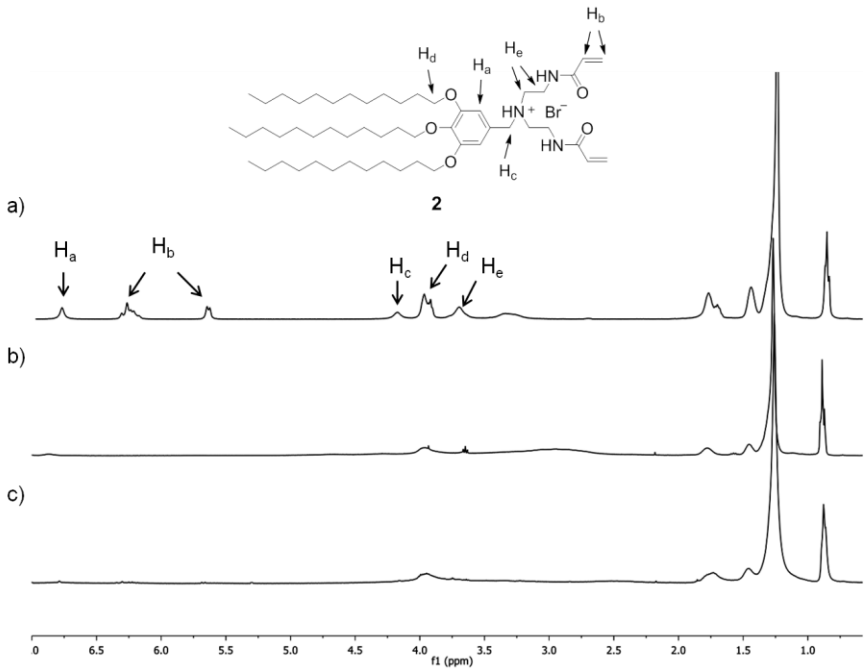

Figure 10. ^{1}H NMR spectra of compound **2** (a) before irradiation in $CDCl_3$, (b) after UV irradiation for 2 h in the reverse-micelle configuration, and (c) after the ICRM was washed with methanol.

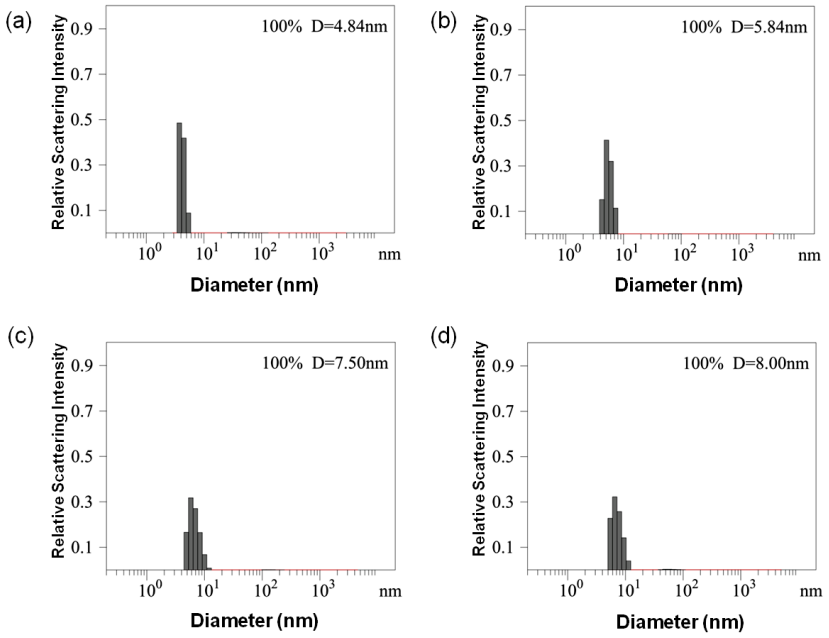

Figure 11. Distribution of the hydrodynamic diameters of ICRM(**2**) in (a) THF, (b) $CHCl_3$, (c) heptane, and (d) toluene determined by DLS.

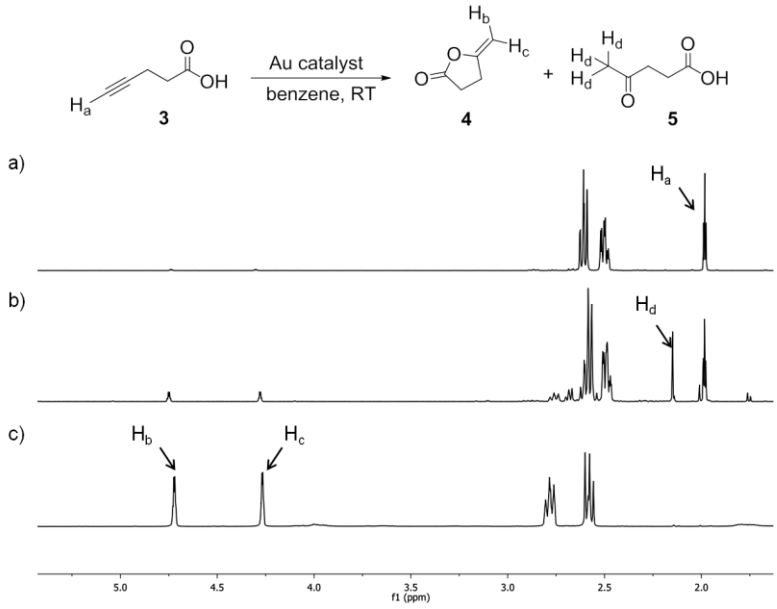

Figure 12. ^{1}H NMR spectra of (a) 4-pentynoic acid, (b) reaction product of 4-pentynoic acid catalyzed by $HAuCl_4$, and (c) reaction product of 4-pentynoic acid catalyzed by Au@ICRM(2) with 10% aurate loading and W_0 = 5. All the reactions were performed with

0.25 mmol of 4-pentynoic acid with 1 mol % gold catalysts in 0.2 mL of benzene-d_6 at room temperature for 3 h.

^{1}H and ^{13}C NMR spectra of key compounds

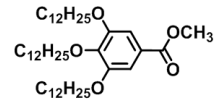

10

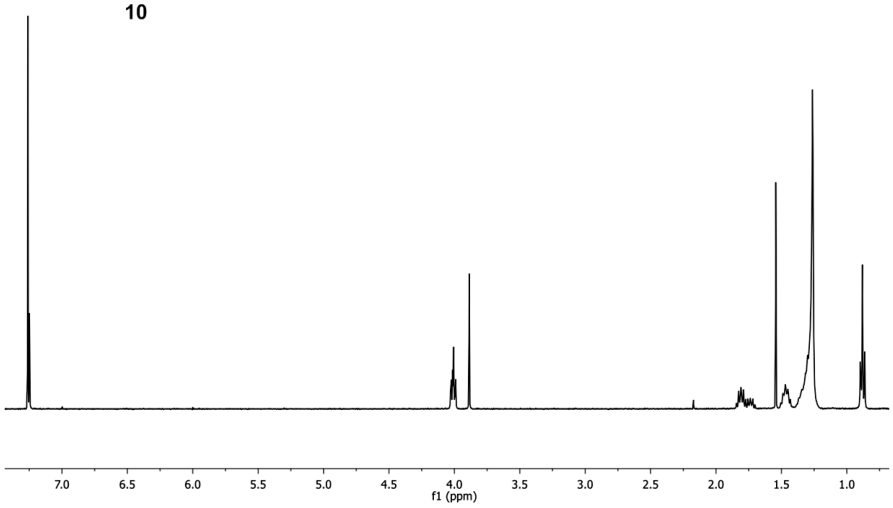

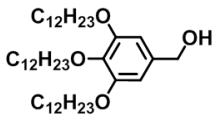

11

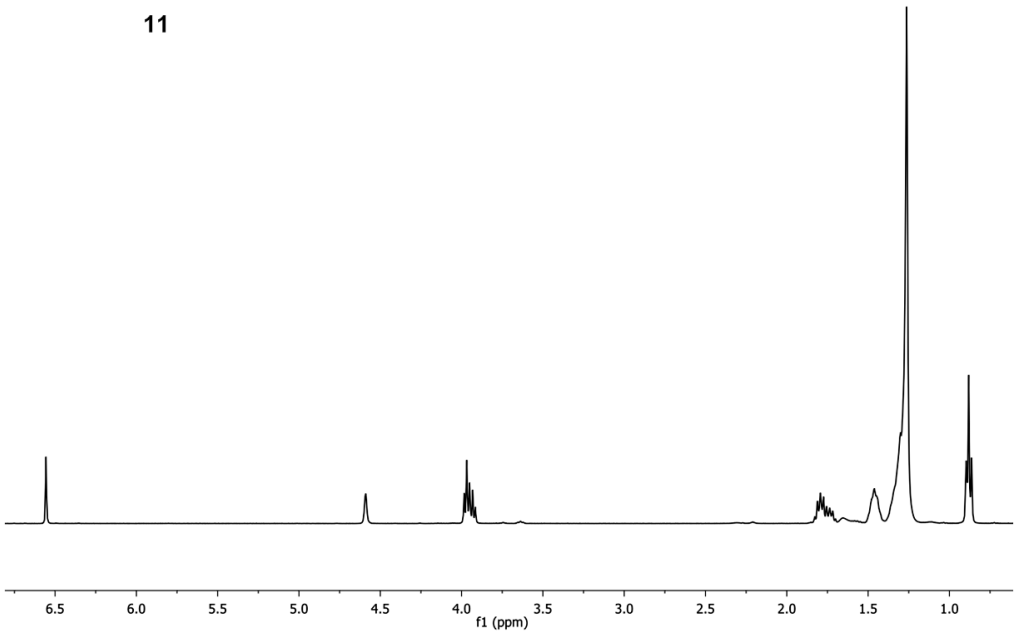

^{1}H and ^{13}C NMR spectra continued

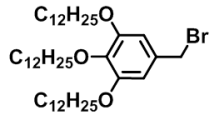

12

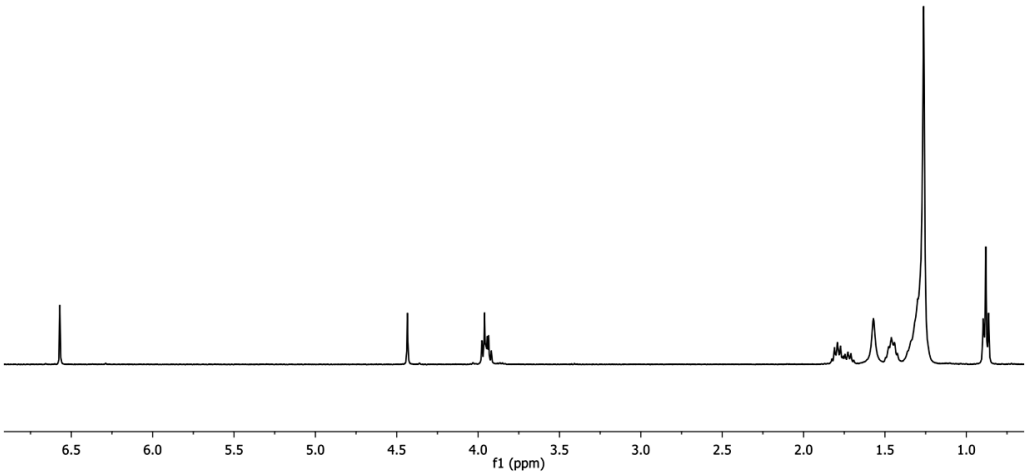

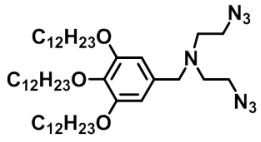

14

^{1}H and ^{13}C NMR spectra continued

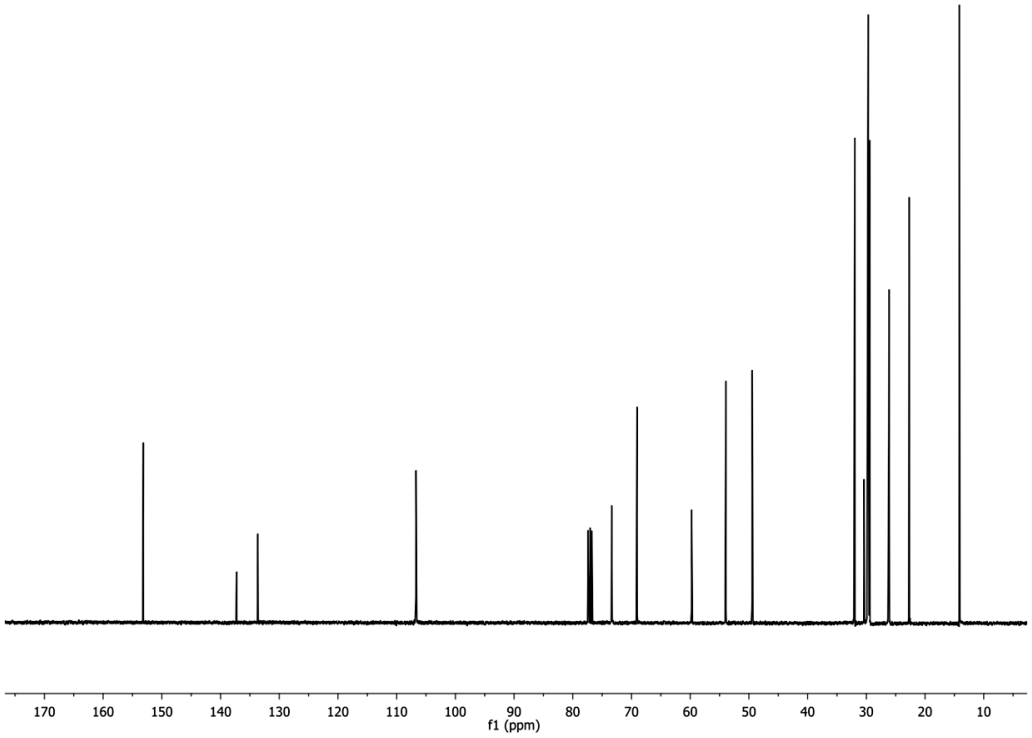

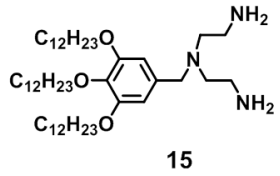

15

^{1}H and ^{13}C NMR spectra continued

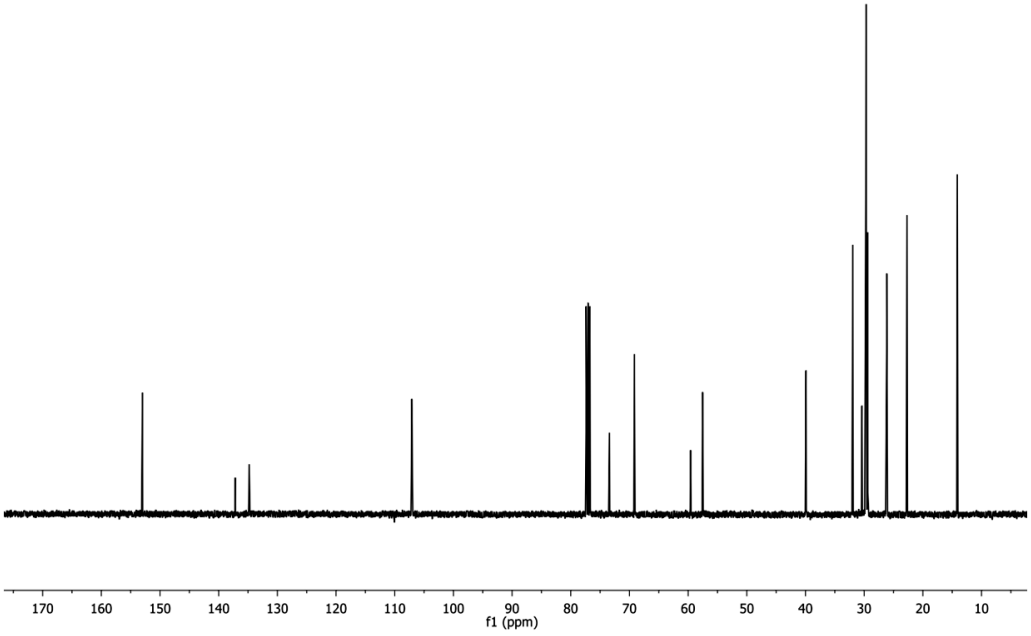

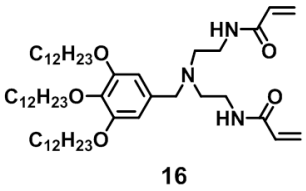

16

^{1}H and ^{13}C NMR spectra continued

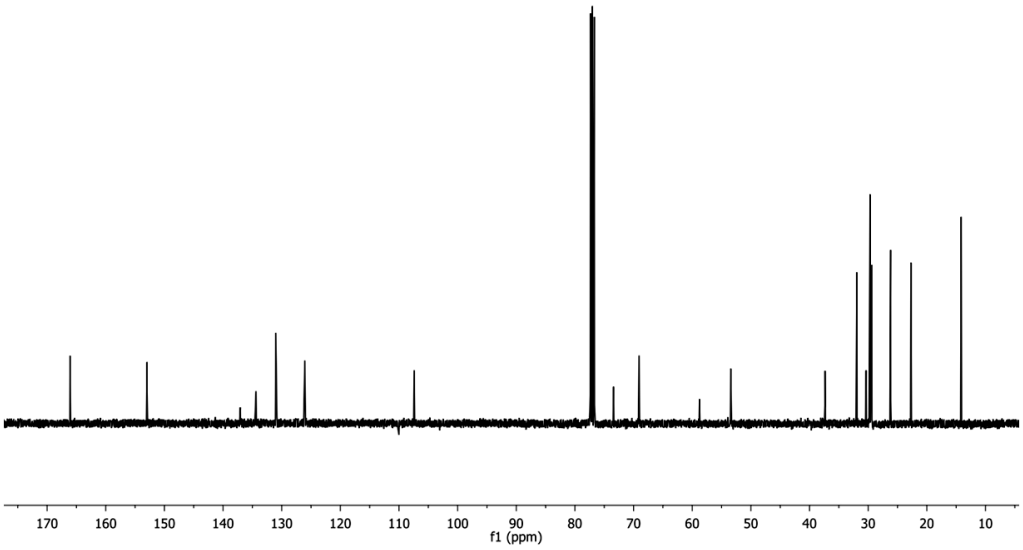

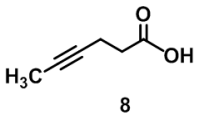

8

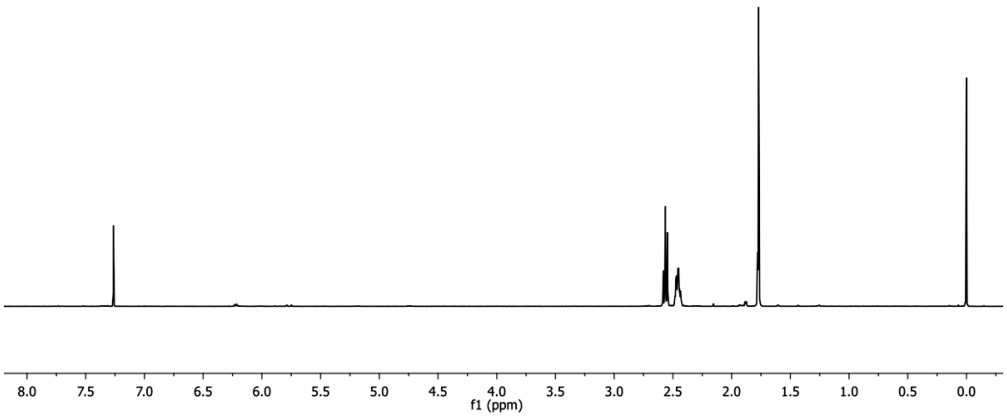

Acknowledgment. We thank the U.S. Department of Energy-Office of Basic Energy Sciences (grant DE-SC0002142) for supporting the research.

References

(1) Jencks, W. P. *Adv. Enzymol. Relat. Areas Mol. Biol.* **1975**, *43*, 219-410.

(2) Das, S.; Brudvig, G. W.; Crabtree, R. H. *Chem. Commun.* **2008**, 413-424.

(3) (a) Atwood, J. L.; Lehn, J. M. *Comprehensive Supramolecular Chemistry*; Pergamon: New York, 1996. (b) Steed, J. W.; Gale, P. A. *Supramolecular Chemistry: From Molecules to Nanomaterials*; Wiley: Weinheim, 2012. (c) Schneider, H.-J.; Yatsimirsky, A. K. *Principles and Methods in Supramolecular Chemistry*; Wiley: New York, 2000.

(4) (a) Rekharsky, M. V.; Mori, T.; Yang, C.; Ko, Y. H.; Selvapalam, N.; Kim, H.; Sobransingh, D.; Kaifer, A. E.; Liu, S.; Isaacs, L.; Chen, W.; Moghaddam, S.; Gilson, M. K.; Kim, K.; Inoue, Y. *Proc. Natl. Acad. Sci. U. S. A.* **2007**, *104*, 20737-20742. (b) Hogben, H. J.; Sprafke, J. K.; Hoffmann, M.; Pawlicki, M.; Anderson, H. L. *J. Am. Chem. Soc.* **2011**, *133*, 20962-20969.

(5) (a) Das, S.; Incarvito, C. D.; Crabtree, R. H.; Brudvig, G. W. *Science* **2006**, *312*, 1941-1943. (b) Pluth, M. D.; Bergman, R. G.; Raymond, K. N. *Science* **2007**, *316*, 85-88. (c) Lee, S. J.; Cho, S.-H.; Mulfort, K. L.; Tiede, D. M.; Hupp, J. T.; Nguyen, S. T. *J. Am. Chem. Soc.* **2008**, *130*, 16828-16829. (d) Shenoy, S. R.; Pinacho Crisóstomo, F. R.; Iwasawa, T.; Rebek, J. *J. Am. Chem. Soc.* **2008**, *130*, 5658-5659. (e) Smejkal, T.; Breit, B. *Angew. Chem. Int. Ed.* **2008**, *47*, 3946-3949. (f) Yoshizawa, M.; Klosterman, J. K.; Fujita, M. *Angew. Chem. Int. Ed.* **2009**, *48*, 3418-3438. (g) Meeuwissen, J.; Reek, J. N. H. *Nat Chem* **2010**, *2*, 615-621. (h) Wiester, M. J.; Ulmann, P. A.; Mirkin, C. A. *Angew. Chem. Int. Ed.* **2011**, *50*, 114-137.

(6) Zhang, S.; Zhao, Y. *ACS Nano* **2011**, *5*, 2637-2646.

(7) Zhang, S.; Zhao, Y. *Langmuir* **2012**, *28*, 3606-3613.

(8) (a) Haruta, M. *Chem. Rec.* **2003**, *3*, 75-87. (b) Hashmi, A. S. K.; Hutchings, G. J. *Angew. Chem. Int. Ed.* **2006**, *45*, 7896-7936. (c) Corma, A.; Garcia, H. *Chem. Soc. Rev.* **2008**, *37*, 2096-2126. (d) Della Pina, C.; Falletta, E.; Prati, L.; Rossi, M. *Chem. Soc. Rev.* **2008**, *37*, 2077-2095. (e) Della Pina, C.; Falletta, E.; Rossi, M. *Chem. Soc. Rev.* **2012**, *41*, 350-369. (f) Zhang, Y.; Cui, X. J.; Shi, F.; Deng, Y. Q. *Chem. Rev.* **2012**, *112*, 2467-2505.

(9) (a) Sanchez, A.; Abbet, S.; Heiz, U.; Schneider, W. D.; Häkkinen, H.; Barnett, R. N.; Landman, U. *J. Phys. Chem. A* **1999**, *103*, 9573-9578. (b) Lopez, N.; Janssens, T. V. W.; Clausen, B. S.; Xu, Y.; Mavrikakis, M.; Bligaard, T.; Nørskov, J. K. *J. Catal.* **2004**, *223*, 232-235. (c) Tsunoyama, H.; Sakurai, H.; Negishi, Y.; Tsukuda, T. *J. Am. Chem. Soc.* **2005**, *127*, 9374-9375. (d) Herzing, A. A.; Kiely, C. J.; Carley, A. F.; Landon, P.; Hutchings, G. J. *Science* **2008**, *321*, 1331-1335. (e) Lee, S.; Molina, L. M.; López, M. J.; Alonso, J. A.; Hammer, B.; Lee, B.; Seifert, S.; Winans, R. E.; Elam, J. W.; Pellin, M. J.; Vajda, S. *Angew. Chem. Int. Ed.* **2009**, *48*, 1467-1471. (f) Liu, Y. M.; Tsunoyama, H.; Akita, T.; Xie, S. H.; Tsukuda, T. *Acs Catal* **2011**, *1*, 2-6. (g) Oliver-Meseguer, J.; Cabrero-Antonino, J. R.; Domínguez, I.; Leyva-Pérez, A.; Corma, A. *Science* **2012**, *338*, 1452-1455.

(10) (a) Lee, L.-C.; Zhao, Y. *Helv. Chim. Acta* **2012**, *95*, 863-871. (b) Lee, L.-C.; Zhao, Y. *ACS Catalysis* **2014**, 688-691.

(11) Lee, L.-C.; Zhao, Y. *Org. Lett.* **2012**, *14*, 784-787.

(12) (a) Genin, E.; Toullec, P. Y.; Antoniotti, S.; Brancour, C.; Genêt, J.-P.; Michelet, V. *J. Am. Chem. Soc.* **2006**, *128*, 3112-3113. (b) Harkat, H.; Weibel, J. M.; Pale, P. *Tetrahedron Lett* **2006**, *47*, 6273-6276. (c) Toullec, P. Y.; Genin, E.; Antoniotti, S.; Genet, J. P.; Michelet, V. *Synlett* **2008**, 707-711. (d) Neaţu, F.; Li, Z.; Richards, R.; Toullec, P. Y.; Genêt, J.-P.; Dumbuya, K.; Gottfried, J. M.; Steinrück, H.-P.; Pârvulescu, V. I.; Michelet, V. *Chem.-Eur. J.* **2008**, *14*, 9412-9418. (e) Harkat, H.; Dembele, A. Y.; Weibel, J. M.; Blanc, A.; Pale, P. *Tetrahedron* **2009**, *65*, 1871-1879. (f) Tomás-Mendivil, E.; Toullec, P. Y.; Díez, J.; Conejero, S.; Michelet, V.; Cadierno, V. *Org. Lett.* **2012**, *14*, 2520-2523.

(13) We did not attempt to exclude moisture in the reaction because the strongly hydrophilic ICRM core was likely to retain water molecules. The residual moisture present in the solvent and the starting material could also be responsible for the hydrolysis of the product, as suggested by Entry 11, Table 1.

(14) Because the reduction of the aurate was induced by the bromide counteranion in the ICRM core, an increase of W_0 increased the number of the surfactant and thus the bromide counterion available for the reduction

(15) Zheng, J.; Nicovich, P. R.; Dickson, R. M. *Annu. Rev. Phys. Chem.* **2007**, *58*, 409-431.

(16) Zheng, J.; Zhang, C.; Dickson, R. M. *Phys. Rev. Lett.* **2004**, *93*, 077402.

(17) The larger cluster size of Au@ICRM(**2**) at W_0 =10 was evident from its longer emission wavelength (496 nm) (Figure S4).

(18) It is not entirely clear to us why ICRM(**2**) gave so much better results than ICRM(**1**). We suspect that the different functional groups in the headgroup of the cross-

linkable surfactant might be responsible. ICRM(**1**), for example, utilized thiol in the cross-linking. If any residual thiol (e.g., from singly reacted DTT) was left in the core, it might greatly suppress the most active catalytic site. In our hands, 1 mol % externally added DTT completely shut down the catalysis.

(19) For some exampls of related encapsulated catalysts, see: (a) Vriezema, D. M.; Aragones, M. C.; Elemans, J.; Cornelissen, J.; Rowan, A. E.; Nolte, R. J. M. *Chem. Rev.* **2005**, *105*, 1445-1489. (b) Akiyama, R.; Kobayashi, S. *Chem. Rev.* **2009**, *109*, 594-642. (c) Price, K. E.; McQuade, D. T. *Chem. Commun.* **2005**, 1714-1716. (d) Helms, B.; Guillaudeu, S. J.; Xie, Y.; McMurdo, M.; Hawker, C. J.; Frechet, J. M. J. *Angew. Chem. Int. Ed.* **2005**, *44*, 6384-6387. (e) Chi, Y. G.; Scroggins, S. T.; Frechet, J. M. J. *J. Am. Chem. Soc.* **2008**, *130*, 6322-6323.

(20) Percec, V.; Peterca, M.; Tsuda, Y.; Rosen, B. M.; Uchida, S.; Imam, M. R.; Ungar, G.; Heiney, P. A. *Chem.–Eur. J.* **2009**, *15*, 8994 -9004.

(21) Gao, Y.; Chen, L.; Zhang, Z.; Gu, W.; Li, Y. *Biomacromolecules* **2010**, *11*, 3102-3111.

(22) (a) Zhang, S.; Zhao, Y. *ACS Nano* **2011**, *5*, 2637-2646. (b) Zhang, S.; Zhao, Y. *Langmuir* **2012**, *28*, 3606-3613.

CHAPTER 6.

PALLADIUM–GOLD BIMETALLIC NANOCLUSTERS WITH LOCALLY TUNED METAL OXIDES FOR ALCOHOL OXIDATION

Li-Chen Lee, Chaoxian Xiao, Wenyu Huang, and Yan Zhao

Abstract

Although metal oxide supports could have profound influence on their supported metal nanoparticle catalysts, it is challenging to fine-tune the metal oxide immediate around the catalyst without changing the bulk solid support. Interfacially cross-linked reverse micelles (ICRMs) readily accommodated anionic gold and palladium metal salts in their ammonium-lined hydrophilic cores and allowed facile control of the metallic composition, as well as the metal oxides in the vicinity of the metals. Deposition onto a solid support (P25 TiO_2) followed by thermal treatment of Pd–Au-containing ICRMs yielded bimetallic nanoclusters with tunable properties. The catalysts allowed efficient oxidation of benzyl alcohol under relatively mild conditions with minimal amounts of oxidant (hydrogen peroxide) in water without any organic solvent.

Introduction

Metal nanoparticles represent an important class of catalysts.[1] Their small size translates to a large surface-to-volume ratio but meantime makes the particles prone to agglomeration. For this reason, metal nanoparticle catalysts are often deposited on a solid support or protected by suitable ligands or polymers. In addition to minimizing the agglomeration of the catalysts, the support/ligands themselves may have strong influence

over the catalytic properties of the metal. In recent years, there has been increasing recognition that the microenvironment around a catalyst could profoundly influence the catalyst's properties.[2] The ultimate examples of such environmental control are found in nature, where the unique microenvironment of an enzyme active site and the catalytic groups within are collectively responsible for the observed catalytic efficiency and selectivity. Similar environmental control also proves highly effective in metal nanoparticle-based catalysts. Dendrimers,[3] for example, may endow size-selectivity,[4] tailored solubility,[5] and improved surface deposition[1f] to entrapped metal nanoparticles.

In many cases, organic and inorganic materials are complementary in their properties as catalyst supports. Although organic scaffolds are characterized by their outstanding structural diversity and tunability, inorganic metal oxides tend to be superior in their stability, making them the support of choice in most heterogeneous catalysis. This dichotomy provides strong motivation for chemists to enhance the stability of organic supports or find ways to manipulate the microstructure of inorganic supports around a catalyst. Towards the latter objective, metal particles that are encapsulated in semipermeable metal oxide shells,[6] deposited on tailored-made support structures,[7] or located within intricately structured mesopores[8] have emerged in the literature. The designed microenvironment has been shown to afford unusual substrate selectivity, extend the catalytic lifetime, and/or enable the catalysts to survive harsh reaction conditions.

We recently reported a method to covalently capture reverse micelles (RMs) through polymerization.[9] The resulting interfacially cross-linked RMs (ICRMs) are core–shell organic nanoparticles tunable in multiple ways including the size of their hydrophilic core,[9] the alkyl density on the surface,[9-10] and internal contents.[9, 11] Herein, we report that ICRMs

could serve as templates to prepare palladium–gold bimetallic nanoclusters. The ICRMs allowed facile tuning of not only the metal composition but also the local metal oxides around the metal clusters, *independent* of the bulk solid support. The significance of this approach is that it potentially can allow one to dope minute amounts of effective (but possibly expensive) metal oxides in the catalyst's immediate surroundings to modulate the catalytic properties.

Experimental Section

General. All reagents and solvents were of ACS certified grade or higher and were used as received from commercial suppliers. Routine ^{1}H and ^{13}C NMR spectra were recorded on a Varian VXR-400 and Bruker DRX-400 spectrometer. Inductively coupled plasma optical emission spectrometry (ICP-OES) was performed on a PerkinElmer Optima 2100 DV. The transmission electron micrographs (TEM) were taken on a TECNAI G^2 F20 at acceleration voltages of 200 kV. Samples were prepared by drop-drying dilute particle suspensions in ethanol onto carbon film stabilized with formvar on 300 mesh Cu grids (Global Electron Microscopy Technology Co.).

Preparation of Pd_mAu_n@ICRM. Preparation of ICRM from **1**,[9] detailed characterization of the materials,[9, 11a] and the template synthesis of Au_n@ICRM[9, 11a] and Pd_m@ICRM[11b] have been reported previously. For the introduction of Pd and Au into the ICRM core, 20 mg of ICRM at $W_0 = 5$ was first dissolved in 2 mL of $CHCl_3$. The appropriate amounts of H_2PdCl_4 and $HAuCl_4$ aqueous solutions were stirred with the above ICRM in $CHCl_3$ for 3h. The

orange-colored organic phase was separated, washed with H_2O (3 × 1 mL), and concentrated in vacuo to give an orange powder (18 mg).

Preparation of Pd_mAu_n-M_xO_y@ICRM. The preparation and characterization of Au_n-M_xO_y@ICRMs were reported in detail previously.[12] To introduce metal oxide into the ICRM core, 20 mg of Pd_mAu_n@ICRM with $[H_2PdCl_4]$/[surfactant] = 30 % , [aurate]/[surfactant] = 30 %, and W_0 = 5 was first dissolved in 2 mL of $CHCl_3$. For easily hydrolyzed metal oxide precursors such as $SnCl_4$, (*s*-BuO)$_3$Al, and Ti(OiPr)$_4$, 2.7 μL of water was added. For Si(OMe)$_4$, 2.7 μL of 6 M HCl aqueous solution was added to facilitate the hydrolysis of the metal oxide precursor. The mixture was stirred vigorously until the water droplets disappeared into the chloroform solution. The appropriate metal oxide precursor ([metal oxide precursor]/[**1**] = 2.0) was then added to the solution with a Hamilton microsyringe. The mixture was stirred at room temperature for 24 h (48 h for Si(OMe)$_4$) to allow the hydrolysis to complete. The $CHCl_3$ solution of the materials was generally used in the next step directly.

Adsorption of Pd_mAu_n-M_xO_y@ICRM onto P25 TiO_2. TiO_2 (Aeroxide(R) P25, surface area 35 to 65 m^2/g) (300 mg) was dispersed in $CHCl_3$ (100 mL) and sonicated for ca 10 min. An aliquot (2 mL) of the above solution of Pd_mAu_n-M_xO_y@ICRM in $CHCl_3$ (2 mL) containing the appropriate amount of Au was injected into the TiO_2 suspension under vigorous stirring. After 12 h, $CHCl_3$ was removed by rotary evaporation and the materials were dried in vacuum for 6 h to give a white powder (300 mg).

Typical Thermal Treatment of Pd_mAu_n-M_xO_y@ICRM on P25 TiO_2. The above Pd_mAu_n-M_xO_y@ICRM on P25 TiO_2 (150 mg) was placed in a quartz-tube oven. The tube was filled with Ar at room temperature. The temperature of the oven was raised to the targeted value at a rate of 5 ^oC/min under the appropriate flowing gas (50 mL/min) and maintained for a total of 7 h.

General Procedure for Oxidation. Benzyl alcohol (90 µL, 0.75 mmol) and H_2O_2 (30 wt % in H_2O; 170 µL, 1.50 mmol) were mixed with water (1.0 mL) and an appropriate amount of the Pd_mAu_n-M_xO_y@ICRM on P25 TiO_2 in a thick-walled glass tube. The tube was sealed with a Teflon plug. The reaction mixture was stirred at 80 ^oC for an appropriate length of time. $CDCl_3$ (1.5 mL) was added to the reaction mixture and the yields of the products (benzaldehyde and benzoic acid) were determined by ^1H NMR spectroscopy.

Inductively Coupled Plasma Optimal Emission Spectrometry (ICP-OES). In a typical experiment, an exact weight of the sample (~5 mg) was digested with 10 ml of aqua regia and 1µL of HF (~40 wt %) at 200 °C for 2 h in an acid digestion vessel (Parr 4744 General Purpose Vessel). The resulting solution was filtered and diluted to 50.0 mL with ultrapure water (18.2 MΩ) before the amounts of gold or palladium in the catalysts were determined by ICP-OES.

Results and Discussion

Scheme 1 shows the synthesis of ICRMs from cross-linkable surfactant **1**, template synthesis of Pd_mAu_n@ICRMs,[9, 11a] and subsequent introduction of metal oxide into the ICRM

core.[12] In general, we first dissolved the cross-linkable surfactant in a heptane/chloroform mixture in the presence of a small amount of water. Chloroform was needed mainly to dissolve dithiothreitol (DTT, a hydrophilic cross-linker) in the RM solution. UV irradiation in the presence of a photoinitiator (2,2'-dimethoxy-2-phenylaceto-phenone) quickly cross-linked the RMs to afford organic-soluble ICRMs in quantitative yield. As demonstrated in our previous work,[9] multiple factors contributed to the success of the covalent capture of the RMs including the location of the polymerizable alkenes at the surfactant/water interface, a high effective concentration of DTT in the central water pool as a result of its hydrophilicity, and the high efficiency of the thiol–ene click reaction.

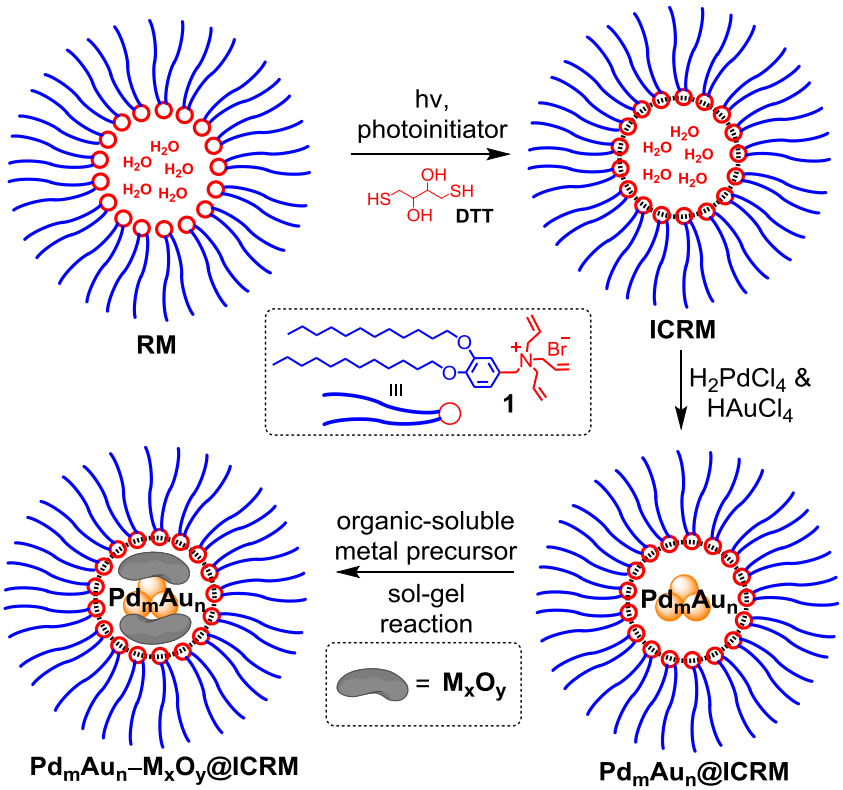

Scheme 1. Preparation of Pd_mAu_n–M_xO_y@ICRM.

The objective of this study is to use the ICRMs as both the templates and the "delivery vehicles" to prepare Pd–Au bimetallic nanoclusters on an inorganic solid support to afford a heterogeneous catalyst. There were several reasons why we chose to study the bimetallic nanoclusters. First, our model reaction is oxidation of benzyl alcohol under green chemistry condition (i.e., minimal usage of oxidant and organic solvent).[13] Palladium is known to enhance the activity of gold nanoparticles for such reactions.[14] The ICRM should allow us to tune the metal composition easily during the template synthesis of the metal clusters. Second, because the metals (in oxidized or reduced forms) are located in the hydrophilic core of the cross-linked RMs and RMs are frequently used as templates to prepare inorganic nanoparticles,[15] we could easily incorporate metal oxides in the ICRM core through sol–gel chemistry to fine-tune the microenvironment around the catalyst. Third, when ICRMs are deposited onto a solid support, the metal oxide and organic shell around the metals potentially could protect them during thermal treatment to minimize metal migration and sintering. Thus, ICRMs could offer multiple ways to fine-tune the structure of the final Pd–Au bimetallic nanoclusters catalysts.

ICRMs have already been shown to produce Au–Pt bimetallic clusters when a mixture of $AuCl_4^-$ and $PtCl_6^{2-}$ were extracted into their hydrophilic cores and reduced by $NaBH_4$.[9] In this work, we initially loaded the ICRMs by extracting a mixture of aqueous $HAuCl_4$ and H_2PdCl_4 with a chloroform solution of ICRM. Our previous work indicates that, once entering the ICRM core, $AuCl_4^-$ undergoes ligand exchange with bromide and a subsequent elimination–disproportionation. The overall reaction is spontaneous reduction within the ICRM core to yield gold clusters with 4–23 gold atoms. The cluster size was

controlled primarily by W_0 (the water/surfactant ratio) and the aurate loading (aurate/surfactant ratio).[9]

In our initial experiments, we kept the metal loading of both $AuCl_4^-$ and $PdCl_4^{2-}$ to 30 mol % of the (cross-linked) surfactant. At too high a metal loading, the ICRMs would not be able to extract all the metal salts from the aqueous solution. We did not attempt to reduce all the metal salts at this point because the reduction was easily done as a standard procedure at the thermal treatment stage using molecular hydrogen at high temperatures.

After extraction of the metal salts to the ICRM core, we added two equivalents (to the surfactant) of chloroform-soluble, hydrolyzable metal oxide precursor—e.g., $Si(OMe)_4$ for SiO_2,[16] $SnCl_4$ for SnO_2, (*s*-$BuO)_3Al$ for Al_2O_3, and $Ti(OiPr)_4$ for TiO_2. The sol–gel hydrolysis of these precursors was expected to take place near the hydrophilic core where water was located. We typically allowed the hydrolysis to continue for 24–48 h at room temperature, depending on the reactivity of the metal precursor. ^{1}H NMR spectroscopy allowed us to monitor the released alcohol side product to confirm the completion of the hydrolysis. All the metal oxide-modified Pd–Au-containing ICRMs, i.e., Pd_mAu_n–M_xO_y@ICRM, were completely soluble in chloroform. In contrast, the same sol–gel hydrolysis of the metal oxide precursors in the absence of ICRMs always yielded precipitate in the chloroform solution in our hands.

In heterogeneous catalysis, TiO_2 is known to have strong interactions with gold nanoparticles and thus is helpful to the latter's deposition and stability.[17] Since we were primarily concerned with tuning the local metal oxides around the metal clusters, we employed commercially available P25-type TiO_2 as the bulk solid support in all our catalysts. Our catalyst preparation is described in detail in the experimental section. Briefly, Pd_mAu_n–

M_xO_y@ICRMs were first ultrasonicated with P25 TiO_2 in a chloroform mixture. After the organic solvent was removed by rotary evaporation, the materials were dried under vacuum before thermal treatment under different conditions (vide infra for a more detailed discussion).

Table 1 summarizes the reaction yields for the oxidation of benzyl alcohol catalyzed by the heterogeneous Pd–Au bimetallic catalysts. Although molecular oxygen also worked with our catalysts, hydrogen peroxide gave better yields and was easy to handle in the optimization of the catalysts. Thus, our standard reaction condition was 0.75 mmol of benzyl alcohol in the presence of 2 equiv of H_2O_2 in 1.0 mL of water at 80 °C for 18 h.

Table 1. Oxidation of benzyl alcohol with hydrogen peroxide catalyzed by Pd–Au bimetallic clusters with locally introduced metal oxides on a P25 TiO_2 support[a]

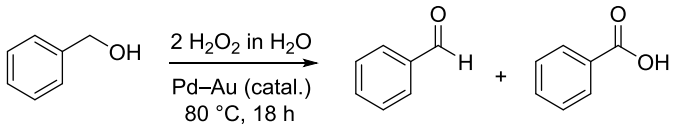

entry	local metal oxide	wt % of Au on TiO_2 support	Au/substrate (%)	yield (%)	activity (h^{-1})[b]	selectivity[c]
1	none	1	1	49	2.7	84:16
2	SnO_2	1	1	90	5.0	87:13
3	SiO_2	1	1	80	4.4	93:7
4	Al_2O_3	1	1	83	4.6	90:10
5	TiO_2	1	1	96	5.3	90:10
6	TiO_2	2.8	1	83	4.6	63:37
7	TiO_2	1	0.2	72	20	80:20
8	TiO_2	0.2	0.2	97	27	83:17

[a] The reaction was performed with 0.75 mmol (90 µL) benzyl alcohol and 2 equiv of H_2O_2 in 1.0 mL of water at 80 °C. The catalysts were prepared by thermal treatment of Pd_mAu_n-M_xO_y@ICRM on P25 TiO_2 at 200 °C for 2 h and 350 °C for 4 h under a 10 % H_2/Ar flowing gas (50 mL/min) in a quartz tube oven. [b] Average activity of the catalyst during the reaction was calculated as mmol of product/mmol of Au per hour. [c] Selectivity = ratio of benzaldehyde to benzoic acid.

The ICRMs contained bromide counterions in the core from surfactant **1**. The anionic aurate and palladate had chloride. It is known that halides can complex fairly strongly with gold[18] and promote sintering during thermal treatment. Bromide is also known to poison gold nanoparticle catalysts.[19] Since hydrogen can remove halide at high temperature (as HX), we heated our catalysts under flowing H_2/Ar gas. We expected the thermal treatment would help removal of the bromide and partly decompose the organic shell (vide infra for more detailed discussion).

The locally introduced metal oxides clearly had a strong impact on the catalysis, even when all the catalysts were supported on the same P25 TiO_2 and went through the same thermal treatment. Without any metal oxide in the ICRM core, the catalyst gave 49% yield in the oxidation, with 84:16 selectivity for benzaldehyde over benzoic acid (Table 1, entry 1). All locally introduced metal oxides improved the reaction yield, with TiO_2 clearly being the best (entries 2–5). The good performance of TiO_2 in a way is not surprising since it is known to interact strongly with gold.[17] However, since the bulk support was the same P25 TiO_2 in all cases, the locally introduced metal oxides must have strongly impacted the catalyst's activity, directly or indirectly.

Our current interpretation for the effects of local metal oxides is that they protected the ICRM-encapsulated metals and reduced their migration/sintering during the thermal treatment. This was probably why locally introduced TiO_2 was particularly helpful even in the large excess of TiO_2 in the bulk. Consistent with the explanation, when the metal loading on the P25 TiO_2 support was increased from 1 to 2.8 wt %, the catalyst under the same thermal treatment became less active, affording 83% yield using the same amount of catalyst in the reaction (compare entries 5 and 6). On the other hand, when the gold loading on the

P25 support was reduced to 0.2 wt %, the catalyst clearly became more active, even with reduced catalyst in the reaction (entry 8).

To further understand the protection of the metal clusters by the ICRMs and the locally introduced metal oxides, we varied the thermal treatment conditions for the catalyst, mainly changing the atmosphere and the temperature while keeping everything else the same (0.2 wt % gold loading on P25 TiO_2 with TiO_2 within the ICRMs). Table 2 shows the reaction yields for the differently prepared catalysts. We reduced the reaction time from 18 to 2–6 h in Table 2, as all catalysts prepared with 0.2 wt % gold loading on P25 TiO_2 were quite reactive.

Table 2. Effects of thermal treatment conditions on the benzyl alcohol oxidation[a]

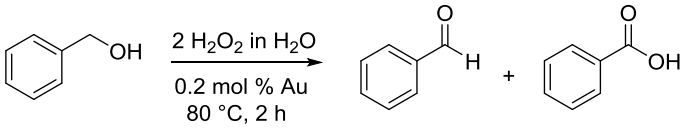

entry	flowing gas (heating time)	temp (°C)	reaction time (h)	yield (%)	activity (h^{-1})[b]	selectivity[c]
1	H_2/Ar (7 h)	350	6	77	64	92:8
2	H_2/Ar (7 h)	250	6	86	72	66:34
3	H_2/Ar (2 h) & air (5h)	250	2	93	233	86:14
4	H_2/Ar (2 h) & air (5h)	400	2	60	150	96:4
5	air (7 h)	250	2	59	148	92:8
6	no thermal treatment	--	2	23	58	97:3

[a] The reaction was performed with 0.75 mmol (90 µL) benzyl alcohol and 2 equiv of H_2O_2 in 1.0 mL of water at 80 °C for 2–6 h. The catalysts were prepared with locally introduced TiO_2 on a P25 TiO_2 support at 0.2 wt % Au loading. The metal loading in the ICRMs was the same as those in Table 1—30 mol % $AuCl_4^-$ and 30 mol % $PdCl_4^{2-}$ relative to the (cross-linked) surfactant. The catalysts were prepared by thermal treatment of Pd_mAu_n-

M_xO_y@ICRM on P25 TiO_2 at the indicated temperature for a total of 7 h under the appropriate flowing gas in a quartz tube oven. [b] Average activity of the catalyst during the reaction was calculated as mmol of product/mmol of Au per hour. [c] Selectivity = ratio of benzaldehyde to benzoic acid.

Since we varied the reaction time in Table 2 (due to different activity of the catalysts), the best way to compare the catalysts' efficiency was their (average) activity defined as mmol of product/mmol of Au per hour during the entire reaction. Our data showed that a decrease of thermal treatment temperature from 350 to 250 °C increased the activity from 64 to 72 h^{-1} using H_2/Ar as the flowing gas (Table 2, entries 1–2). Considering that the organic shell of ICRM was unlikely to decompose under H_2/Ar atmosphere, after treating the materials with H_2/Ar for 2h, we switched the flowing gas to air while keeping the total thermal treatment time (7 h) the same. This change dramatically enhanced the catalyst's activity, with the activity value increasing to 233 h^{-1} with the thermal treatment temperature of 250 °C (entry 3). Possibly, the oxygen in air facilitated decomposition of the organic shell around the metal clusters and might have improved the mass transfer of the substrate to the clusters. After all, a closed shell of organic materials around the catalysts, even partially carbonized, might make it difficult for the substrate to approach the protected metal clusters.

We noticed that the lower thermal treatment temperature (250 °C) gave better results than higher temperature (350 or 400 °C), regardless of the flowing gas (Table 2, entries 1–4). It seems the ICRM and local metal oxides had difficulty protecting the clusters from sintering at too high a temperature. As expected, hydrogen turned out critical to the catalyst's preparation, since thermal treatment with air as the flowing gas yielded less active material (entry 5). Without thermal treatment, although the material still could catalyze the oxidation,

the activity was very low (entry 6). The result further supports the importance of removing the halides and thermally decomposing the organic shell.

Using the best thermal treatment conditions (2 h under H_2/Ar and 5 h under air at 250 °C), we studied two additional parameters for the catalyst's preparation. The ICRMs up to this point all had W_0 = 5. Since the water/surfactant ratio influenced the size of the gold clusters formed (Scheme 1).[9, 11a,20] we thought this parameter might also be important because differently sized clusters should have different abilities to migrate and thus affect the size of the final Pd–Au nanoclusters after thermal treatment. Our experiments showed that the W_0 value indeed had an effect, but the effect was modest (Table 3, entries 1–3). On the other hand, with the same W_0 = 20, the metal composition made a huge difference in the catalyst's activity. A clear synergistic effect was observed for the two metals: the bimetallic clusters outperformed pure palladium or gold clusters, with the highest catalytic activity obtained with Pd/Au = 2:1 (entry 5).[21,22] Note that the reaction time was reduced further to 0.5 in Table 3 because the catalysts were quite active after the previous optimizations.

Table 3. Effects of W_0 and metal composition on the benzyl alcohol oxidation[a]

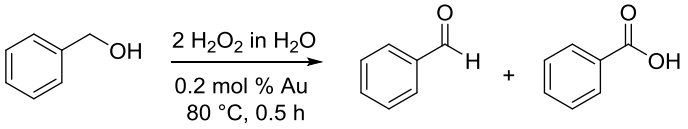

entry	W_0	Metal composition	yield (%)	activity (h^{-1})[b]	selectivity[c]
1	5	Pd/Au = 30/30	78	780	93:7
2	10	Pd/Au = 30/30	86	860	86:14
3	20	Pd/Au = 30/30	87	870	91:9
4	20	Pd/Au = 60/0[d]	11	110	--[e]
5	20	Pd/Au = 40/20	95	950	92:8
6	20	Pd/Au = 20/40	84	840	88:12
7	20	Pd/Au = 0/40	4	40	--[e]

[a] The reaction was performed with 0.75 mmol (90 µL) benzyl alcohol and 2 equiv of H_2O_2 in 1.0 mL of water at 80 °C for 30 min. The catalysts were prepared with locally introduced TiO_2 on a P25 TiO_2 support at 0.2 wt % Au loading. The catalysts were prepared by thermal treatment at 250 °C under 10 % H_2/Ar for 2 h and under air for 5 h in a quartz tube oven. [b] Average activity of the catalyst during the reaction was calculated as mmol of product/mmol of Au per hour. The activity value was calculated based on 0.2 mol % of gold (or Pd in entry 4) catalysts. [c] Selectivity = ratio of benzaldehyde to benzoic acid. [d] All reactions were performed with the amount of gold kept the same (0.2 mol % Au to benzyl alcohol) except this one which was performed with 0.2 mol % Pd. [e] The selectivity was not determined because of the low yield.

Figure 1 shows the TEM images of our optimized Pd–Au containing ICRMs and final bimetallic catalysts on the P25 TiO_2 support. Before thermal treatment (Figure 1a,b), no visible metal clusters could be identified, consistent with our previous results showing the subnanometer size of the gold clusters within ICRMs.[9] After thermal treatment, metal nanoparticles were clearly visible, typically 2.5 nm in size and showed no agglomeration. These particles, however, were only those observable by TEM. The active catalyst could be these nanoparticles and/or smaller ones not detected by TEM.

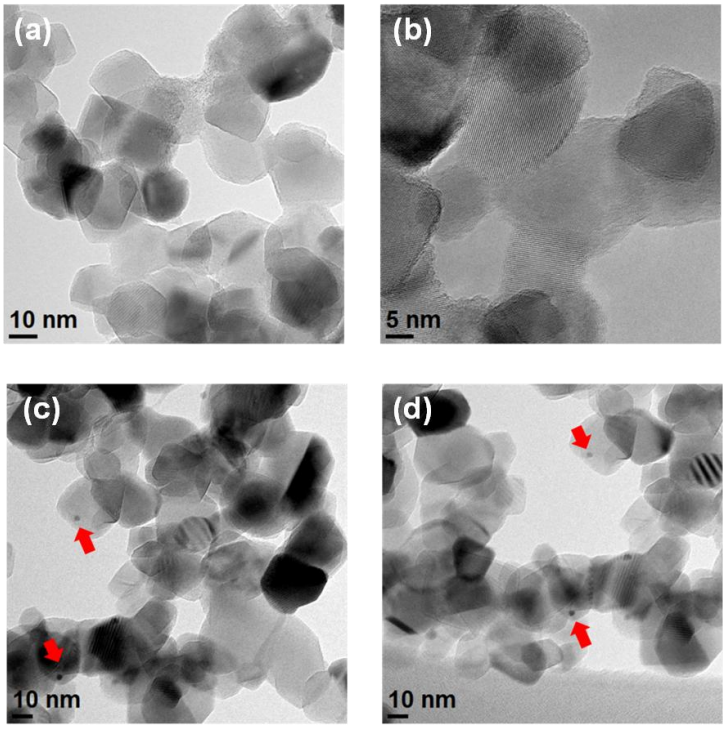

Figure 1. TEM images of (a, b) Pd_mAu_n–M_xO_y@ICRMs deposited on P25 TiO_2 and (c, d) the Pd–Au bimetallic heterogeneous catalyst after thermal treatment. $[H_2PdCl_4]$: $[HAuCl_4]$: [cross-linked **1**] = 0.4/0.2/1 during template synthesis. The gold loading on P25 TiO_2 was 0.2 wt %. The catalysts were prepared by thermal treatment at 250 °C under 10% H_2/Ar for 2 h and under air for 5 h in a quartz tube oven.

We also performed ICP-OES analysis of the materials in Table 3, entries 3–7. The results showed nearly constant loading of gold (0.12–0.13 wt %) on TiO_2 (except in 4, which contained no Au), consistent with our procedures. The systematic error (from the calculated 0.2 wt %) suggested that the actual activity of the catalysts should be about 60% higher than those reported in Table 3, as the calculation overestimated the amounts of catalysts in the reactions. In general, the Pd/Au ratio in the sample was in agreement with our initial

loadings: the 40/20, 30/30, and 20/40 Pd/Au samples, for example, had measured Pd/Au ratios of 2.76, 1.21, and 0.71, respectively.

Conclusions

To summarize, ICRMs allowed us to fine-tune the microenvironment around the Pd–Au bimetallic clusters readily. Metal composition was controlled in the template synthesis using a mixture of the metal precursors. Metal oxides could be introduced selectively in the vicinity of the metal catalysts and have been clearly shown to impact the activity of final catalysts even when the bulk support (P25 TiO_2) was the same. ICRMs can be prepared easily from the cross-linkable surfactant. Their most useful benefit in the preparation heterogeneous catalysts is the possibility of doping minute amounts of potentially expensive co-catalysts right where the catalyst is located. As shown in this work, they enabled many ways to control the composition and the microenvironment of bimetallic metal clusters. Their large tunability in structures[9-11] should make them useful as both templates and "delivery vehicles" of metal cluster catalysts.

Acknowledgment. We thank the U.S. Department of Energy-Office of Basic Energy Sciences (grant DE-SC0002142) for supporting the research.

References

(1) (a) *Nanoparticles and Catalysis*; Astruc, D., Ed.; Wiley-VCH: Weinheim, Germany, 2008. (b) Bell, A. T. *Science* **2003**, *299*, 1688-1691. (c) Burda, C.; Chen, X.; Narayanan, R.; El-Sayed, M. A. *Chem. Rev.* **2005**, *105*, 1025-1102. (d) Somorjai, G. A.; Contreras, A. M.; Montano, M.; Rioux, R. M. *Proc. Natl. Acad. Sci. U. S. A.* **2006**, *103*, 10577-10583. (e) Tsung, C. K.; Kuhn, J. N.; Huang, W.; Aliaga, C.; Hung, L. I.; Somorjai, G. A.; Yang, P. *J. Am. Chem. Soc.* **2009**, *131*, 5816-5822. (f) Somorjai, G. A.; Li, Y. M. *Top. Catal.* **2010**, *53*, 832-847.

(2) (a) Das, S.; Brudvig, G. W.; Crabtree, R. H. *Chem. Commun.* **2008**, 413-424. (b) Rakowski DuBois, M.; DuBois, D. L. *Chem. Soc. Rev.* **2009**, *38*, 62-72.

(3) Crooks, R. M.; Zhao, M. Q.; Sun, L.; Chechik, V.; Yeung, L. K. *Acc. Chem. Res.* **2001**, *34*, 181-190.

(4) Zhao, M.; Crooks, R. M. *Angew. Chem. Int. Ed.* **1999**, *38*, 364-366.

(5) (a) Chechik, V.; Zhao, M.; Crooks, R. M. *J. Am. Chem. Soc.* **1999**, *121*, 4910-4911. (b) Chechik, V.; Crooks, R. M. *J. Am. Chem. Soc.* **2000**, *122*, 1243-1244.

(6) Wu, S. H.; Tseng, C. T.; Lin, Y. S.; Lin, C. H.; Hung, Y.; Mou, C. Y. *J. Mater. Chem.* **2011**, *21*, 789-794.

(7) Lu, J.; Fu, B.; Kung, M. C.; Xiao, G.; Elam, J. W.; Kung, H. H.; Stair, P. C. *Science* **2012**, *335*, 1205-1208.

(8) Joo, S. H.; Park, J. Y.; Tsung, C.-K.; Yamada, Y.; Yang, P.; Somorjai, G. A. *Nat. Mater.* **2009**, *8*, 126-131.

(9) Zhang, S.; Zhao, Y. *ACS Nano* **2011**, *5*, 2637-2646.

(10) Lee, L.-C.; Zhao, Y. *Org. Lett.* **2012**, *14*, 784-787.

(11) (a) Zhang, S.; Zhao, Y. *Langmuir* **2012**, *28*, 3606-3613. (b) Lee, L.-C.; Zhao, Y. *Helv. Chim. Acta* **2012**, *95*, 863-871.

(12) Lee, L.-C.; Zhao, Y. *ACS Catalysis* **2014**, 688-691.

(13) (a) Della Pina, C.; Falletta, E.; Prati, L.; Rossi, M. *Chem. Soc. Rev.* **2008**, *37*, 2077-2095. (b) Della Pina, C.; Falletta, E.; Rossi, M. *Chem. Soc. Rev.* **2012**, *41*, 350-369. (c) Tsunoyama, H.; Sakurai, H.; Negishi, Y.; Tsukuda, T. *J. Am. Chem. Soc.* **2005**, *127*, 9374-9375. (d) Abad, A.; Almela, C.; Corma, A.; Garcia, H. *Chem. Commun.* **2006**, 3178-3180. (e) Hu, J.; Chen, L.; Zhu, K.; Suchopar, A.; Richards, R. *Catal. Today* **2007**, *122*, 277-283. (f) Miyamura, H.; Matsubara, R.; Miyazaki, Y.; Kobayashi, S. *Angew. Chem. Int. Ed.* **2007**, *46*, 4151-4154. (g) Tsunoyama, H.; Ichikuni, N.; Sakurai, H.; Tsukuda, T. *J. Am. Chem. Soc.* **2009**, *131*, 7086-7093. (h) Liu, H.; Liu, Y.; Li, Y.; Tang, Z.; Jiang, H. *J. Phys. Chem. C* **2010**, *114*, 13362-13369.

(14) (a) Enache, D. I.; Edwards, J. K.; Landon, P.; Solsona-Espriu, B.; Carley, A. F.; Herzing, A. A.; Watanabe, M.; Kiely, C. J.; Knight, D. W.; Hutchings, G. J. *Science* **2006**, *311*, 362-365. (b) Dimitratos, N.; Lopez-Sanchez, J.; Lennon, D.; Porta, F.; Prati, L.; Villa, A. *Catal. Lett.* **2006**, *108*, 147-153. (c) Villa, A.; Janjic, N.; Spontoni, P.; Wang, D.; Su, D. S.; Prati, L. *Appl. Catal., A* **2009**, *364*, 221-228. (d) Marx, S.; Baiker, A. *J. Phys. Chem. C* **2009**, *113*, 6191-6201. (e) Kesavan, L.; Tiruvalam, R.; Rahim, M. H. A.; bin Saiman, M. I.; Enache, D. I.; Jenkins, R. L.; Dimitratos, N.; Lopez-Sanchez,

J. A.; Taylor, S. H.; Knight, D. W.; Kiely, C. J.; Hutchings, G. J. *Science* **2011**, *331*, 195-199. (f) Balcha, T.; Strobl, J. R.; Fowler, C.; Dash, P.; Scott, R. W. J. *Acs Catal* **2011**, *1*, 425-436. (g) Murugadoss, A.; Sakurai, H. *J. Mol. Catal. A-Chem.* **2011**, *341*, 1-6. (h) Xie, S.; Tsunoyama, H.; Kurashige, W.; Negishi, Y.; Tsukuda, T. *Acs Catal* **2012**, *2*, 1519-1523.

(15) Pileni, M. P. *Structure and Reactivity in Reverse Micelles*; Elsevier: Amsterdam, 1989.

(16) The reaction for the Si(OMe)4 was facilitated by using 6 M HCl aqueous solution instead of water in the ICRM core.

(17) (a) Haruta, M. *Catal. Today* **1997**, *36*, 153-166. (b) Haruta, M. *Chem. Rec.* **2003**, *3*, 75-87. (c) Chen, M. S.; Goodman, D. W. *Chem. Soc. Rev.* **2008**, *37*, 1860-1870.

(18) Habib, M. A. In *Comprehensive Treatise of Electrochemistry*; Bockris, J. O. M., Conway, B. E., Yeager, E., Eds.; Plenum Press: New York, 1980; Vol. 1, p 135-220.

(19) (a) Oxford, S. M.; Henao, J. D.; Yang, J. H.; Kung, M. C.; Kung, H. H. *Appl. Catal., A* **2008**, *339*, 180-186. (b) Chandler, B. D.; Kendell, S.; Doan, H.; Korkosz, R.; Grabow, L. C.; Pursell, C. J. *Acs Catal* **2012**, *2*, 684-694.

(20) Because the reduction of the aurate was induced by the bromide counteranion in the ICRM core, an increase of W_0 increased the number of the surfactanst and thus the bromide counterions available for the reduction. Since the palladium salt would be reduced by hydrogen during the thermal treatment, we did not attempt to determine the oxidation states of palladium at the stage of metal-salt-extraction into ICRMs.

(21) The reactions in Table 3 were performed with 0.2 mol % gold catalysts (0.2 mol % palladium in entry 4). If the total amounts of metal were used to calculate the activity, the catalyst with Pd/Au =1:2 was the most active.

(22) Hutchings, G. J.; Kiely, C. J. *Acc. Chem. Res.* **2013**, *46*, 1759-1772.